PERFORMANCE OF ASSISTED HISTORY MATCHING TECHNIQUES WHEN UTILIZING MULTIPLE INITIAL GEOLOGIC MODELS

A Thesis

by

AKSHAY AGGARWAL

Submitted to the Office of Graduate Studies of
Texas A&M University
in partial fulfillment of the requirements for the degree of

MASTER OF SCIENCE

December 2011

Major Subject: Petroleum Engineering

Performance of Assisted History Matching Techniques When Utilizing Multiple Initial Geologic Models

PERFORMANCE OF ASSISTED HISTORY MATCHING TECHNIQUES WHEN UTILIZING MULTIPLE INITIAL GEOLOGIC MODELS

A THESIS

by

AKSHAY AGGARWAL

Submitted to the Office of Graduate Studies of
Texas A&M University
in partial fulfillment of the requirements for the degree of

MASTER OF SCIENCE

Approved by:

Chair of Committee,	Michael J. King
Committee Members,	Duane A. McVay
	Rick Gibson
Head of Department,	Stephen A. Holditch

December 2011

Major Subject: Petroleum Engineering

ABSTRACT

Performance of Assisted History Matching Techniques When Utilizing Multiple Initial Geologic Models. (December 2011)

Akshay Aggarwal, B.Tech, Indian School of Mines

Chair of Advisory Committee: Dr. Michael J King

History matching is a process wherein changes are made to an initial geologic model of a reservoir, so that the predicted reservoir performance matches with the known production history. Changes are made to the model parameters which include rock and fluid parameters (viscosity, compressibility, relative permeability, etc.) or properties within the geologic model. Assisted History Matching (AHM) provides an algorithmic framework to minimize the mismatch in simulation, and aids in accelerating this process. The changes made by AHM techniques, however, cannot ensure a geologically consistent reservoir model. In fact, the performance of these techniques depends on the initial starting model. In order to understand the impact of the initial model, this project explored the performance of the AHM approach using a specific field case, but working with multiple distinct geologic scenarios.

This project involved an integrated seismic to simulation study, wherein I interpreted the seismic data, assembled the geological information, and performed petrophysical log evaluation along with well test data calibration. The ensemble of static models obtained was carried through the AHM methodology. I used sensitivity analysis

to determine the most important dynamic parameters that affect the history match. These parameters govern the large scale changes in the reservoir description and are optimized using the Evolutionary Strategy Algorithm. Finally, the streamline based techniques were used for local modifications to match the water cut well by well.

The following general conclusions were drawn from this study-

a) The use of multiple simple geologic models is extremely useful in screening possible geologic scenarios and especially for discarding unreasonable alternative models. This was especially true for the large scale architecture of the reservoir.

b) The AHM methodology was very effective in exploring a large number of parameters, running the simulation cases, and generating the calibrated reservoir models. The calibration step consistently worked better if the models had more spatial detail, instead of the simple models used for screening.

c) The AHM methodology implemented a sequence of pressure and water cut history matching. An examination of specific models indicated that a better geologic description minimized the conflict between these two match criteria.

ACKNOWLEDGEMENTS

I would like to thank my committee chair, Dr. Michael King, and my committee members, Dr. McVay and Dr. Gibson, for their guidance and support throughout the course of this research.

I want to extend my thanks to the PETE 400 course Teaching Assistants and my teammates in that course. I also wish to express my gratitude to the MCERI research group who financially supported me in two summers. I also thank my friends Mohan and Satyajit who helped me time to time in doing the research work. Thanks also go to my other friends and colleagues and the department faculty and staff for making my time at Texas A&M University a great experience

Finally, thanks to my mother, father, brother, and sister who have always stood behind me and motivated me to finish my Master's degree.

NOMENCLATURE

AHM	Assisted History Matching
FOPT	Total Field Oil Production
FOPTH	Total Field Oil Production History
TDRM	Top Down Reservoir Modeling
GTTI	Generalized Travel Time Inversion
NTG	Net to Gross Ratio
λ_{total}	Total Mobility
k_{ro}	Relative Permeability to Oil Fraction
k_{rw}	Relative Permeability to Water Fraction
μ_o	Oil Viscosity
μ_w	Water Viscosity
STB	Stock-Tank Barrel
ϕ	Porosity
OOIP	Original Oil in Place
B	Oil Formation Volume Factor

V_{sh}	Shale Volume
ρ_{ma}	Matrix Density
ρ_{fl}	Fluid Density
GR	Gamma Ray

TABLE OF CONTENTS

Page

ABSTRACT iii

ACKNOWLEDGEMENTS v

NOMENCLATURE vi

TABLE OF CONTENTS viii

LIST OF FIGURES xi

LIST OF TABLES xiv

1. INTRODUCTION 1

2. THEORY 6

    2.1 Evolution Strategy 6
        2.1.1 Recombination 6
        2.1.2 Mutation 7
    2.2 Generalized Travel Time Inversion 8

3. METHODOLOGY 10

    3.1 Overview 10
    3.2 Procedure 11

4. PETROPHYSICAL ANALYSIS 12

    4.1 Introduction 12
    4.2 Shifting of Data 12
    4.3 Lithology 14
    4.4 Shale Volume 15
    4.5 Porosity 16
    4.6 Permeability 18
        4.6.1 Deterministic Approach 18
        4.6.2 Stochastic Approach 23
    4.7 Net Sand Determination 25
    4.8 Fluid Contact 26

Page

5. PRESSURE TRANSIENT ANALYSIS 28

5.1 Methodology 28
5.2 Intermediate Parameters 28
5.3 Well Test Interpretation 29
5.4 Results Summary 32
5.5 PTA Observations 32
5.6 Log and well test data Calibration 33

6. MATERIAL BALANCE ANALYSIS 36

6.1 Data Preparation 36
6.2 Material Balance Plots and Analysis 37
6.3 Uncertainty Quantification 39
6.4 Results and Interpretation 42

7. STATIC MODEL CONSTRUCTION 43

7.1 Geological Setting 43
7.2 Geologic Scenarios 46
7.3 Channel Architecture 47
7.4 Porosity Modeling and Aspect Ratio 48
7.5 Permeability Trend Modeling 49
7.6 Porosity - Permeability Modeling 49
7.7 Dynamic Uncertainties 51
7.8 Dynamic Base Case and Uncertainty Range 51
7.8.1 Fault Transmissibility 51
7.8.2 Rock Compressibility 51
7.8.3 Aquifer Strength 52
7.8.4 Permeability Multipliers 53
7.8.5 Pore Volume Multipliers 53
7.8.6 K_v/K_h Ratio 53
7.8.7 Relative Permeability 54

8. DYNAMIC DATA CALIBRATION 57

8.1 Case 1 63
8.2 Case 2 66
8.3 Case 3 68
8.4 Case 4 74
8.5 Case 5 80

Page

8.6 Case 6 85
8.7 Case 7 86
8.8 Case 8 88

9. DISCUSSION AND CONCLUSIONS 94

REFERENCES 103

VITA 106

LIST OF FIGURES

Page

Fig. 1- Core Porosity and Density Porosity match 13

Fig. 2 - Neutron Density Crossplot of M2 Sand 14

Fig. 3 - Shale Effect on Neutron Density Crossplot of M3 Sand 15

Fig. 4 - Core Picture shows Laminated Shale 17

Fig. 5 - Core Porosity – Density Porosity Crossplot 17

Fig. 6 - Core Permeability – Core Porosity Crossplot 18

Fig. 7 - Core Permeability – V_{sh} Crossplot 19

Fig. 8 - Core Permeability – Core Porosity Crossplot with V_{sh} as filter 20

Fig. 9 - Core Permeability – Core Porosity Crossplot for different V_{sh} 21

Fig. 11 - Match between Core Measurements and Log Calculations 23

Fig. 12 - Permeability compared from Cloud Transform 24

Fig. 13 - Plot of PD vs. PHID showing a Porosity cutoff 25

Fig. 14 - V_{sh} vs. PHID showing a V_{sh} cutoff 26

Fig. 15 - OWC inferred in a Well Log 27

Fig. 16 - Well A1 - Log - Log Diagnostic Plot 30

Fig. 17 - Well A2 - Log – Log Diagnostic Plot 31

Fig 18 - Well Test and Log Permeability Comparison 34

Fig. 19 - Individual Well Pressures 37

Fig. 20 - MBAL Pressure History Match by Analytical Approach 38

Page

Fig. 21 - Pressures and Cumulative Oil Production 38

Fig. 22 - Energy Plot..... 39

Fig. 23 - Probability Function vs OOIP..... 41

Fig. 24 - CDF vs OOIP..... 41

Fig. 25 - Reservoir Structure 44

Fig. 26 - M2 Structure Map with Dip (BB') and Strike (AA') Direction 44

Fig. 28 - Uncertainties Considered..... 46

Fig. 29 - Average Rock Compressibility vs. Net Confining Pressure..... 52

Fig. 30 - Mobility Calculation..... 55

Fig. 31- Initial and Adjusted Relative Permeabilities..... 56

Fig. 32 - Global error – NTG parameter..... 57

Fig. 33 - Global error – Porosity parameter..... 58

Fig. 34 - Global error – Permeability parameter 59

Fig. 35 - Global error – Permeability approach..... 60

Fig. 36 - Initial Regions..... 63

Fig. 37 - Tornado Chart for Case 1..... 64

Fig. 38 - Simplest Model Match..... 65

Fig. 39 - Tornado Chart for Case 2..... 66

Fig. 40 - Case 2 Results..... 67

Fig. 41 - Case 3 Results..... 69

Fig. 42 - Case 1 - 3 Comparison..... 70

Page

Fig. 43 - New Regions Defined 74

Fig. 44 - Tornado Chart for Case 4 75

Fig. 45 - Case 4 Results 76

Fig. 46 - Case 4 Reservoir Description 77

Fig. 47 - Case 4 Adjusted Aquifer Results 79

Fig. 48 - Tornado Chart for Case 5 80

Fig. 49 - Case 5 Results 81

Fig. 50 - Case 5 Adjusted Aquifer Results 82

Fig. 51 - Water Breakthrough Profile in Case 3 83

Fig. 52 - Water Breakthrough Profile in Case 4 84

Fig. 53 - Water Breakthrough Profile in Case 5 84

Fig. 54 - Tornado Chart for Case 6 86

Fig. 55 - Case 7 Results compared with Case 5 87

Fig. 56 - Tornado Chart for Case 8 89

Fig. 57 - Tornado Chart for A8 water cut 89

Fig. 58 - Case 8 Results 91

Fig. 59 - Case 8 Results with Adjusted Aquifer Strength 92

Fig. 60 - Simulation Cases Compared 93

Fig. 61 - Forward Predictions compared for different Cases 101

LIST OF TABLES

Page

Table 1 - Permeability Prediction at 30% Porosity for different V_{sh} 21

Table 2 - Net Pay Zone Thickness for Wells 29

Table 3 - Parameters used in Well Test Analysis 29

Table 4 - Well A1 Results 30

Table 5 - Well A2 Results 31

Table 6 - Individual Well Test Results 32

Table 7 - Well Test and Log Permeability Results 34

Table 8 - MBAL Input Parameters 36

Table 9 - Input Aquifer Parameters 40

Table 10 - Standard Deviation and Probability Function 40

Table 11 - Different Static Models 50

Table 12 - Initial Mobility 55

Table 13 - OOIP for different Cases 95

Table 14 - Pore Volume and Permeability Multipliers for different Cases 96

Table 15 - Aquifer Strength for different Cases 97

Table 16 - Rock Compressibility for different Cases 97

Table 17 - Total Oil Production after 20 Years 101

1. INTRODUCTION

The initial geological model is fundamental when we develop an acceptable reservoir description in a reservoir simulation study. The initial geologic model here refers to the spatial distribution of facies and reservoir properties like net-to-gross (NTG), porosity, and permeability in a 3D grid representing the reservoir structure. Building a good descriptive geological model requires time, expertise, and data. Usually the geologic models are large (millions of cell) and are upscaled prior to the start of the history match. However, even that does not guarantee a good predictive simulation model and often it undergoes large changes in the calibration process. The conventional approach has been to match a base model and then run sensitivities on it for reservoir performance. However, a single model is insufficient to capture both the information and uncertainty for a field with significant production history. In contrast, BP's Top Down Reservoir Modeling Approach, TDRM (Williams et al. 2004) proposes a different methodology by constructing multiple geologic reservoir models to incorporate uncertainty in various parameters like channel orientation/width, kv/kh ratio, aquifer strength, formation compressibility etc. Assisted History Matching (AHM) is then utilized to perform the history match for each model. The idea is to get a sense on how the dynamic model is reconciled with our static model without using too much geologic detail initially. Its application to a field case has been discussed by Moulds et al. (2005) for the Magnus Field, North Sea.

This thesis follows the style of *SPE Journal.*

The AHM techniques have offered a faster and potentially more robust approach to the integration of dynamic data with the static model. This history matching methodology helps simplify the steps involved in traditional history matching described by Williams et al. (1998). The key steps in traditional history matching are to first obtain an overall energy balance and second to identify the gridblocks in the model which affect the water production for a well. Properties are changed according to the mismatch in water production. Emanuel and Milliken (1998) used 3D streamline simulation for this purpose. The streamlines are the preferential flowpaths that fluids traverse in the reservoir. The fluids travel from source (injector/aquifer) to sink (producer). Each gridblock in the model is assigned to the producer where the streamline passing through it terminates. Once the gridblocks are allocated to different producers, the properties are changed to minimize the mismatch in water cut. Milliken et al. (2000) described the utility of this technique. However, this technique was limited to changes in the geologic model such as permeability, porosity, and NTG. This technique worked one well at a time and the changes made for one well could impact the production adversely at other wells as described in Cheng et al. (2004).

The uncertainty in history matching has also been approached using Experimental Design (Box and Draper 1987; Myers and Montgomery 1995) through the method of response surfaces (Eide et al. 1994; Friedmann et al. 2001; White et al. 2001; White and Royer 2003; Landa and Guyagular 2003). The sensitivity coefficients are calculated to construct the response surface from a pre-determined set of experimental runs. The response surface, which is a polynomial equation, can be constructed for a

predefined objective function and then acts as a proxy for the actual simulation runs. The locations of minima below a certain threshold can be calculated on a response surface and those points can be included for Monte Carlo simulation. However, prediction error will always be present in response surface predictions as they do not represent the actual simulation results. This error can sometimes be significant. Moreover, a more complete response surface includes the linear, quadratic, and interaction terms between the parameters, which require substantially more simulation runs (Ligero et al. 2005). The response surface approach has the limitation that the changes to different parameters are made at once without any hierarchy in the parameters. It may bring in unnecessary input parameters in the forecast that may not affect history match. Therefore, the experimental design should be designed efficiently so as to minimize the variables that we need to explore.

Other recent global search algorithms utilize an evolutionary approach as described in Castellini et al. (2006) and Cheng et al. (2008). These algorithms find the optimized values for uncertain parameters within their specified probable range working under the requirement to minimize the objective function. The genetic algorithms and the evolutionary strategy are the two most commonly used evolutionary algorithms in reservoir engineering application.

The above two methods introduce changes that are global in nature e.g. multipliers to the pore volume or to the permeability field. Their usability is limited when the changes are meant to be localized, i.e., fine tuning the water cut match well by well. The streamline based GTTI (Generalized Travel Time Inversion) technique

(discussed later) is able to perform local changes. It alters the permeability inside the model to minimize the water production data time misfit. But its functionality doesn't extend to modifying the overall energy balance.

We thus have two competing history matching strategies. The first utilizes TDRM principles to work with multiple simple geologic models and screen the reservoir uncertainty through them. The second is AHM which emphasizes the calibration of a single model using a sequential process to screen and optimize the parameter values to minimize misfit with historical data. However, a single calibrated model cannot adequately explore subsurface uncertainty, adding uncontrolled risk when making development decisions. This study is an attempt to explore how working with multiple models improves on the performance of AHM techniques and helps us in understanding the reservoir characteristics. In this study, I shall apply both AHM techniques and TDRM principles on a field case. Following TDRM, the reservoir models developed are initially simplistic in nature, but cover multiple geologic scenarios. These models are built without sophisticated geological modeling expertise. This study can also anchor a detailed geological model construction and subsequent AHM analysis. This study also highlights a structured approach to a reservoir history matching study in which we sequentially explore uncertainty, screen possible geologic scenarios, calibrate dynamic parameters and then extend the subsurface uncertainties. In this approach, I combine the best elements of TDRM and conventional AHM.

The field data has been provided by a major oil and gas producer for research and education purposes. Some information in this study has been picked from the literature

related to the specific field. I have refrained from citing the references to the literature for reasons of confidentiality.

2. THEORY

The theory related to the two techniques I am using in the Assisted History Matching methodology for this study is discussed in this section.

2.1 EVOLUTION STRATEGY

Evolution Strategy (ES) is a subclass of evolutionary algorithms. ES was primarily developed by Rechenberg (1973) and Schwefel (1975) to solve complex parameter optimization problems. It works on the principle of Natural Evolution. The ES works by randomly creating some pre-determined sets of parameters (λ). The value of a fitness function is then found by running the simulation for each set. Based on the fitness function, μ ($\mu < \lambda$) set of experiments are selected and they are recombined to form λ new parameter sets called children. The parameter vectors contained in these sets are then modified by mutation. The parent population is then selected anew from the experiments run using new produced children sets. The process is continued until the fitness function can no longer be improved or the algorithm has reached the maximum number of iterations. The theory given below for recombination and mutation process involved in ES is referred from Back (1996) and Back et al. (1997).

2.1.1 Recombination

Recombination creates λ children from the μ individuals selected as parent population ($\lambda > \mu$). This operator can select β ($1 \leq \beta \leq \mu$) individuals to evolve a single

offspring. The recombination operators in Evolution Strategy can be classified as either discrete recombination or intermediate recombination. In discrete recombination, the vector component in the offspring is copied from either of the parent individual at random. In intermediate recombination, the vector component is the arithmetic mean of the parent's component, which can be generalized by assigning weight factors other than 0.5 to each component.

2.1.2 Mutation

The individuals in ES consist of two components – object variables (uncertainty parameters) and strategy parameters. For an individual $\vec{a} = (\vec{x}, \vec{\sigma}) \in I$

$\vec{x}$ is the n-dimensional object variable. Each individual $\vec{a}$ thus may contain 1 to n different standard deviations σ_i ($1 \leq i \leq$ n) where n is the number of uncertainty parameters.

Given an objective function $f : IR^n \longrightarrow IR$ for n-dimensional object parameter vectors $\vec{x} \in IR^n$, for an individual $\vec{a} \in I$, the fitness function is given by function ϕ which is similar to f.

$$\phi(\vec{a}) = f(\vec{x})$$

The components other than object variable component $\vec{x}$ for individual $\vec{a}$ are called strategic parameters for the individual $\vec{a}$. These components govern the mutation process for the offspring obtained from recombination. The mutation is performed as –

$$x_i' = x_i + \sigma_i' . N_i(0,1)$$

where $N_i(0,1)$ is random value from a standard normal distribution. The σ_i' is determined from the following expression –

$$\sigma_i' = \sigma_i \,.\exp[\,\tau'.N(0,1) + \tau\,.N_i(0,1)]$$

where $\tau' \propto \left(\sqrt{2n}\,\right)^{-1}$ and $\tau \propto \left(\sqrt{2\sqrt{n}}\,\right)^{-1}$. The proportionality constants are normally one for both $\tau' and\, \tau$. The notation $N(0,1)$ refers to a single realization whereas $N_i(0,1)$ refers to a new realization for each object variable component.

2.2 GENERALIZED TRAVEL TIME INVERSION

Wu and Datta-Gupta (2002) proposed a streamline based approach called generalized travel time inversion (GTTI) to reconcile the production data with the geological model. This method was an extension of the streamline based fluid flow travel time inversion method of Vasco et al. (1999). The traditional amplitude matching techniques works by minimizing the misfit between prediction and data, versus time. The data here corresponds to the pressure data or production data. However, this method is highly non-linear, computational intensive and will have difficulties in convergence if the initial model is far from the correct one. The travel time inversion method is an improvement over amplitude method based on aligning the model prediction at a particular time with the production history. The inversion is implemented using a streamline based method which modifies the properties in the model. The travel time could be either water breakthrough time or a peak in the production history. This method greatly reduces the non-linearity in the misfit objective function and thus gives faster convergence. Typically, after completing the travel time inversion, amplitude matching

is used to fine tune the match to the entire production history. The GTTI also works like the travel time inversion; however here the prediction is aligned with production over all time until the cross correlation between prediction and field response is maximized. Though it doesn't utilize the concept of conventional amplitude matching; the approach near the solution is analogous to amplitude inversion (He et al. 2001). This technique was proposed in the context of wave equation travel time tomography (Luo and Schuster 1991).

3. METHODOLOGY

3.1 OVERVIEW

This project involves an integrated seismic to simulation study, wherein I interpret the seismic data, assemble the geological information, and perform petrophysical log evaluation along with well test data calibration. The interpreted seismic data is used to build the structural model of the field and thus set up the grid model. Based on the performed log interpretation, the petrophysical properties were distributed inside the grid model. The ensemble of static models thus obtained is taken through the AHM workflow in which sensitivity analysis is used to determine the most important dynamic parameters among several others that affect the history match. These parameters govern the large scale changes in the reservoir description and are optimized using the Evolutionary Strategy Algorithm. Finally, the streamline based techniques are used for local modifications to match the water cut well by well.

In the history matching workflow, I first identify the key parameters that most affect the history match using a sensitivity method. This method creates experiments by varying one uncertainty parameter at a time to either its lower or upper limit, which is called a “one factorial” design method. If we have ‘n’ uncertainty parameters, the total experiments including the base case will be ‘2n+1’. The base case is defined as the experiment using the initial uncertainty parameter values as input. The impact of different parameters on the base case is displayed in a tornado diagram computed using the upper and lower limits for each parameter. The Evolution Strategy is then used as a

global search algorithm for the key parameters identified from the sensitivity analysis. Thereafter, in order to improve the water cut match well wise, the streamline based approach is used to make localized changes in the model. . The results obtained from different starting models are then compared to understand the performance of AHM methodology. This also led to a few general observations on the history matching process which shall be discussed in the discussions and conclusion section.

3.2 PROCEDURE

For this purpose, the field seismic data was first interpreted to pick the horizons as well as the faults present in the reservoir using Seisvision in the Landmark Geographix suite. There are three sand units in this reservoir which are referred to as M1, M2, and M3 sands. The M2 sand is the major producing unit. The seismic trend maps were prepared in GeoAtlas and the petrophysical evaluation in Prizm, both in the Geographix suite. Based on this analysis, I constructed the 3D geologic model using Roxar's Reservoir Modeling System (RMS) application. The dynamic predictions were then performed using Schlumberger's Eclipse 100 simulator. I used the MEPO application to run the parameter sensitivities to get the energy match. After that, the water cut history match is optimized using the GTTI technique in the in-house developed Destiny application. I then analyzed the quality of the history match and the reservoir description achieved.

4. PETROPHYSICAL ANALYSIS

4.1 INTRODUCTION

The petrophysical analysis of the field was done to come up with a valid log interpretation model. Our analysis included determination of lithology, shale volume, porosity, water saturation, permeability, net sand and the fluid contacts. We had log data available for all the wells which consisted of Gamma Ray (GR), Neutron Porosity, Bulk Density, Deep Resistivity, Shallow Resistivity, Caliper and Sonic measurements. Moreover special core analysis, description, and photos were available for four wells that were cored conventionally. Sidewall core data was also provided for a few wells.

4.2 SHIFTING OF DATA

The core data was depth matched with the log data. The core porosity was matched with the density porosity for this purpose. I also used core permeability as another criterion so that the high core permeability matches with low gamma rays and high density porosity (which indicates clean sand). Fig. 1 shows the match achieved between core porosity and density porosity after depth shifting.

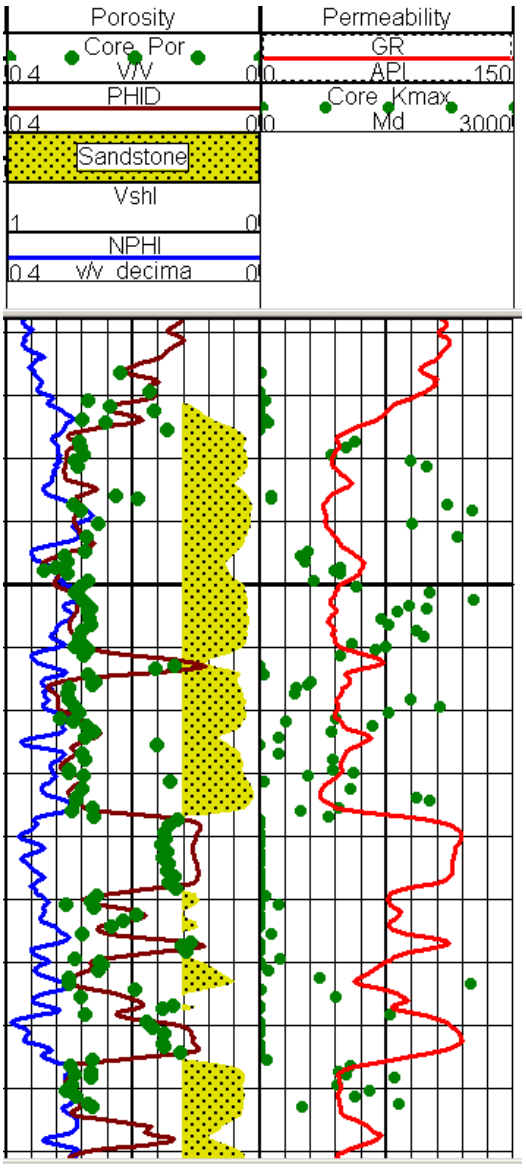

Fig. 1- Core Porosity and Density Porosity match

4.3 LITHOLOGY

I used Density-neutron cross plots to determine the following:

a) Lithology

b) Shale effect

Fig. 2 shows the formation lithology of the sand interval of M2 stratigraphic package in a well as sandstone (matrix density of 2.65g/cc). Shale is characterized by high neutron porosity. Shale effect is prevalent in M3 due to bound water with shale bulk density of 2.5 g/cc (Fig. 3). From the given core description of a well, 80% of the channel sand is quartz, which confirms the reservoir is sandstone.

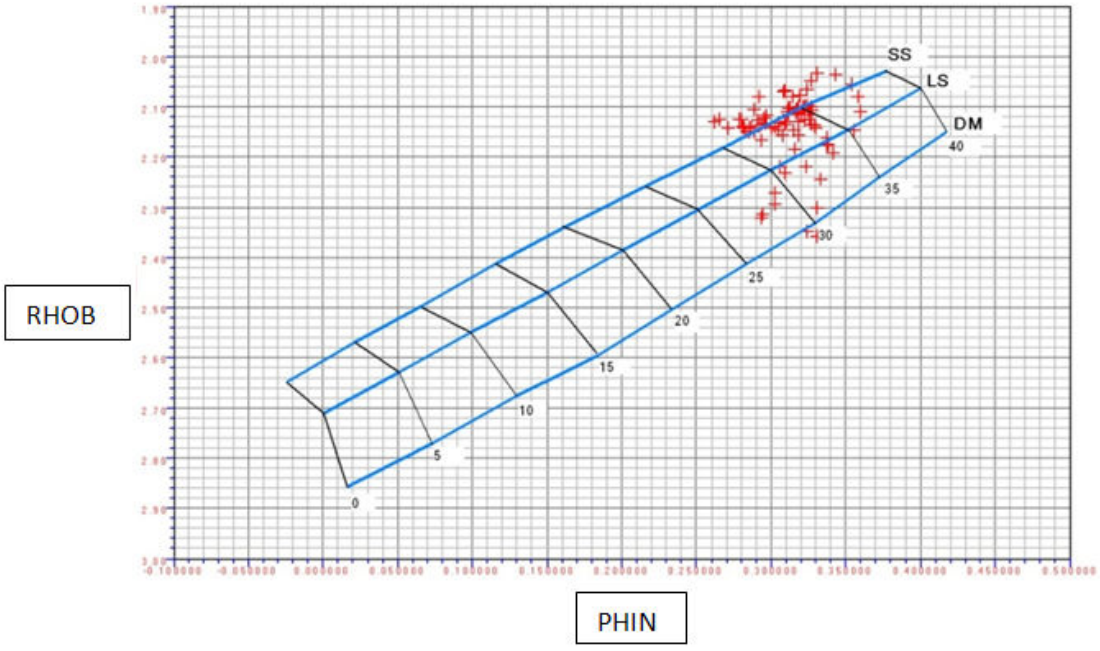

Fig. 2 - Neutron Density Crossplot of M2 Sand

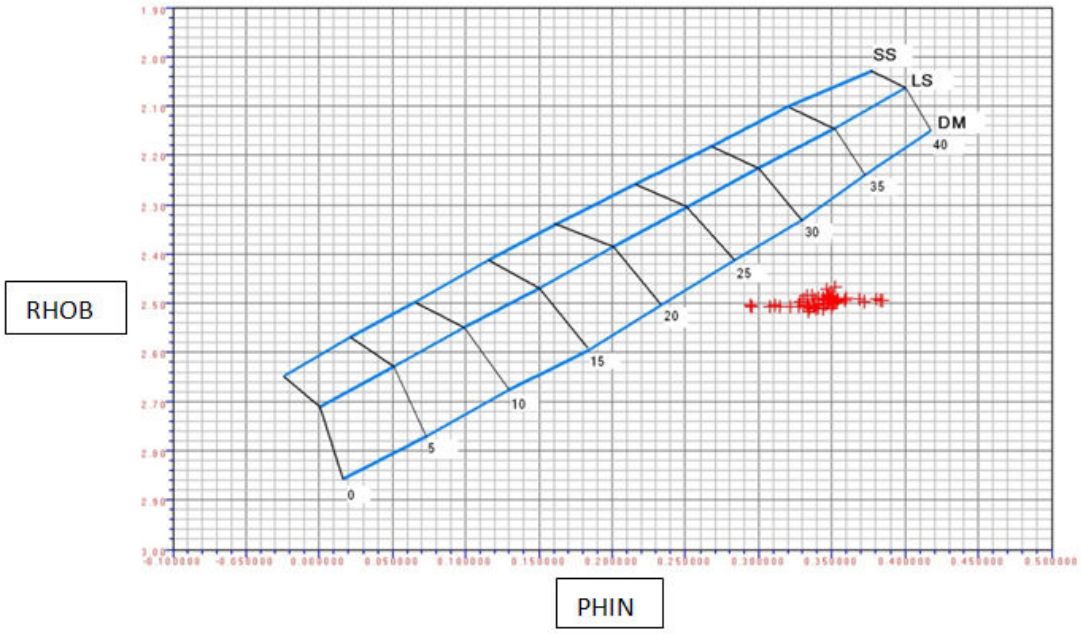

Fig. 3 - Shale Effect on Neutron Density Crossplot of M3 Sand

4.4 SHALE VOLUME

Shale volume is an important parameter that has significant effect on many other petrophysical parameters such as porosity, permeability and water saturation. It is also used in lithology identification and facies classification. Since the spontaneous potential (SP) log was not available, I used the GR log to determine shale volume. Sand and shale base lines were identified on the gamma ray log in order to select GR minimum and maximum values which came out to be 30 API and 120 API, respectively. The shale index was calculated using Eq. 1. The shale index provides a linear relationship of Vsh with Gamma Ray count. However, non-linear relationships are more optimistic indicator of Vsh (≤ Ish). There have been many relationships suggested of which Clavier et al. (1971) and Steiber (1970) are most commonly used.

$$I_{sh} = \frac{GR - GR_{\min}}{GR_{\max} - GR_{\min}} \text{.....} Eq.1$$

$$V_{sh} = 1.7 - (3.38 - (I_{sh} + 0.7)^2)^{0.5} \text{.....} Eq.2 \quad (Clavier)$$

$$V_{sh} = 0.5 * (I_{sh} / (1.5 - I_{sh})) \text{.....} Eq.3 \quad (Steiber)$$

I used the minimum estimate among these three as the V_{sh} estimation.

4.5 POROSITY

I calculated the density porosity from the expression in Eq. 4. The matrix density of 2.65 g/cm3 was used from the neutron-density cross plot. I used fluid density of 0.85 g/cm3 in eq. 4, since the wells were drilled with oil based mud.

$$\phi_D = \frac{\rho_{ma} - \rho_b}{\rho_{ma} - \rho_{fl}} \text{.....} Eq.4$$

The neutron porosity is not accurate because of the shale effect in shaly sand. The neutron porosity is greater than the density porosity in shaly sand zones and therefore does not match the core porosity as well as the density porosity. The core photos (Fig. 4) show laminated shales in the reservoir. Since laminated shale does not decrease the interconnected pore spaces as dispersed shale does, the correlation $\phi_E = \phi(1 - V_{sh})$ is not used in this study. The neutron porosity was ignored in the model as the core porosity matched well with density porosity as seen in the crossplot (Fig. 5).

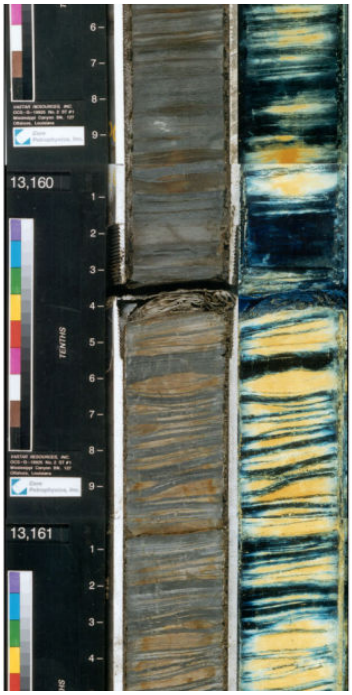

Fig. 4 - Core Picture shows Laminated Shale

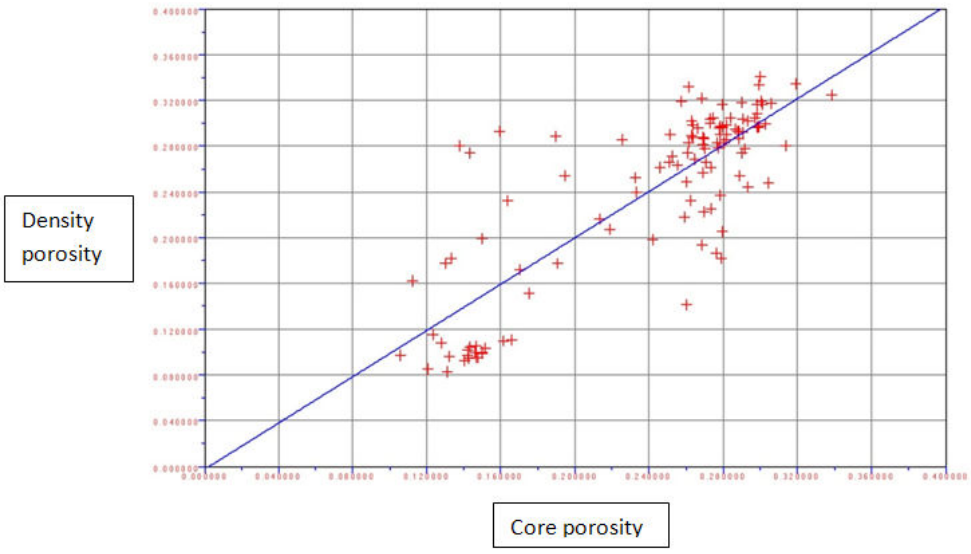

Fig. 5 - Core Porosity – Density Porosity Crossplot

4.6 PERMEABILITY

4.6.1 Deterministic Approach

Fig. 6 shows the permeability – porosity plot of clean sand (blue dots), laminated sand (red dots), shaly sand (green dots) and shale (purple crosses) based on the core data description. Core data with permeability less than 10 md were excluded from the porosity – permeability relationship because of high shale content in those data.

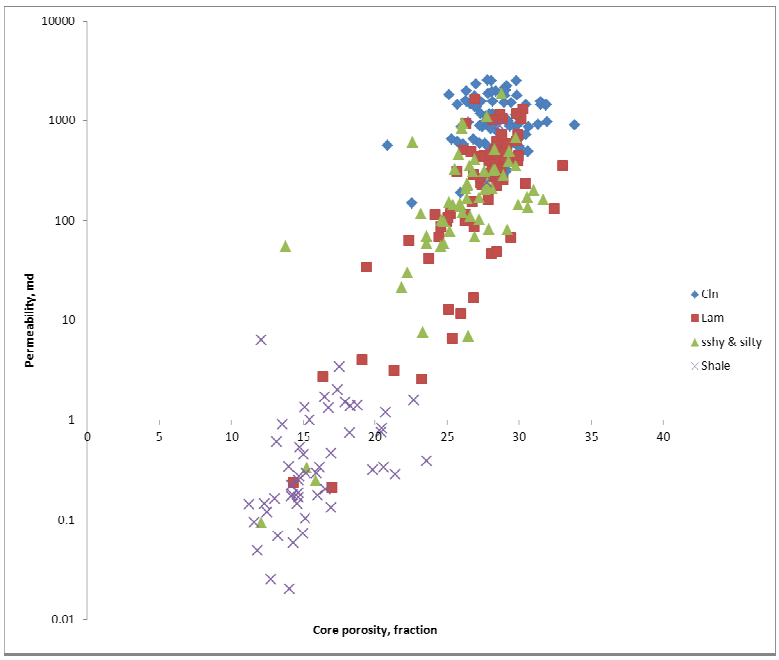

Fig. 6 - Core Permeability – Core Porosity Crossplot

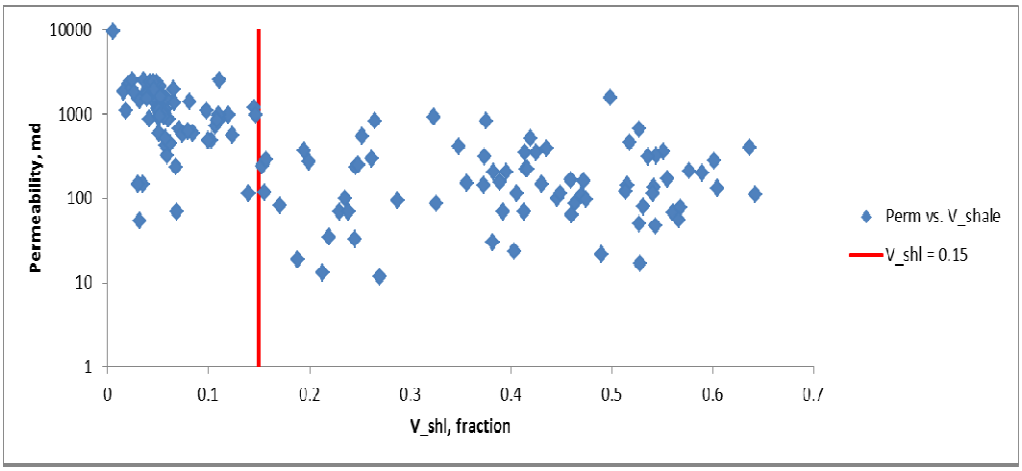

Fig. 7 - Core Permeability – V_{sh} Crossplot

Based on the permeability – V_{sh} crossplot (Fig. 7), two different behaviors were observed. When V_{sh} is less than 15%, permeability is high and a negative relationship between permeability and V_{sh} was observed. The sandstones with less than 15% V_{sh} are called as "clean sand". When V_{sh} is higher than 15%, most of the core permeability is low (less than 1000 md) and no relationship between permeability and V_{sh} is observed. These sandstones are called as "shaly sand". The permeability – porosity plot of the "clean sand" and "shaly sand" is shown in Fig. 8.

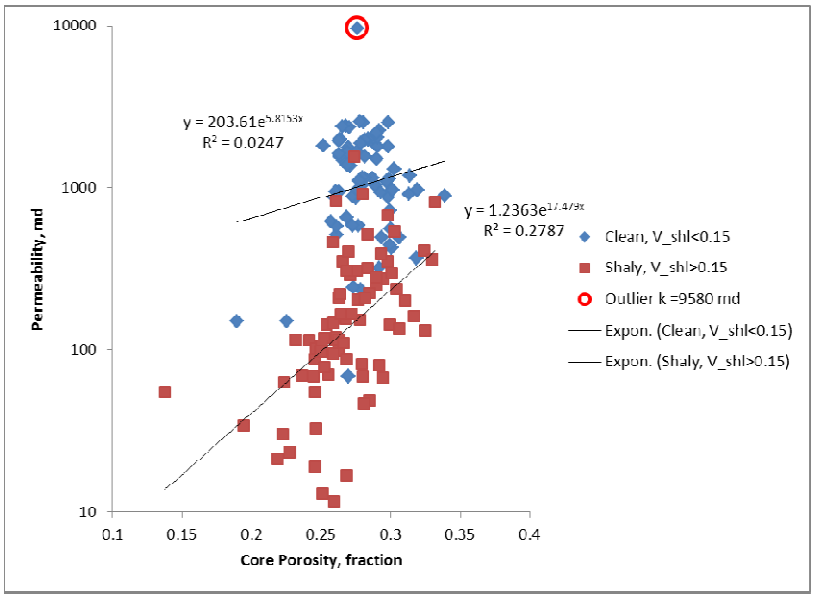

Fig. 8 - Core Permeability – Core Porosity Crossplot with V_{sh} as filter

$$k = \exp(2.6027 + 18 \times \phi_D - 11.734 \times V_{sh}) \quad when\ V_{sh} < 15\%$$

$$k = 1.2363 \times \exp(17.479 \times \phi_D) \quad when\ V_{sh} > 15\%$$

The "shaly sand" correlation and the "clean sand" correlation with various V_{sh} values are plotted on semi-log porosity-permeability scale in Fig. 9. All of the relationships have different slopes (1.8 for "clean sand" and 17.5 for "shaly sand") and intercepts. Table 1 shows the calculated permeability for different shale volumes at 30% porosity.

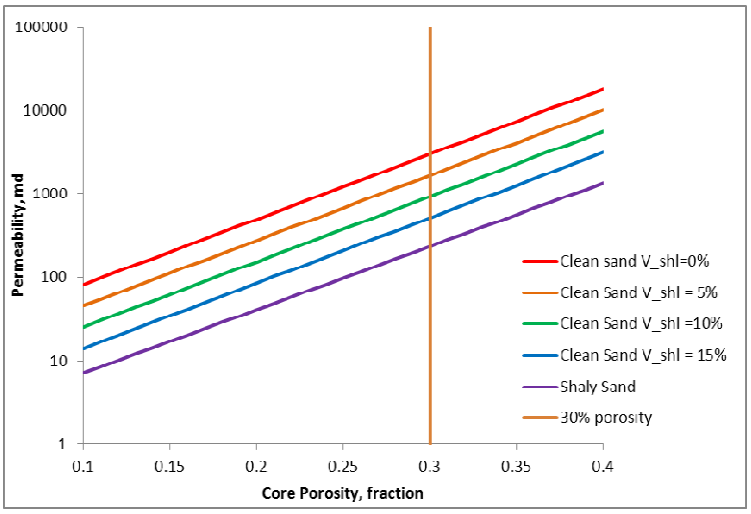

Fig. 9 - Core Permeability – Core Porosity Crossplot for different V_{sh}

Table 1 - Permeability Prediction at 30% Porosity for different V_{sh}

V_{shl}	k,md
0%	2989
5%	1662
10%	925
15%	514
Shaly	234

In general, I obtained good agreement between core permeability and log permeability, core porosity and log porosity as shown in Fig. 10 and Fig. 11.

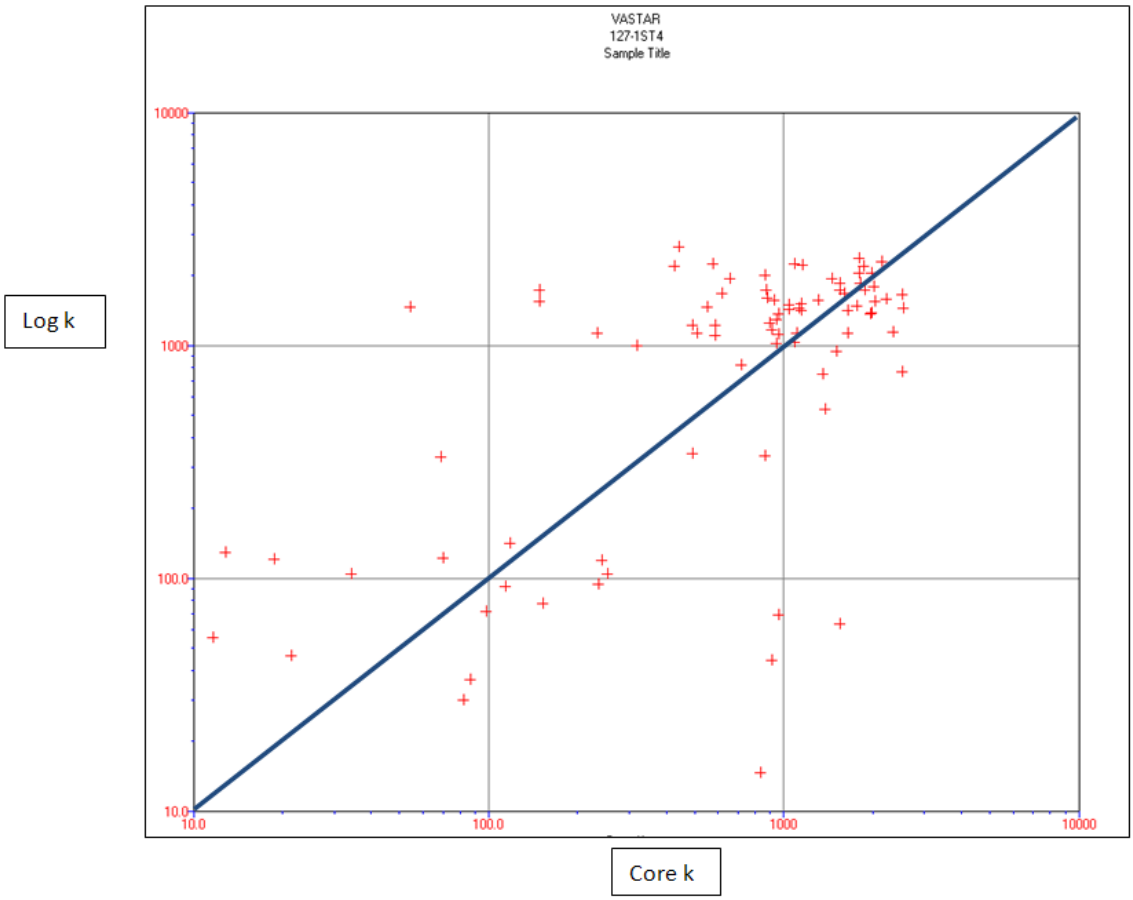

Fig. 10 - Log Permeability – Core Permeability Crossplot

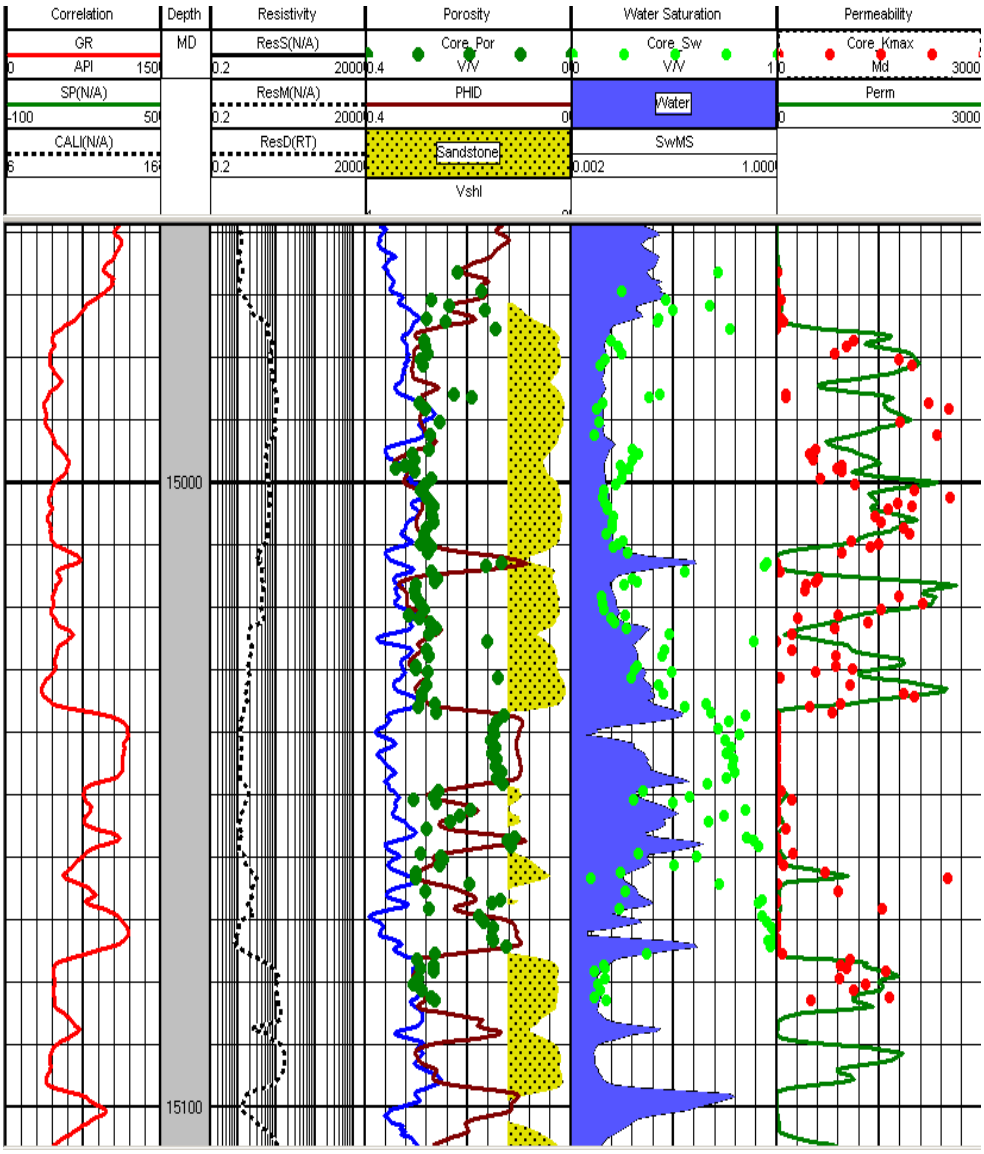

Fig. 11 - Match between Core Measurements and Log Calculations

4.6.2 Stochastic Approach

I used another method to calculate permeability based on the cloud transform (Fig. 12). The core permeability was plotted against the core porosity for a given core data on a semilog graph. I then evaluated the permeability based on the best fit line

equation. To the calculated value, a random error was added which was based on the standard deviation observed for the error between calculated value and the actual core permeability. To accomplish this, the inverse of the standard normal distribution for a random generated probability and standard deviation as calculated previously was added as random error.

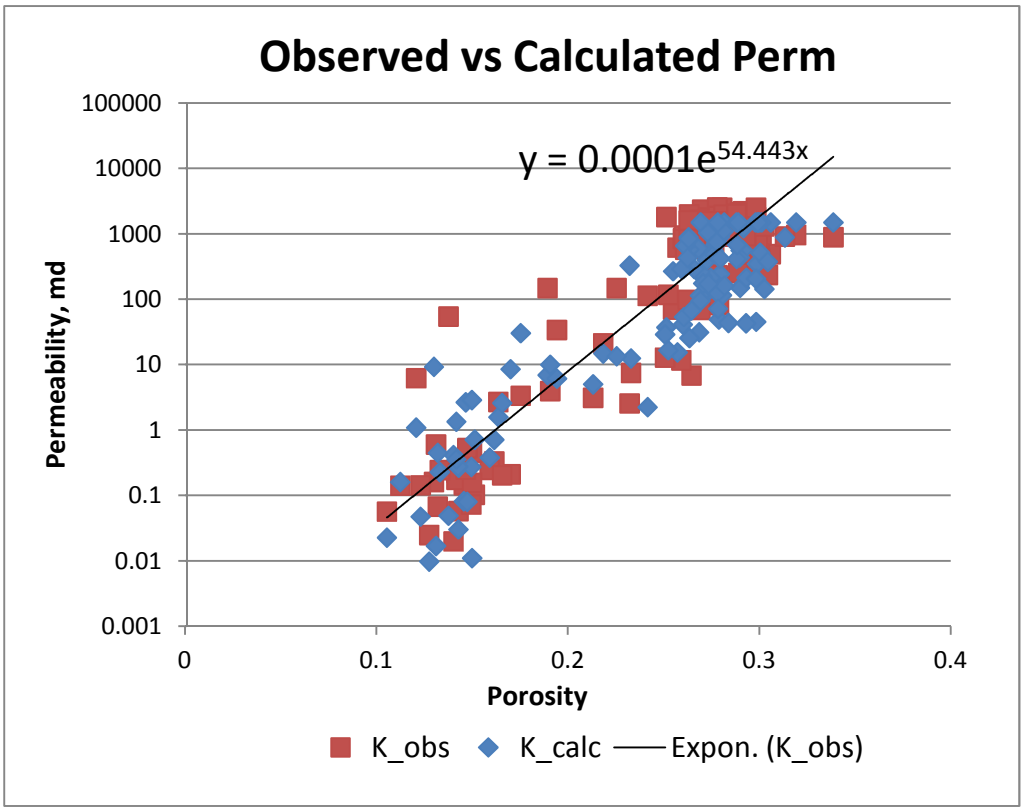

Fig. 12 - Permeability compared from Cloud Transform

4.7 NET SAND DETERMINATION

Net sand is defined as that part of the reservoir which meets the shale volume cutoff and porosity cut off. I determined the porosity cutoff by plotting the equivalent pore throat diameter $\left(\frac{k}{\emptyset}\right)^{0.5}$ versus effective porosity (Worthington 2008) for the M sand. It was selected as 15% where the pore throat diameter starts rising on the plot (Fig. 13).

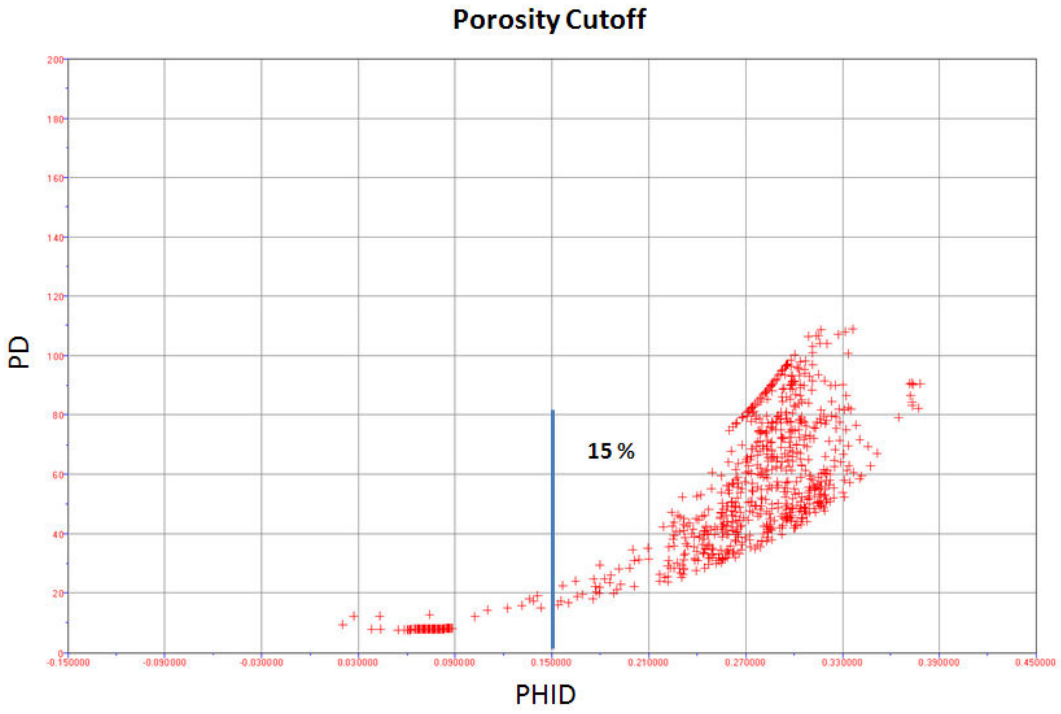

Fig. 13 - Plot of PD vs. PHID showing a Porosity cutoff

The V_{sh} cut off was determined from the corresponding porosity cutoff value (Fig. 14).

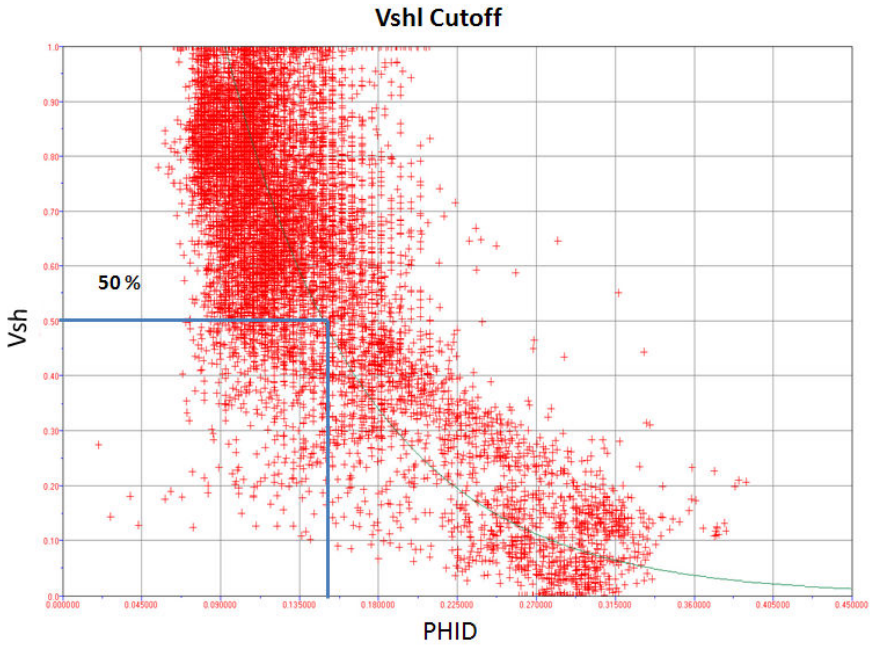

Fig. 14 - V_{sh} vs. PHID showing a V_{sh} cutoff

4.8 FLUID CONTACT

The literature review on the field mentioned the oil-water contact was not penetrated in any well and is assumed to be at approximately 14,300 ft TVDSS in the main part of the reservoir. I also corroborated this from a well log (Fig. 15), which substantiates that the OWC is near about 14,300 ft TVD.

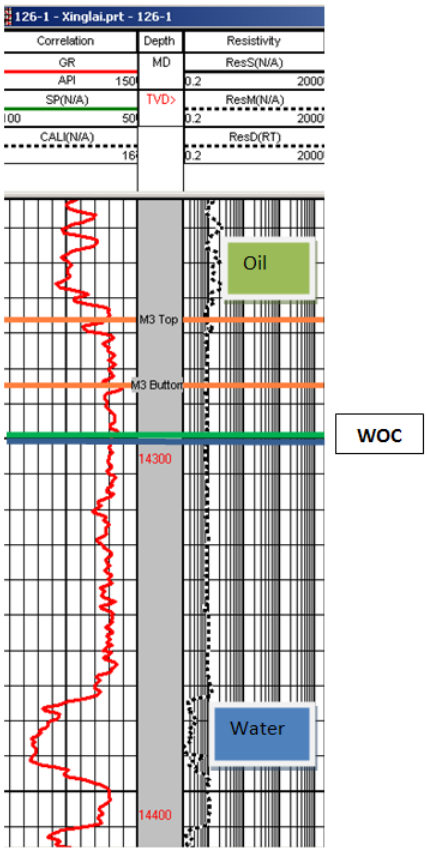

Fig. 15- OWC inferred in a Well Log

5. PRESSURE TRANSIENT ANALYSIS

5.1 METHODOLOGY

Permanent downhole gauges were installed in each of the producing wells. The permanent downhole gauge data consisted of multiple pressure build ups. The longer build ups among them were selected for analysis. I analyzed three build ups in each well to see the effect on permeability and skin during the course of production with one build up taken early and one taken in the late time in the course of production.

5.2 INTERMEDIATE PARAMETERS

The well test analysis requires an average estimate of the following parameters: – porosity, pay zone thickness, formation volume factor, oil viscosity, and total compressibility. I applied the net apparent vertical thickness of the perforation zone in each well for the analysis (Table 2). The wells were first reviewed to identify the sand zones completed. Most of the wells were fully completed in the M2 sand, except for wells A5 and A8. The well radius was the same for all the wells. A common value was used for the formation volume factor and oil viscosity when determined for each well as their reservoir pressure didn't show significant variation. The porosity was taken equal to the average reservoir porosity. The total compressibility was assumed equal to the average rock compressibility (1.38E-5 1/psia) as it is significantly greater than the oil and water compressibility. The values of the parameters as discussed are summarized in Table 3.

Table 2 – Net Pay Zone Thickness for Wells

Thickness, ft									
	A-1	A-2	A-3	A-4	A-5	A-8	A-9	A-6	A-7
M2	85	141	212	168	143	87	120	41.5	86.9
M1						0			
M3						53		8.9	

Table 3 – Parameters used in Well Test Analysis

B	1.3
phi	0.27
visc, cp	0.693
Ct, psi^{-1}	1.38E-05
rw, ft	0.56

5.3 WELL TEST INTERPRETATION

Most of the wells showed channel flow characteristics at late time, while some of the wells were modeled using an intersecting fault model. The modeled match for the build up in two wells, A1 and A2 (Fig. 16 and Fig. 17 respectively), are discussed here. I selected an intersecting fault model to match the derivative response in both the wells. The results for both the wells are summarized in Table 4 and Table 5 respectively.

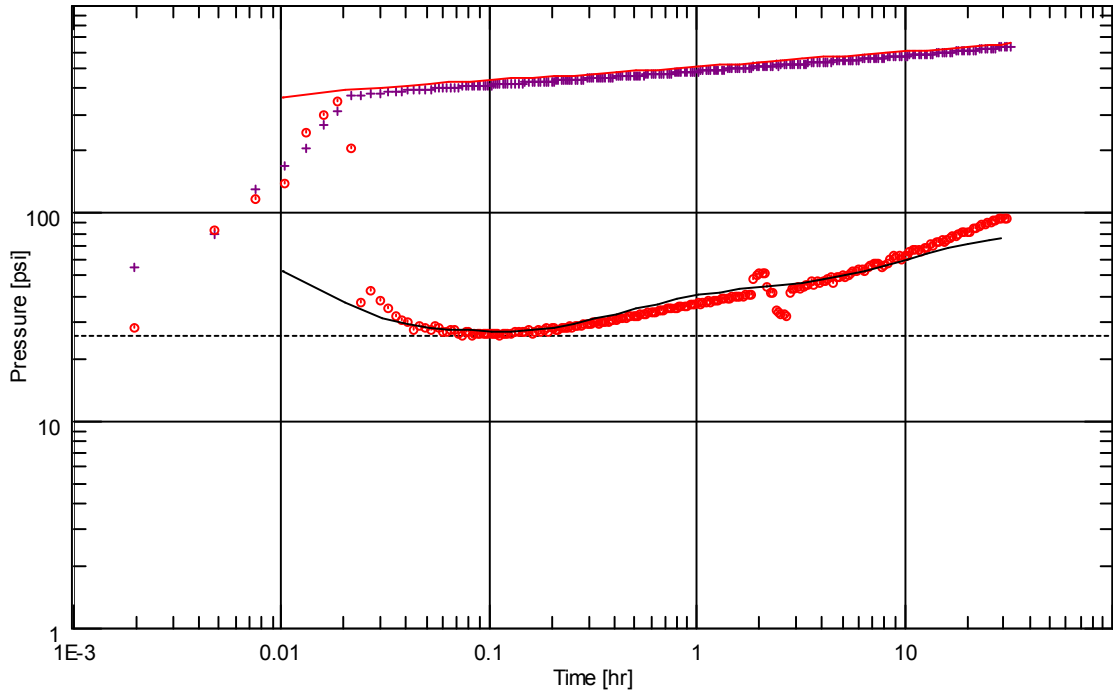

Fig. 16 - Well A1 - Log - Log Diagnostic Plot

Table 4 – Well A1 Results

Model Option	Standard Model
Well	Vertical
Reservoir	Homogeneous
Boundary	Intersecting faults - Any angle
TMatch	2990 [hr]-1
PMatch	0.0196 [psia]-1
C	0.00692 bbl/psi
Total Skin	3.3
k.h, total	48600 md.ft
k, average	572 md
Pi	6932.85 psia
C	0.00692 bbl/psi
Skin	3.3
Pi	6932.85 psia
k.h	48600 md.ft
k	572 md
L1 - No flow	170 ft
L2 - No flow	830 ft
Angle	98.2029 °
Delta P (Total Skin)	168.301 psia
Delta P Ratio (Total Skin)	0.256403 Fraction

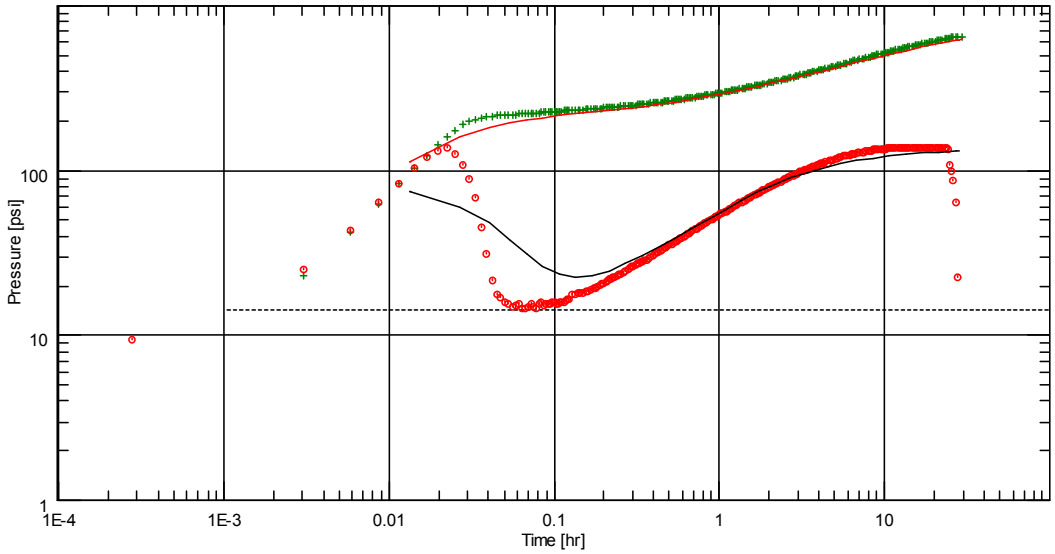

Fig. 17 - Well A2 - Log – Log Diagnostic Plot

Table 5 – Well A2 Results

Model Option	Standard Model
Well	Vertical
Reservoir	Homogeneous
Boundary	Intersecting faults - Any angle
TMatch	477 [hr]-1
PMatch	0.0347 [psia]-1
C	0.0489 bbl/psi
Total Skin	2.5
k.h, total	54800 md.ft
k, average	388 md
Pi	6636.49 psia
C	0.0489 bbl/psi
Skin	2.5
Pi	6636.49 psia
k.h	54800 md.ft
k	388 md
L1 - No flow	105 ft
L2 - No flow	102 ft
Angle	37.7372 °
Delta P (Total Skin)	72.0288 psia
Delta P Ratio (Total Skin)	0.114354 Fraction

The results for different wells are summarized in Table 6.

5.4 RESULTS SUMMARY

Table 6 – Individual Well Test Results

Well	Permanent	Model	Distances, ft	K	Avg Pr	Skin
A1	BU 12/13/2002	intersecting fault	170 / 830	572	6933	3.3
	BU 1/22/2003	intersecting fault	170 / 830	572	6820	2.5
	BU 5/23/2003	intersecting fault	234 / 1146	488	6318	1.22
A2	BU 1/22/2003	intersecting fault	104 / 100.5	380	6658	2.51
	BU 2/12/2003	intersecting fault	102 / 100	371	6502	2.12
	BU 5/1/2003	intersecting fault	102 / 100	371	6060	1.2
A3	BU 11/13/2003	intersecting fault	155 / 481	461	6402	2.92
A4	BU 2/12/2003	radial composite		351	6564	7
	BU 5/24/2003	radial composite, one fault	1200	277	6085	6.23
A5	BU 3/21/2003	parallel fault	280 / 293	413	6985	3.2
	BU 5/1/2003	parallel fault	295 / 309	402	7153	3
	BU 11/13/2003	parallel fault	305 / 319	391	7187	7
A-8	BU 5/19/2003	parallel fault	101 / 463	419	5913	0.171
	BU 10/13/2004	parallel fault	103 / 472	381	5913	0.152
A-9	BU 11/13/2003	parallel fault	162 / 164	239	7929	0
	BU 9/13/2004	parallel fault	175 / 177	224	8824	2

5.5 PTA OBSERVATIONS

Our model selects parallel faults for well A5 and A8. Their location is in the midst of a channel trend as visualized in the seismic RMS amplitude map of the M2 sand in figure on Page 45. The parallel faults represent the channel boundaries in the reservoir as the reservoir is deposited in a channel levee depositional system. The width of the

channel can be estimated from the distances between the faults boundaries which vary from 800-1500 ft.

The permeability as expected decreases in later build ups as the effective permeability to oil will decrease as oil saturation decreases with respect to time. The skin doesn't show any specific trend. It decreases with time in wells A1 & A4; remains almost the same in wells A2 & A8; and increases in well A5.

There is uncertainty associated with these results. The derivative curve could be matched using other boundary models and reservoir models also, but I selected the model which documents the field geology. Also, the intermediate well test input parameters may affect the results. However, these results represent the best estimates of each of these parameters based on the data available. The estimated channel widths will be used to constrain our 3D geologic models. I do not expect these estimates to vary significantly if the well test model is changed.

5.6 LOG AND WELL TEST DATA CALIBRATION

The permeabilities calculated from the well test interpretation and log evaluation are compared in Table 7 and Fig 18.

Table 7 - Well Test and Log Permeability Results

Well	k(PTA), md	k(log), md	Net Reservoir, TVD ft	Net Reservoir, MD ft	Dip (degrees)
A1	572	540	85	124	46.7
A2	388	489	141	160	28.2
A3	461	1096	212	230	22.8
A4	351	383	168	238	45.1
A5	413	719	143	222	49.9
A8	419	323	140	178	38.1
A9	239	731	120	255	61.9

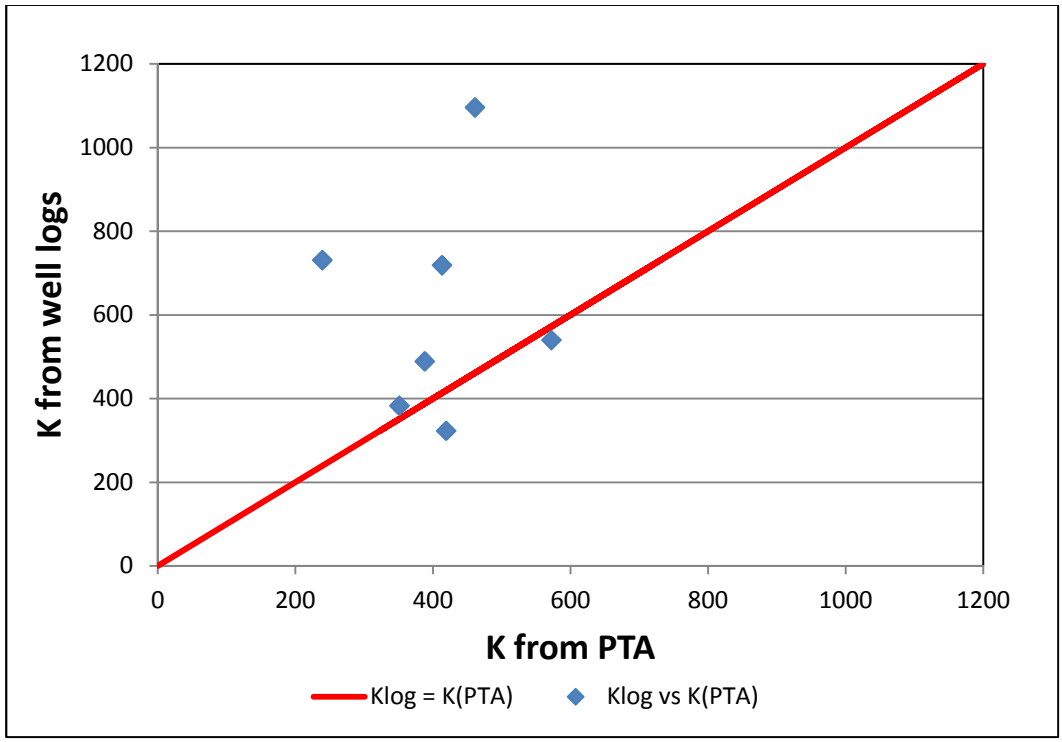

Fig 18 - Well Test and Log Permeability Comparison

The well test permeabilities match well with log calculated values except for well A3, A5, and A9. The uncertainty in well test permeability may be due to the net sand thickness used in the calculation. The thickness I used in the calculation corresponds to the apparent vertical depth in the well trajectory, which doesn't represent actual formation thickness of a dipping stratum. Therefore, the thickness used in the well test interpretation can be referred to as the apparent formation thickness. This would result in low estimation of permeabilities in well test interpretation as is the case in most of the wells.

6. MATERIAL BALANCE ANALYSIS

6.1 DATA PREPARATION

Individual well shut in pressures were averaged to be used in Material Balance (MBAL) history match. Since the permeability across the reservoir is high, the well shut in pressures are assumed to provide reservoir pressure. The available pressure production history from Nov-2002 to May-2008 was provided in MBAL in order to do the history match. The Modified Van Everdingen and Hurst aquifer model was used to fine tune the aquifer strength. The values of the oil in place and aquifer properties obtained were quite reasonable. Table 8 shows the input data used in building the material balance model.

Table 8 - MBAL Input Parameters

Property	Field Data
Reservoir	
Formation Pressure, psig	7081
Temperature, deg F	184
Porosity	0.27
Connate water saturation	0.12
Original oil in place, MMSTB	218
Fluid	
Gas gravity, sp.gravity	0.73
Gas oil ratio, scf/stb	780
Water salinity, sp.gravity	80,000
Hurst-van Everdingen-Modified Aquifer Model	
Outer/Inner Radius ratio	11.5
Encroachment Angle	28°
Aquifer Permeability, md	150

6.2 MATERIAL BALANCE PLOTS AND ANALYSIS

Fig. 19 shows the individual well shut-in pressures. These shut in pressures were average out and used as reservoir pressures. Fig. 20 and Fig. 21 shows the history match obtained after regression in MBAL. The energy plot in Fig. 22 shows the water influx as the dominating drive mechanism in the field.

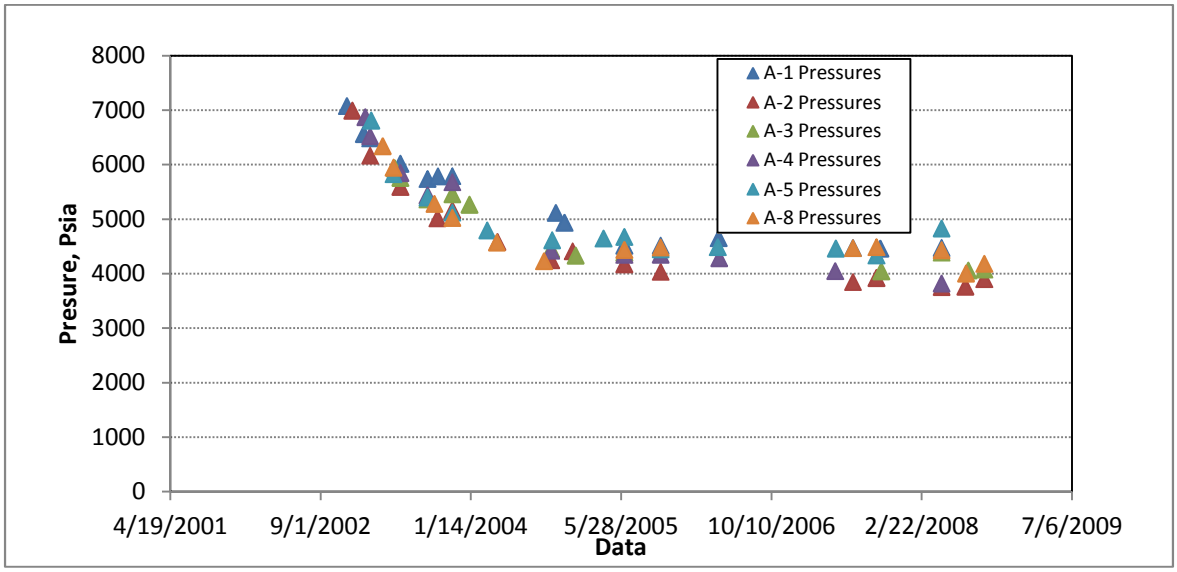

Fig. 19 - Individual Well Pressures

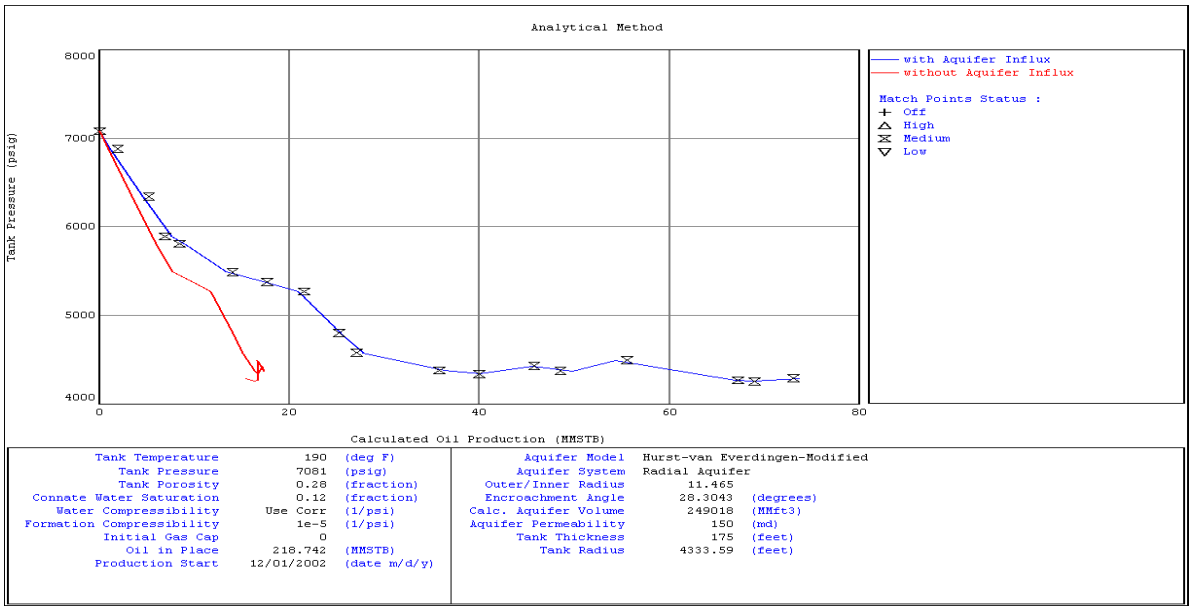

Fig. 20 - MBAL Pressure History Match by Analytical Approach

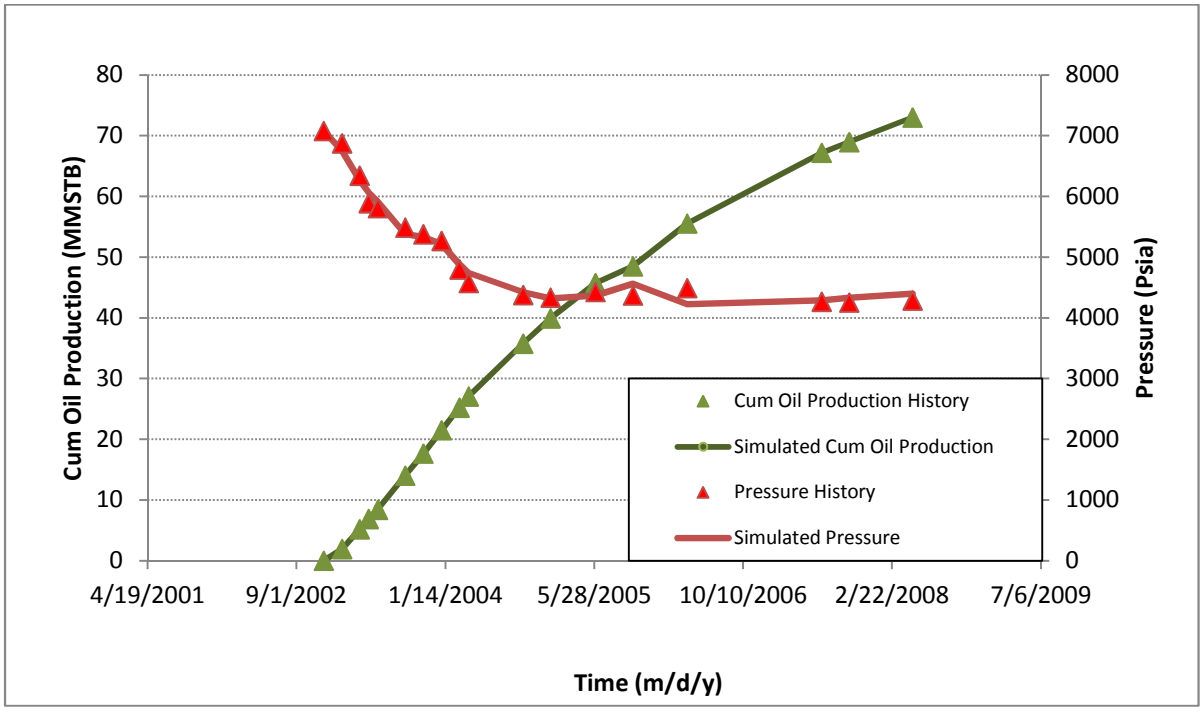

Fig. 21 - Pressures and Cumulative Oil Production

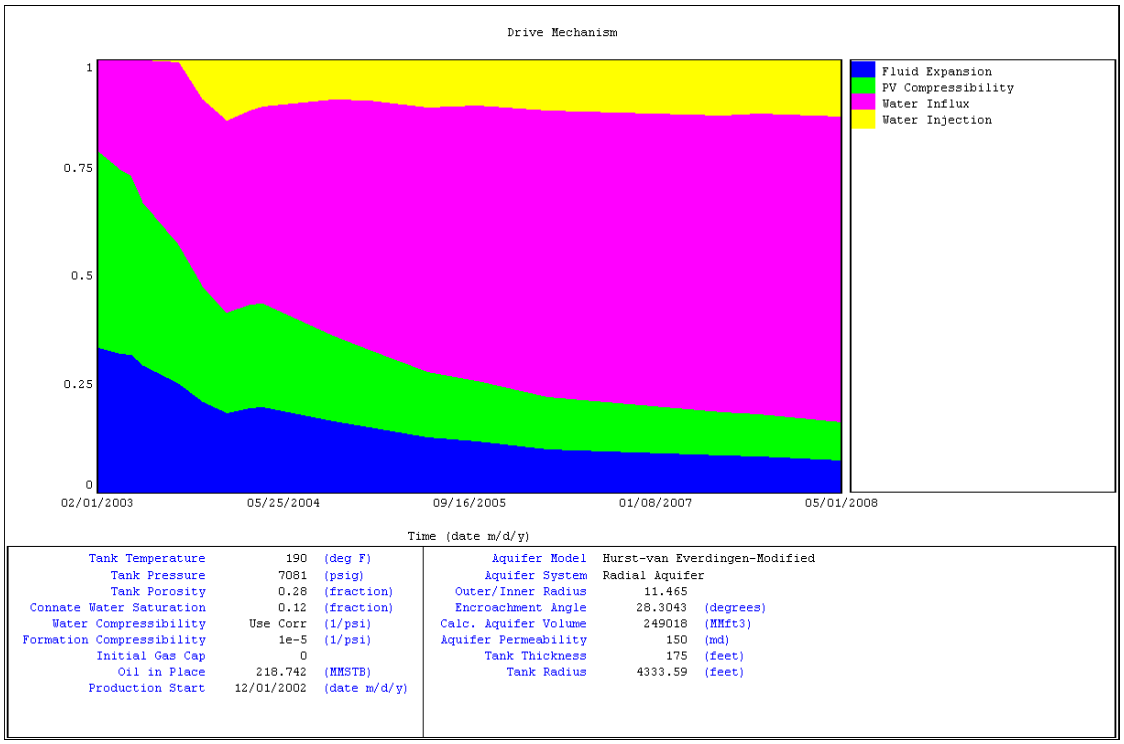

Fig. 22 - Energy Plot

6.3 UNCERTAINTY QUANTIFICATION

For the base case, the aquifer parameters are shown in Table 9. The pressure history for different OOIP cases were matched with encroachment angle values within 25° - 31°. For each attempt, I noted the standard deviation after the regression. Based on this, I generated probability distribution function (Table 10) to quantify uncertainty in OOIP. The probabilistic variation for OOIP is shown in Fig. 23 and the corresponding cumulative distribution curve is shown in Fig. 24**.**

Table 9 – Input Aquifer Parameters

Outer/Inner Radius	11.4
Reservoir Radius	4333 ft
Encroachment Angle	28°
Aquifer Perm	150 md

Table 10 – Standard Deviation and Probability Function

OOIP (MMSTB)	SD	Probability function
170	0.571051	0.027016172
180	0.453579	0.133687837
190	0.364532	0.35189585
200	0.297655	0.633759341
210	0.24835	0.906250643
220	0.214202	1.117844882
230	0.195371	1.23845744
240	0.194045	1.24698246
250	0.2124	1.129319687
260	0.2495	0.899383744
270	0.3021	0.611706297
280	0.367143	0.343077116
290	0.4421	0.153254324

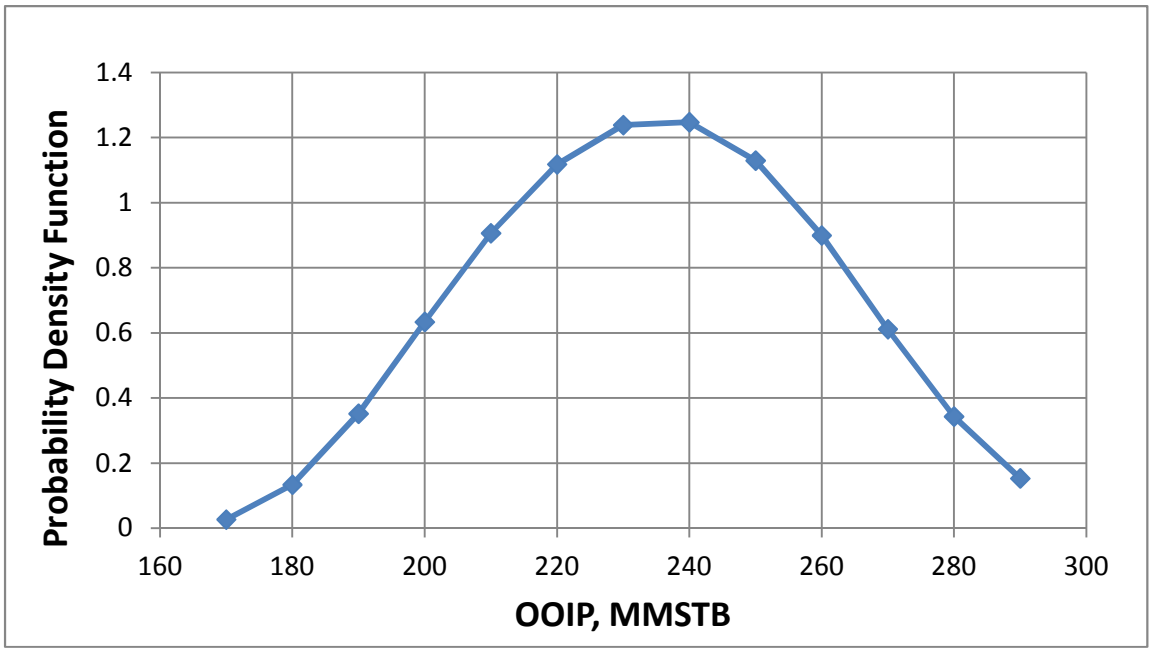

Fig. 23 – Probability Function vs OOIP

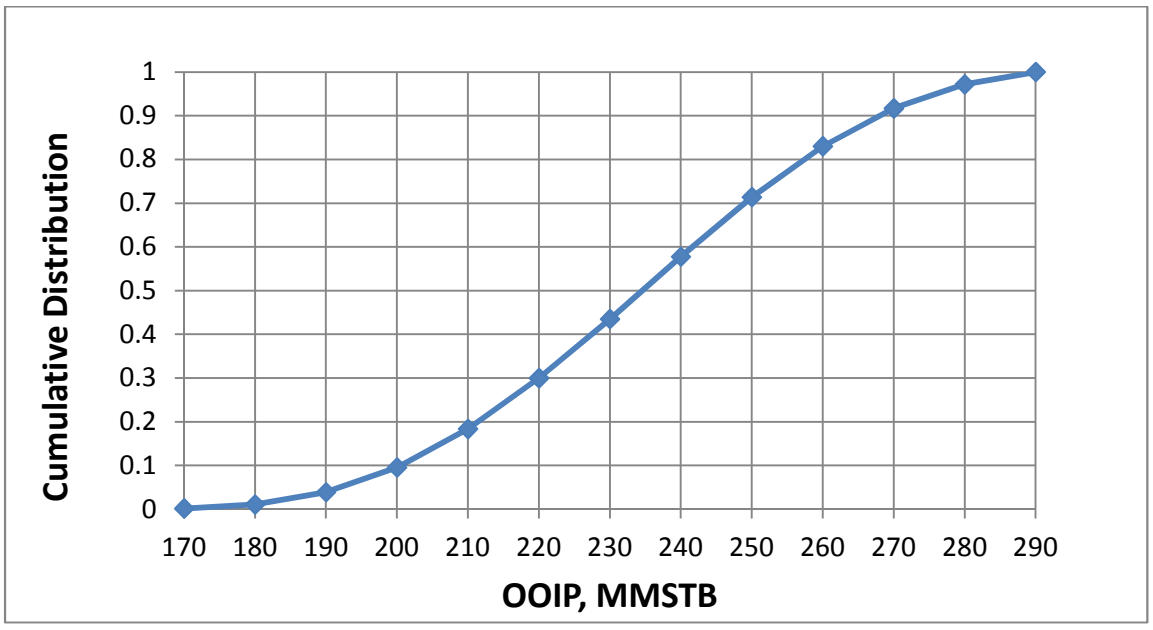

Fig. 24 – CDF vs OOIP

6.4 RESULTS AND INTERPRETATION

The probable material balance oil in place after the uncertainty analysis came out to be around 230 MMSTB. The energy plot indicates that all the four drive mechanisms provide contribution to the reservoir production. The water influx is the dominant drive.

7. STATIC MODEL CONSTRUCTION

7.1 GEOLOGICAL SETTING

The reservoir in the case field produces oil from middle Miocene sands. The field has a combination of structural and stratigraphic traps. Fig. 25 shows the reservoir structure of the field. It is bounded on the northeast by a W.E fault that dips northwards, stratigraphic pinch outs on the eastern and northeastern flanks, and salt dome lying on the western edge (Fig. 26). The OWC is identified at 14300 ft from the literature survey and log evidence. The reservoir rock is composed of sand, silt and shale laminations. Information from the well logs and cores indicate that the reservoir facies can be divided into two main subcategories 1) Clean channel-fill sands, and 2) Low-quality overbank deposits. The low quality overbank deposits can be further subdivided into proximal levee and distal levee facies, which have increasing shale content. Fig. 27 shows the seismic RMS amplitude map in the grid layout. The RMS map was extracted from SeisVision, the seismic interpretation application in Geographix, as point data. This point data was then converted to surface data and laid out on the grid. The bright regions typically correspond to hydrocarbon presence which is generally linked to high NTG areas or channel sands. But there is considerable uncertainty associated with this.

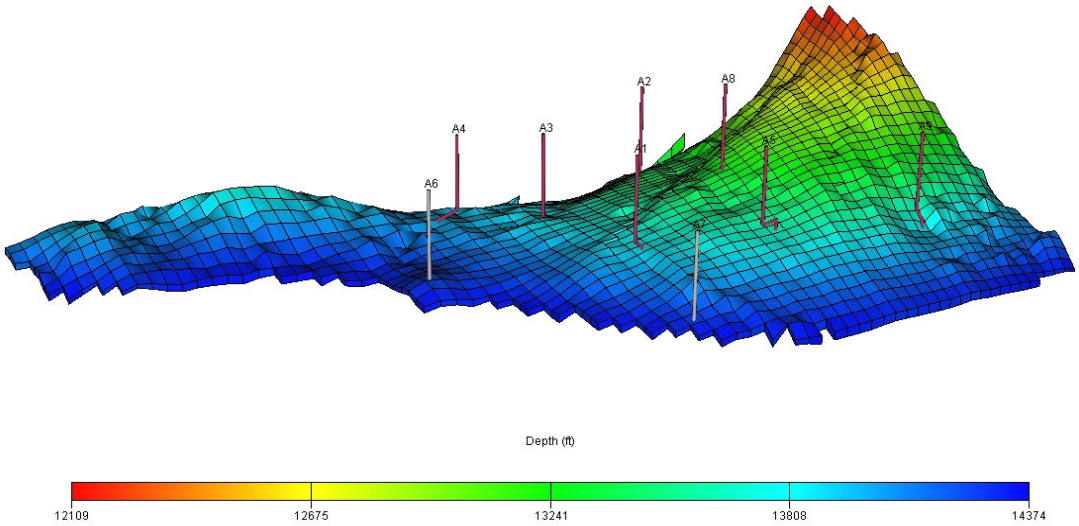

Fig. 25 - Reservoir Structure

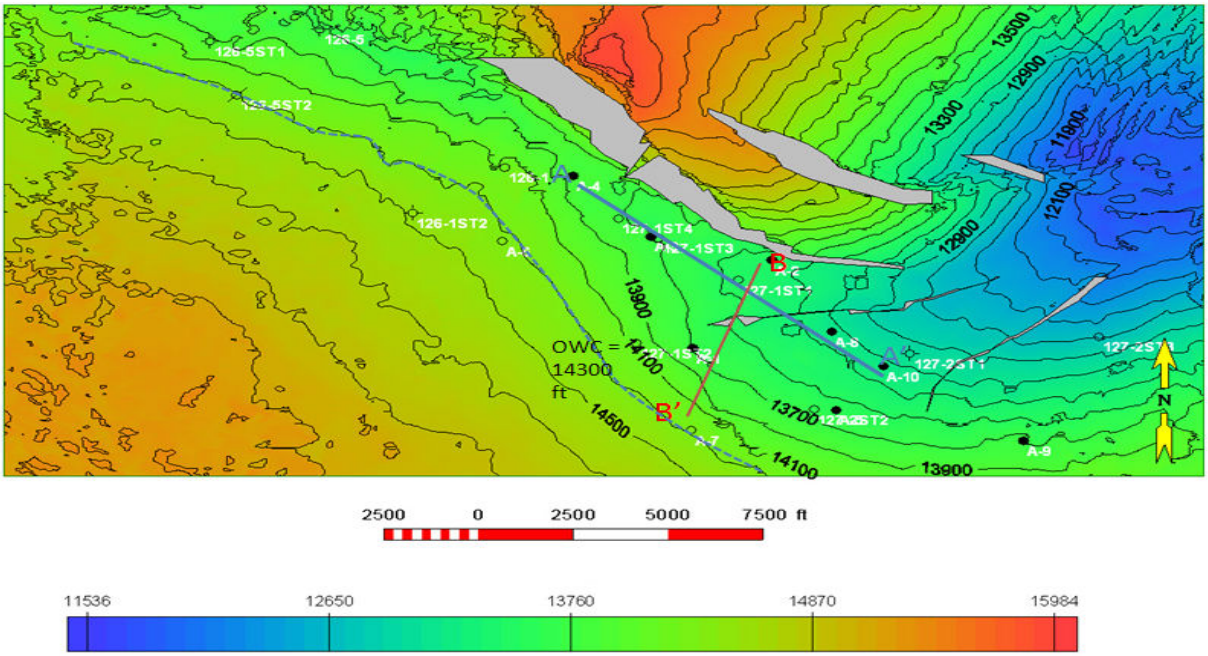

Fig. 26 - M2 Structure Map with Dip (BB') and Strike (AA') Direction

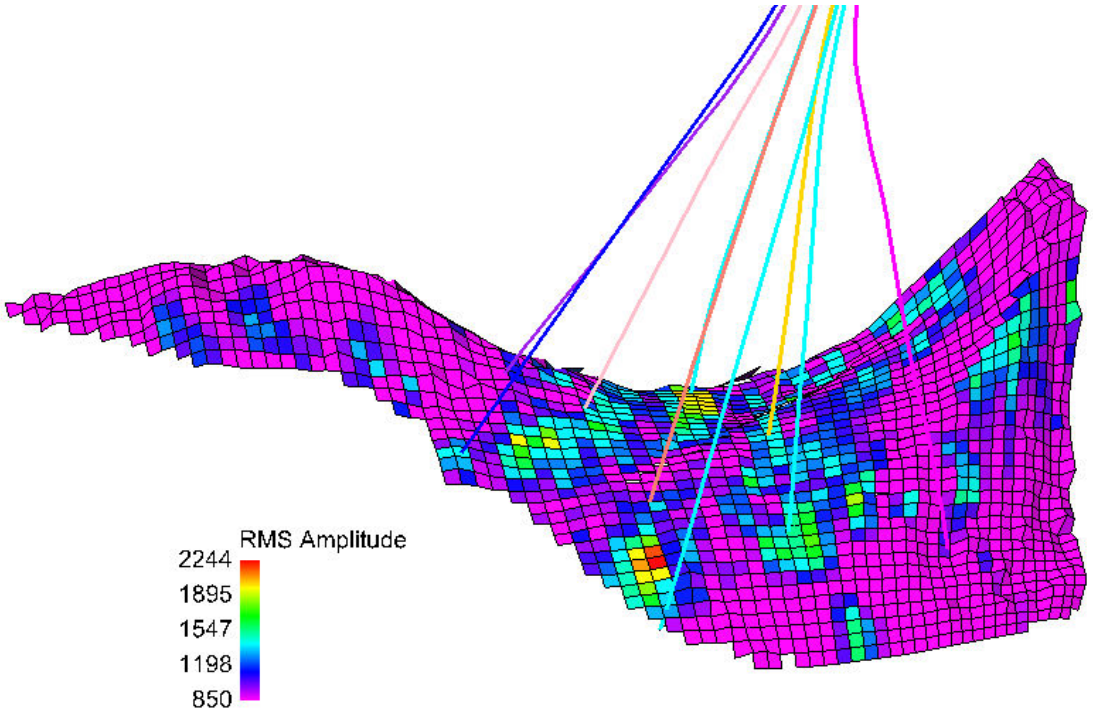

Fig. 27 – Seismic RMS Amplitude Map on the Grid

The seismic data was first interpreted in Seisvison to pick three different sand intervals. The picked horizons and faults files were then imported to the RMS application for geo-modeling. The interpreted logs as well as the deviation survey for each well were also imported. The NTG maps for each sand unit were generated and contoured based on the seismic RMS amplitude map in GeoAtlas to obtain the areal trend. The maps were imported into the RMS application. I then made the structural model using the imported horizons and faults and then constructed the 3D modeling

grid. The M1 and M3 sands are kept as single layers, whereas the M2 is divided into 3 layers for the low resolution and 20 layers for the high resolution model.

7.2 GEOLOGIC SCENARIOS

The different geologic scenarios and dynamic uncertainties I considered in the study are illustrated in Fig. 28.

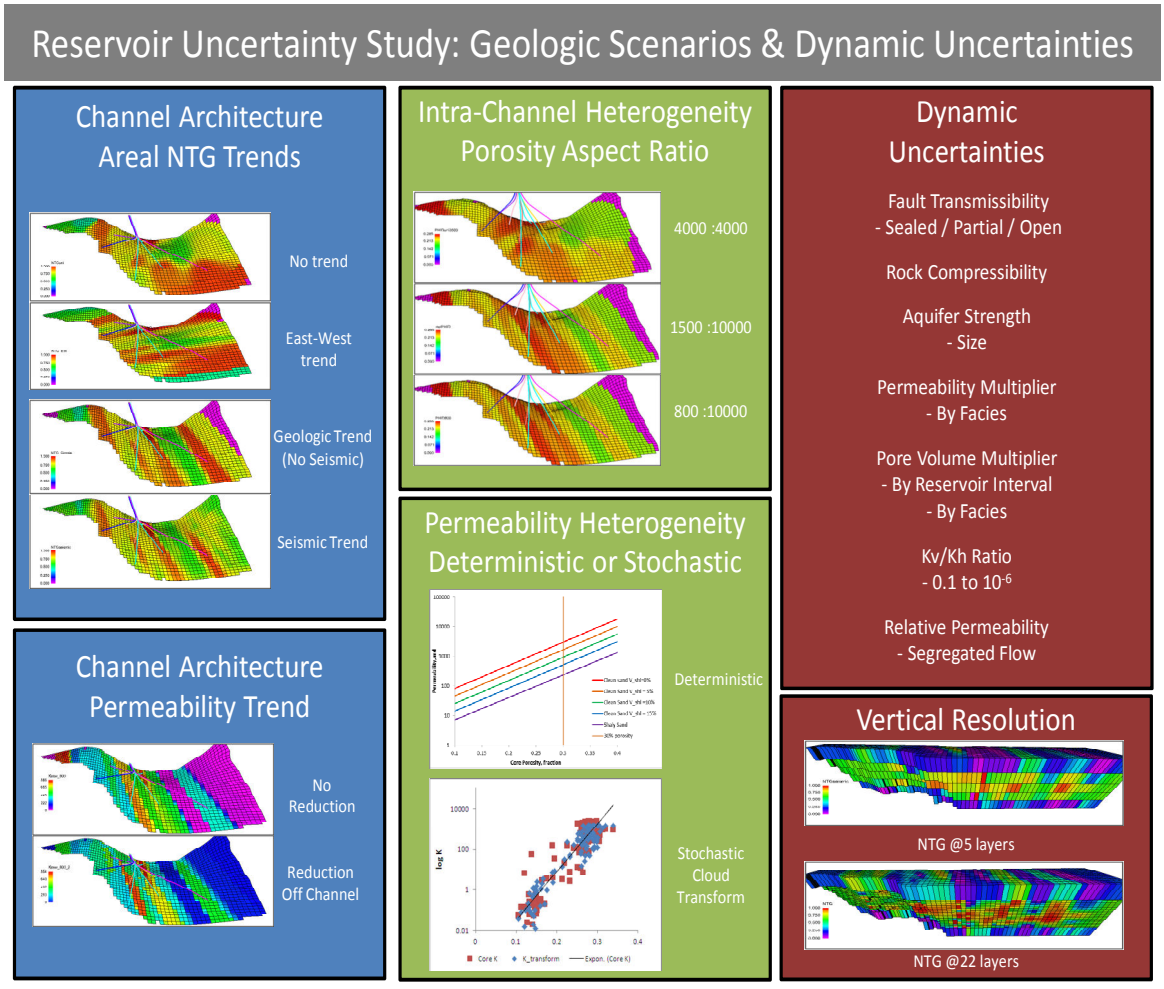

Fig. 28 – Uncertainties Considered

I shall now describe each aspect of our subsurface uncertainties.

7.3 CHANNEL ARCHITECTURE

I considered four different areal trends for NTG in our models. All models were conditioned to the well data, but they differed between wells. The four different representations of NTG areal trends are discussed below.

a) The simplest model populated the NTG uniformly with no imposed channel orientation.

b) The NTG is populated with an E-W channel orientation, which is expected to be inconsistent with the actual reservoir description. I included this areal trend to compare its initial performance ranked with the models having anticipated geological trend and check whether there are evidences that discard this scenario completely.

c) The NTG is populated along a general N-S geological trend.

d) The NTG is populated along the geological trend and is conditioned with the seismic RMS amplitude. For this, a base map having average NTG values at each well location is contoured based on a seismic RMS amplitude surface map provided in the background. I used GeoAtlas application in Geographix for this purpose. So, for each three layers, separate NTG trends were obtained which were then imported in RMS application and interpolated in the respective sand layers. These trends were then conditioned with well data to have distinct values in every layer.

The NTG correlation length was kept at 4000 m for the simplest model to cover all the field area. For the other three trends, the correlation length was kept at 1500 m in the channel direction as inferred from the well test interpretation results.

7.4 POROSITY MODELING AND ASPECT RATIO

Since the NTG parameter is used to account for the geometry of the non-net sand channels, I used net porosity in the model. The log data was imported in the RMS application. While constructing the static model, the log values were blocked (averaged) in the well intersecting grid blocks with values in non-net sand sections filtered out as a bias log. The net porosity is then determined in those gridblocks as –

$$\Phi_A = \frac{\sum_{i=1}^{N} w_i \Phi_i}{\sum_{i=1}^{N} w_i}, \quad where \;\; w_i \; is \; the \; bias \; \log$$

The blocked values were used to generate the spatial distribution inside the grid model with varying correlation lengths. For each NTG model, I developed two models of porosity to address the intra channel heterogeneity. One model has the same correlation length as NTG, whereas for the second model, I reduced the correlation length to 800 m to allow for proximal & distal levee facies contrast near the channel boundary. So corresponding to each areal trend, there are two different porosity distributions, so a total of 8 initial models that still need to be populated with permeability parameter.

7.5 PERMEABILITY TREND MODELING

The permeability was blocked similarly to the porosity and populated spatially using the same correlation length as of the porosity parameter in a particular model. There are now eight initial models. However, in the M2 sand, the channel sequences have high NTG values of above 0.8, whereas the NTG off-channel varies from 0.4 to 0.8. But, the permeability in low resolution model varies from 700 – 800 md in channel sequences, whereas from 400 – 600 md in off-channel. In Fig. 7, the permeability for core plugs having low Vsh fraction is around 1000 md, whereas those having high Vsh fraction is around 100 md. Such a contrast in permeability could not be obtained for these eight models. Therefore, it was considered necessary to reduce the permeability off-channel and try it as sensitivity to know whether high permeability contrast is essential or not. Therefore, for each eight model, one more model having permeability reduction off channel was made. Therefore, there are a total of 16 different initial geologic models now.

7.6 POROSITY - PERMEABILITY MODELING

As discussed in the petrophysical section, I calculated the log permeability in two ways –

a) **Deterministic Approach** - Using Vshale as an additional variable in K-phi relationship.

b) **Stochastic Approach** – Using the cloud transform in the K-Phi relationship. I performed this transformation at the log scale since that data is at the highest spatial resolution available.

Each of the 16 models described above was made for both the approaches. Thus, a total of 32 different static models were made for initial screening. Table 11 shows a summary of these static models.

Table 11 – Different Static Models

Models	NTG	Porosity correlation	Permeability	Initial OOIP
1, 17	E-W	Correlation as NTG	Reduction off channel	845.4
2, 18	E-W	Reduced Correlation	No reduction	846
3, 19	E-W	Reduced Correlation	Reduction off channel	846
4, 20	E-W	Correlation as NTG	No Reduction	845.4
5, 21	Seismic	Correlation as NTG	Reduction off channel	742.3
6, 22	Seismic	Reduced Correlation	No reduction	742
7, 23	Seismic	Reduced Correlation	Reduction off channel	742
8, 24	Seismic	Correlation as NTG	No Reduction	742.3
9, 25	Geologic	Correlation as NTG	Reduction off channel	730.3
10, 26	Geologic	Reduced Correlation	No reduction	730
11, 27	Geologic	Reduced Correlation	Reduction off channel	730
12, 28	Geologic	Correlation as NTG	No Reduction	730.3
13, 29	Uniform	Correlation as NTG	Reduction off channel	796.8
14, 30	Uniform	Reduced Correlation	No reduction	797.3
15, 31	Uniform	Reduced Correlation	Reduction off channel	797.3
16, 32	Uniform	Correlation as NTG	No Reduction	796.8

*Models 1-16: Deterministic permeability

*Models 17-32: Permeability by Cloud Transform

7.7 DYNAMIC UNCERTAINTIES

Apart from the static model uncertainties, I also considered several dynamic uncertainties which may affect the history match results. The uncertainties studied were the rock compressibility, aquifer strength, regional pore volume multipliers, regional permeability multipliers, the K_v/K_h ratio, relative permeabilities to oil & water, and the fault transmissibility. The initial values for rock compressibility, K_v/K_h ratio, and relative permeabilities to oil & water were determined from the data provided.

7.8 DYNAMIC BASE CASE AND UNCERTAINTY RANGE

7.8.1 Fault Transmissibility

The faults in the reservoir do not separate the reservoir into separate fault blocks. Therefore, the fluid flow is not believed to be affected by the faults. Only the fault present between the well A2 and A8 might affect the fluid flow to well A2. So, I have kept zero transmissibility across the faults for base case and kept the faults open as the other limit.

7.8.2 Rock Compressibility

The rock compressibility value for the base case was established at 13.88E-6 1/psi from the given rock compressibility and net confining pressure data. When plotted, the average rock compressibility for the major production time period comes out to be 13.88E-6 1/psi. For uncertainty analysis, I kept the rock compressibility in the range from 1E-6 1/psi to 3E-5 1/psi. This interval brackets the possible value range of rock compressibility around the base case value as reflected in Fig. 29.

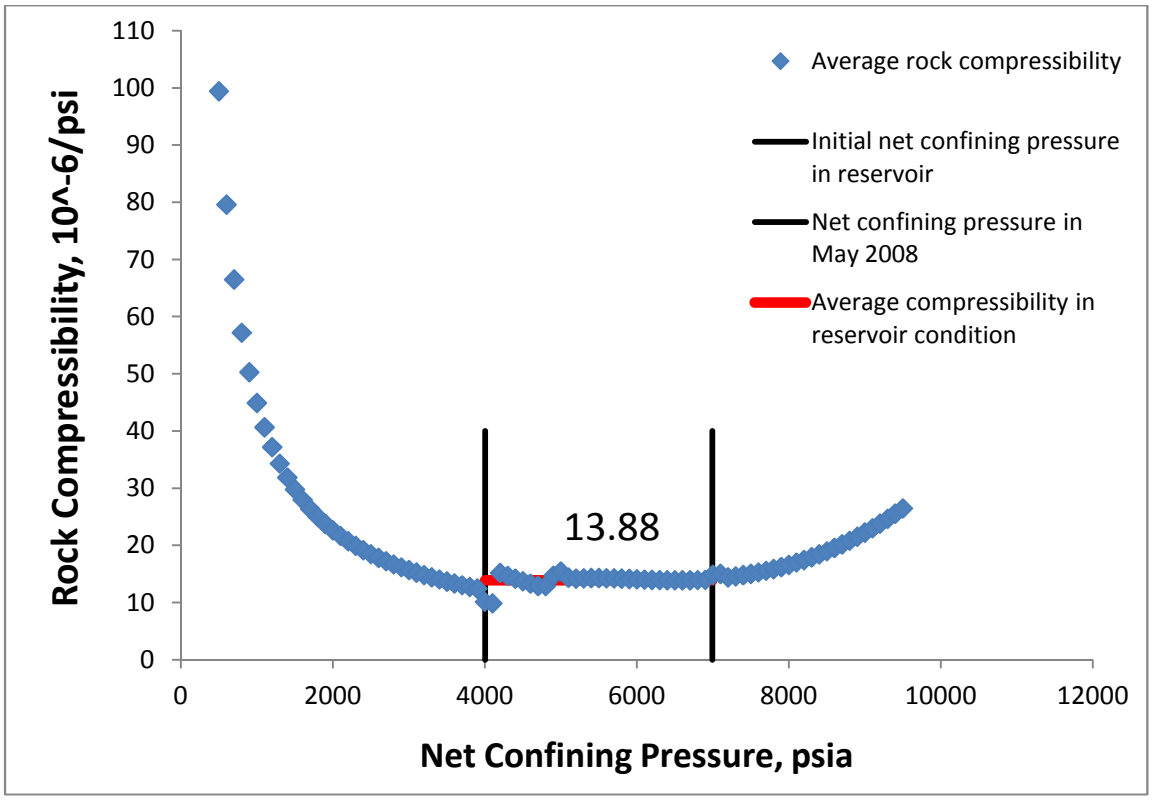

Fig. 29 - Average Rock Compressibility vs. Net Confining Pressure

7.8.3 Aquifer Strength

I used Carter Tracy aquifer in the simulation study. The aquifer connections were made to all the cells at oil water contact. I used the same aquifer permeability as modeled in Material Balance study. There was considerable uncertainty associated with other aquifer parameters. I fixed the other parameters for aquifer but its radius which varied its strength. The aquifer height was kept as 175 ft (from material balance),

whereas the encroachment angle was kept as 80°. Based on a few manual runs, the aquifer radius range was kept from 300 ft (low active) to 3000 ft (highly active).

7.8.4 Permeability Multipliers

The permeability multipliers are used in the cases which have regions defined based on facies. The core plugs had maximum permeability of around 1500 md. However, the maximum permeability in the low resolution model was around 850 md. Therefore, I kept the maximum permeability multiplier limit of 2 for the channel regions. For the non-channel regions, the low permeability multiplier limit was set at 0.2 which brings the permeability in those regions in the range 10-50 md which is also supported from core data.

7.8.5 Pore Volume Multipliers

The pore volume inside the initial model was large as compared to the OOIP estimate from the material balance. The initial models have average OOIP of 750 MMSTB, whereas that estimated from material balance is 230 MMSTB. Based on these, I kept the lower limit of PV multipliers to 0.2 which is slightly lower to the ratio of the above OOIP values.

7.8.6 K_v/K_h Ratio

The K_v/K_h ratio provided in oriented field core data analysis had an average value of 3.5E-5. However, for uncertainty analysis, I kept the Kv/Kh ratio in the range from 1E-6 – 0.1. I used a fairly wide range of K_v/K_h to determine whether it has an impact on the history match or not. The upper limit if set to 1 would have represented a

completely disorganized reservoir. Keeping the upper limit at 0.1 provides dimensions to the virtual shale barriers. The lower is to include any possibility of lower $Kv/K_{h.}$

7.8.7 Relative Permeability

I obtained the rock relative permeability curve from the field data which was used in the base case. Table 12 shows the calculated values of total mobility and fractional flow for water from these curves. However, when total mobility calculated is plotted (Fig. 30), there is a characteristic drop in it as the water saturation starts increasing. For a two phase fluid flow, this is an extreme case. The relative permeability sensitivity is made under the constraint that fractional flow for oil and water remains the same as the rock case; however the total mobility of the system is adjusted close to linear trend such that relative permeability curves remain monotonic.

$$\lambda_{\text{total}} = \frac{k_{ro}}{\mu_o} + \frac{k_{rw}}{\mu_w}$$

$$\textit{Fractional Flow}, F = \frac{\frac{k_r}{\mu}}{\lambda_{total}}$$

Table 12 - Initial Mobility

Sw	Krw	Kro	Total Mob	Mob Oil	Mob Wat	Fw
0.1361	0	1	1.428571	1.428571	0	0
0.2875	0.0262	0.576	0.875257	0.822857	0.0524	0.059868
0.392	0.056	0.306	0.549143	0.437143	0.112	0.203954
0.5243	0.101	0.0946	0.337143	0.135143	0.202	0.599153
0.6917	0.188	0.0153	0.397857	0.021857	0.376	0.945063
0.7388	0.244	0.00933	0.501329	0.013329	0.488	0.973414
0.8196	0.34	0	0.68	0	0.68	1

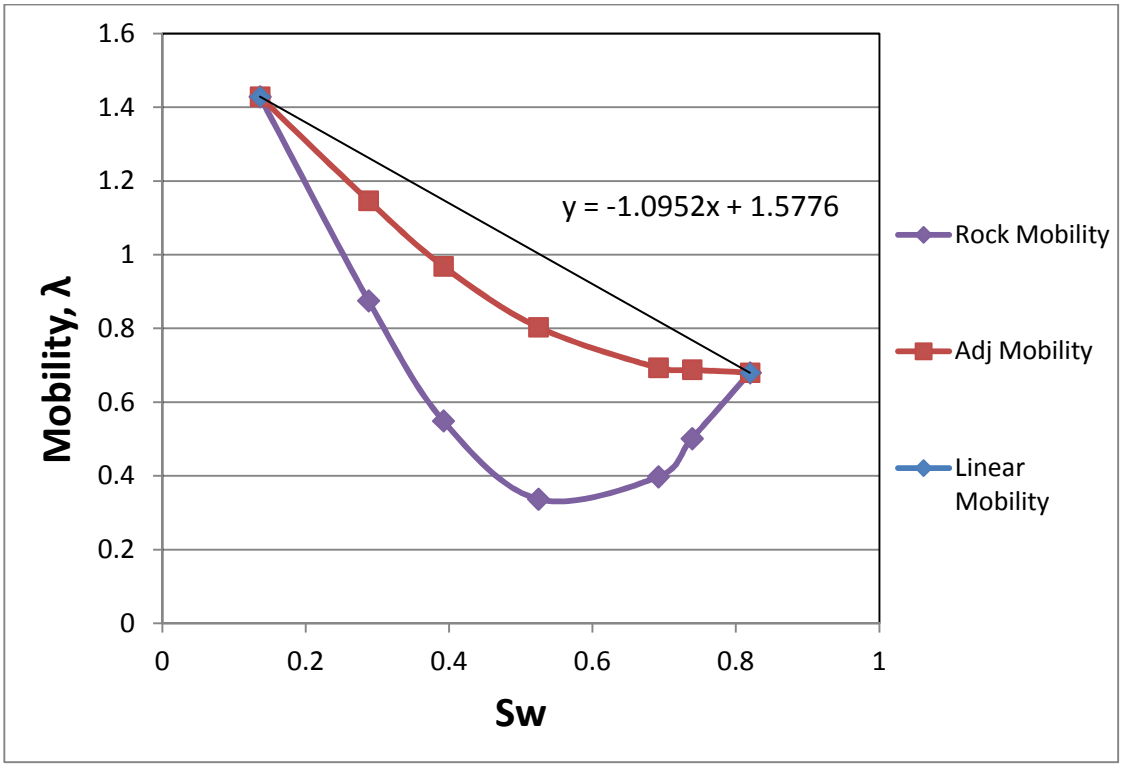

Fig. 30 – Mobility Calculation

The total mobility for initial rock curves was calculated and plotted against water saturation. The values for total mobility for completely segregated flow are linear. Based on the initial and linearly calculated total mobility value, an intermediate value for total mobility was calculated. The relative permeability for oil and water were then back calculated from the adjusted mobility values for the same fractional flow at different water saturation points. The newly calculated relative permeabilities curves are compared to the initial rock curves in Fig. 31.

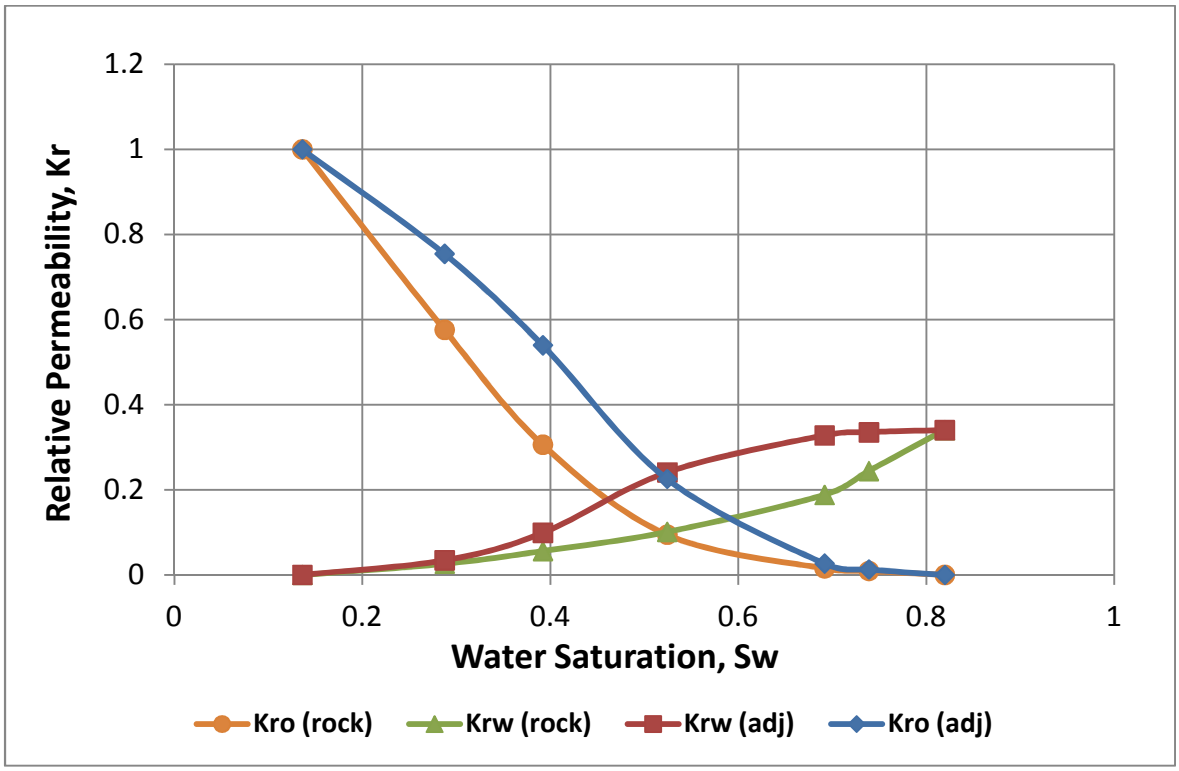

Fig. 31 – Initial and Adjusted Relative Permeabilities

8. DYNAMIC DATA CALIBRATION

The 32 static models were screened in a sensitivity run in MEPO to rank their fitness based on an objective function which was constructed from the observed and computed values for bottom hole pressures of each well. The reservoir pressure always remained above the bubble point pressure during the production history. Therefore, the simulations were run on liquid rate control. The performance of different static initial models is compared in Fig. 32 - Fig. 35.

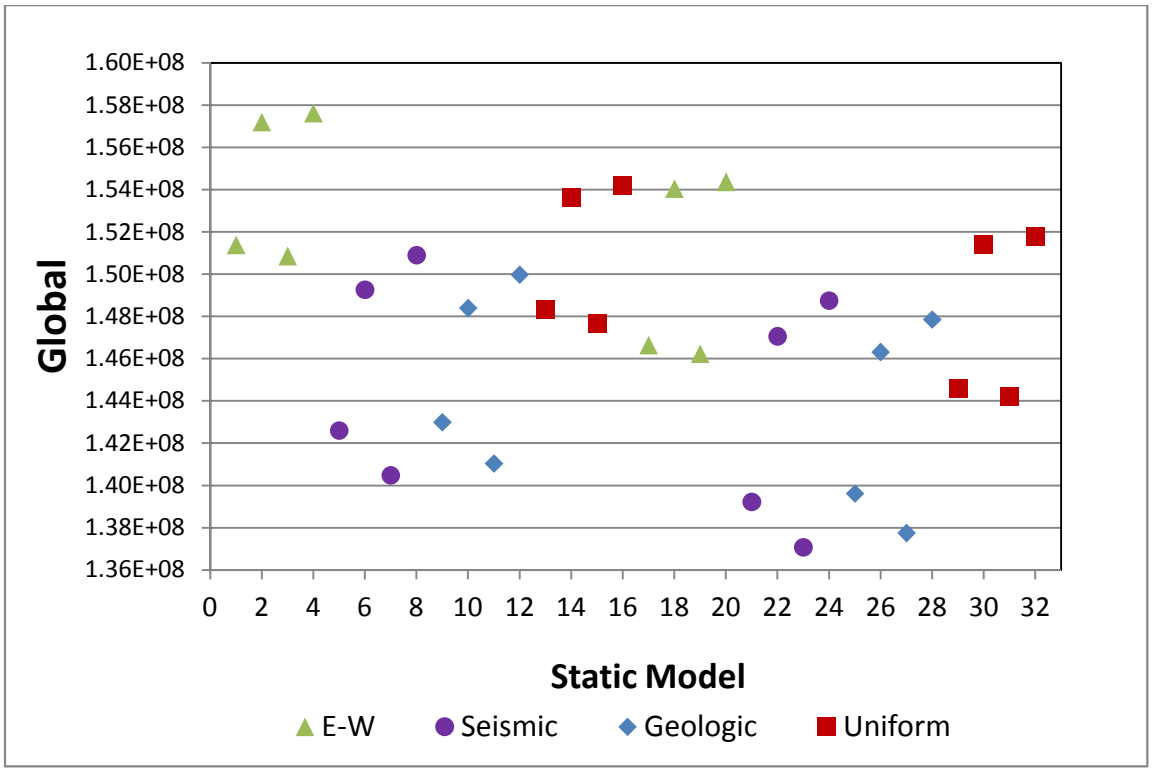

Fig. 32 – Global error – NTG parameter

The models with geological trends perform distinctly better than the models with E-W or uniform trend. The E-W trend model performs poorer than the uniform trend models.

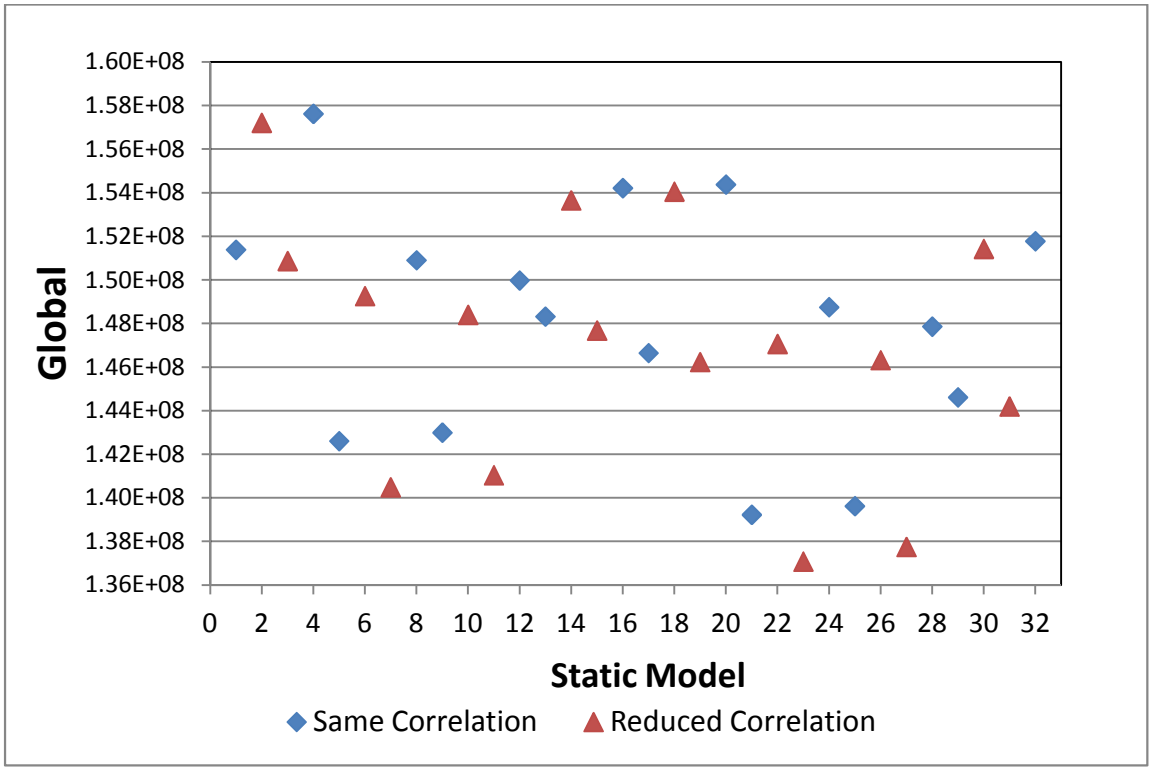

Fig. 33 – Global error – Porosity parameter

The scatter in both the porosity correlation cases is as spread as in the other. However, the models with reduced correlation length fare better than the models with the same correlation length as of NTG. Even though the impact does not seem to be significant, this may imply that lower pore volume in the model gives better results.

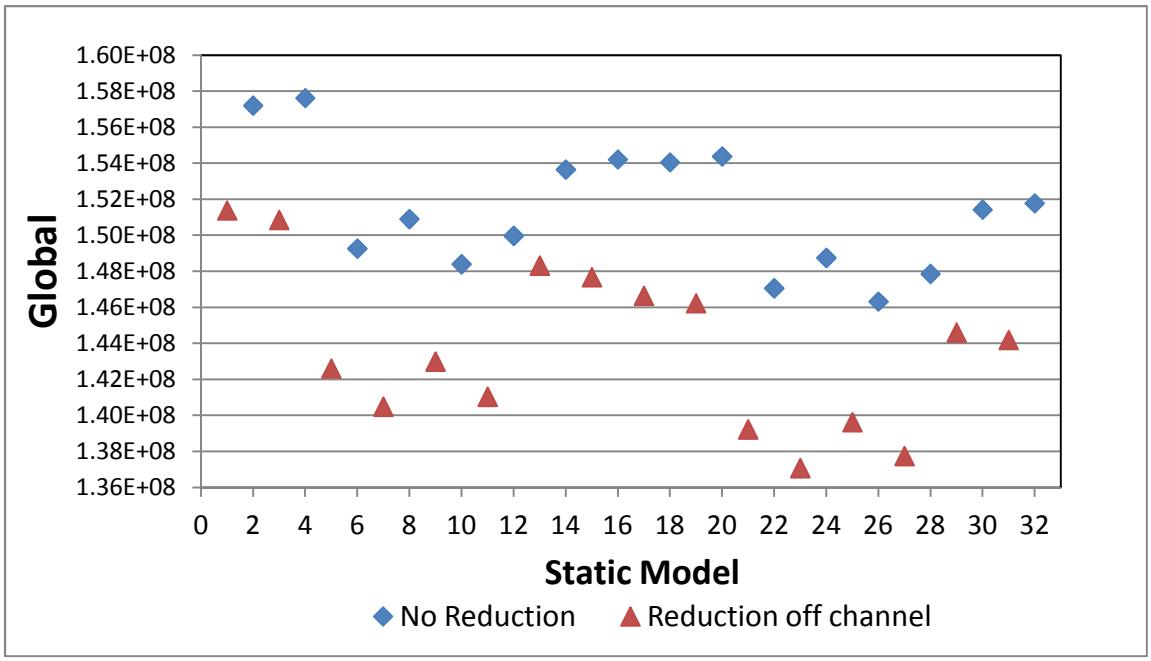

Fig. 34 – Global error – Permeability parameter

The permeability contrast between channel and non-channel facies clearly affects the model performance. It is inferred that all the models with higher permeability contrast fare better than their counterparts.

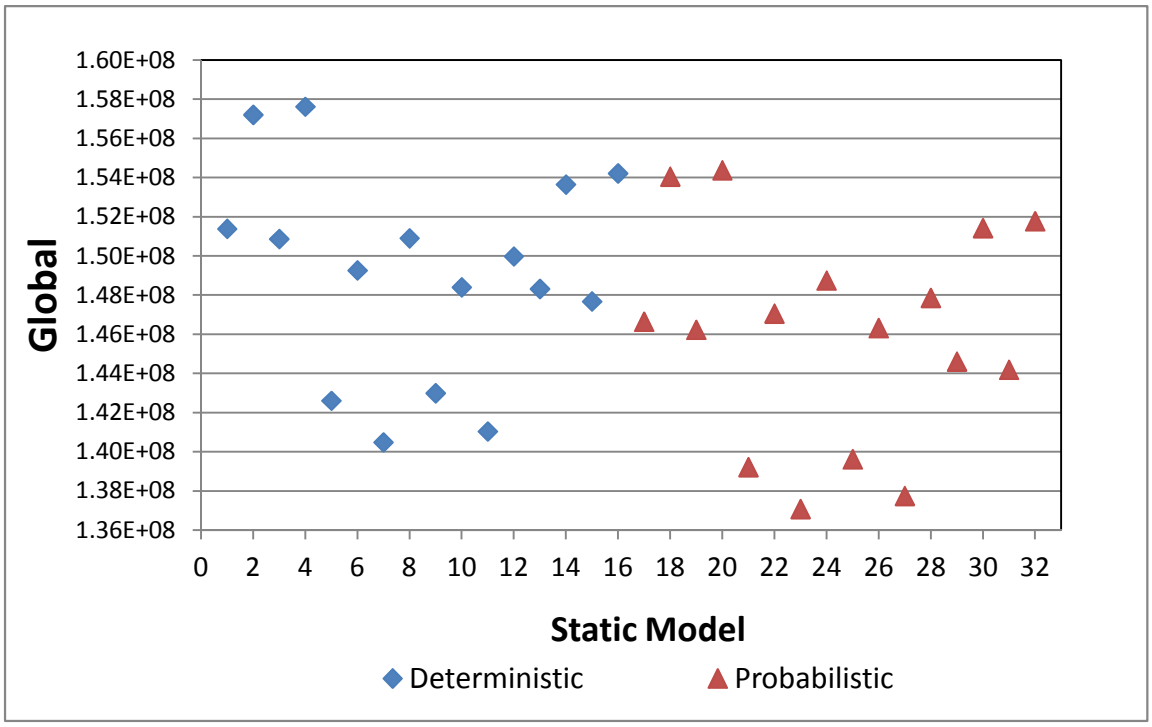

Fig. 35 – Global error – Permeability approach

The permeability calculation approach doesn't impact significantly the starting model, though models based on permeability calculated by the cloud transform have lesser error. The scatter is equally spread for the two cases.

In summary, the model with reduced porosity correlation length and enhanced permeability contrast yield the minimum error among its subset class. The permeability contrast has a big impact on the performance of the model. The models with E-W NTG trend had the maximum error. The seismic trend model turned out to be the model with minimum error among all. This model had the permeability calculation based on cloud transform. This screening can rule out the incorrect channel direction if not known beforehand.

Thereafter, I started the history matching study with three different classes of models which showed minimum error in the static model sensitivity. These three classes were –

a) Uniform Trend Model – where no trend/orientation in properties is considered.
b) Geological Trend Model – where NTG was given the known geologic trend (N-S orientation) but without seismic conditioning.
c) Seismic Trend Model

Of these static models, I selected the following features as they gave the minimum error in the screening study –

- Permeability reduction off-channel
- Lower porosity correlation length
- Cloud transform for permeability

The initial dynamic parameters that affect the energy balance in a reservoir were included in the uncertainty evaluation. These were –

a) Pore Volume Multipliers for each sand unit as the OOIP calculated from the initial geologic models are greater than that estimated from material balance.
b) Aquifer Strength –
c) Rock Compressibility

The impacts of these parameters for the initial model were first studied through a sensitivity run in MEPO which generates the Tornado Plot. This plot depicts the impact of each parameter to the defined objective function (now extended to include field oil production also) and ranks them accordingly. The main affecting parameters were then

decided. The optimized values of the selected parameters were then found using the Evolution Strategy Algorithm in MEPO. The MEPO optimized output was input to Destiny, which then varied the permeability field within the minimum and maximum input range to minimize water cut mismatch well wise using GTTI technique. Initially, I made five different regions in the model (Fig. 36):

a) Region 1 – M1 Sand
b) Region 2 – M2 Sand
c) Region 3 – M3 Sand
d) Region 4 – Western Part
e) Region 5 – Eastern Part

The western and eastern parts in our model are defined as separate regions 4 & 5 as they are far from the main part of the reservoir and thus have little impact on production. The simulations were run on total liquid control mode. I will next discuss the results.

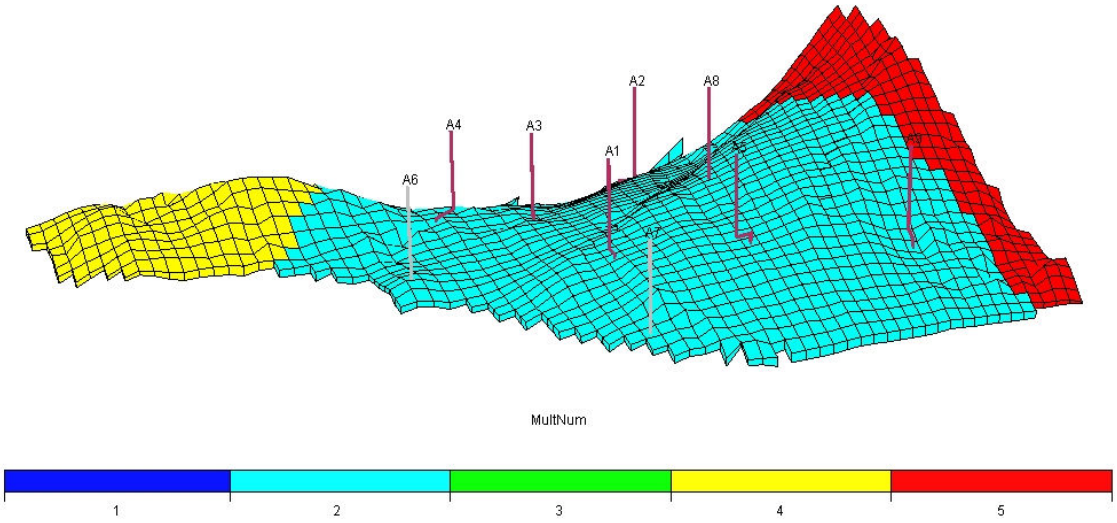

Fig. 36 – Initial Regions

8.1 CASE 1

Geologic Model – Uniform Trend Model

Initial Parameters – PV1, PV2, PV3, PV4, PV5, aquifer radius, K_v/K_h ratio, rock compressibility

Selected Parameters – PV2, rock comp, aq radius

These three parameters were selected as they ranked highest in the Tornado chart for this case (Fig. 37). The same criterion is used to select the parameters for other cases.

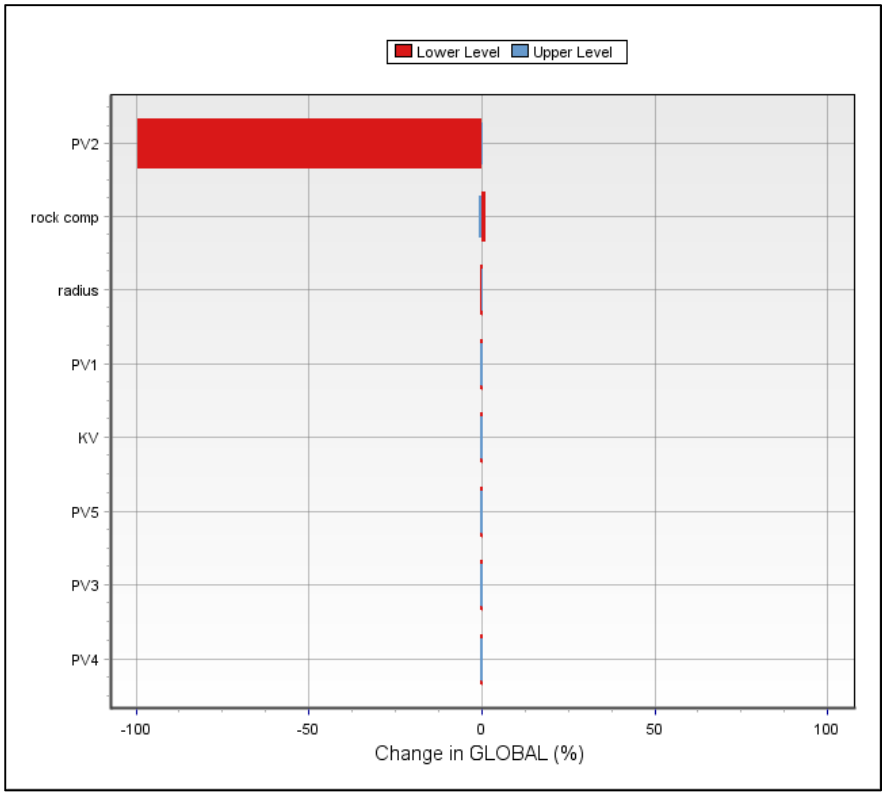

Fig. 37 – Tornado Chart for Case 1

Fig. 38 shows the match for the uniform trend model.

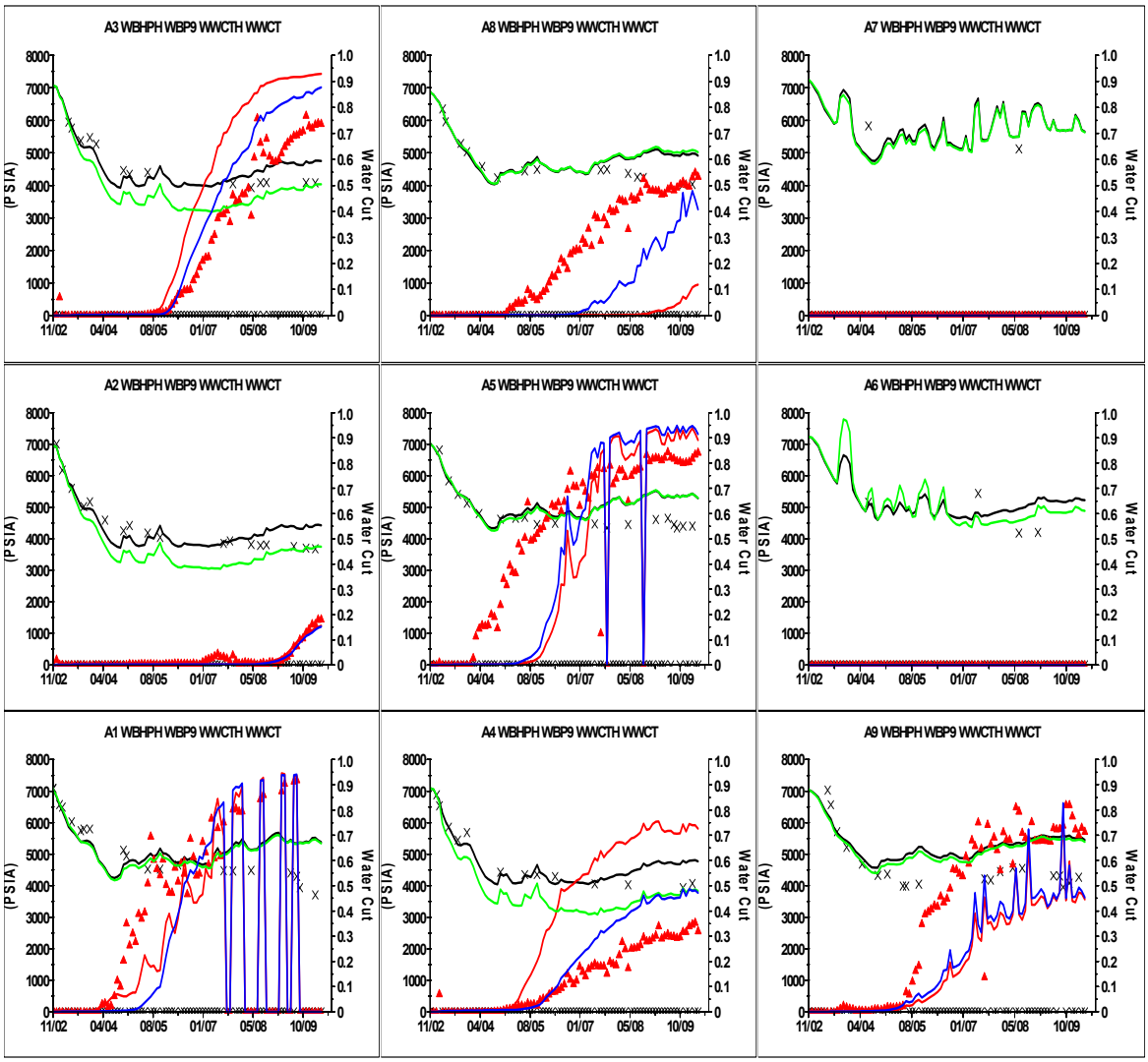

Fig. 38 – Simplest Model Match

(Black and Red curves represent the match obtained after energy balance in MEPO. Green and Blue curves represent modified match after the Destiny run.)

The assisted techniques have a hard time for this model to get a good match. The pressure match quality in each well gets worse after the Destiny run.

8.2 CASE 2

Geologic Model - Geologic Trend Model

Initial Parameters – PV1, PV2, PV3, PV4, PV5, aquifer radius, Kv/Kh ratio, rock compressibility

Selected Parameters – PV2, rock comp, aq radius (Fig. 39)

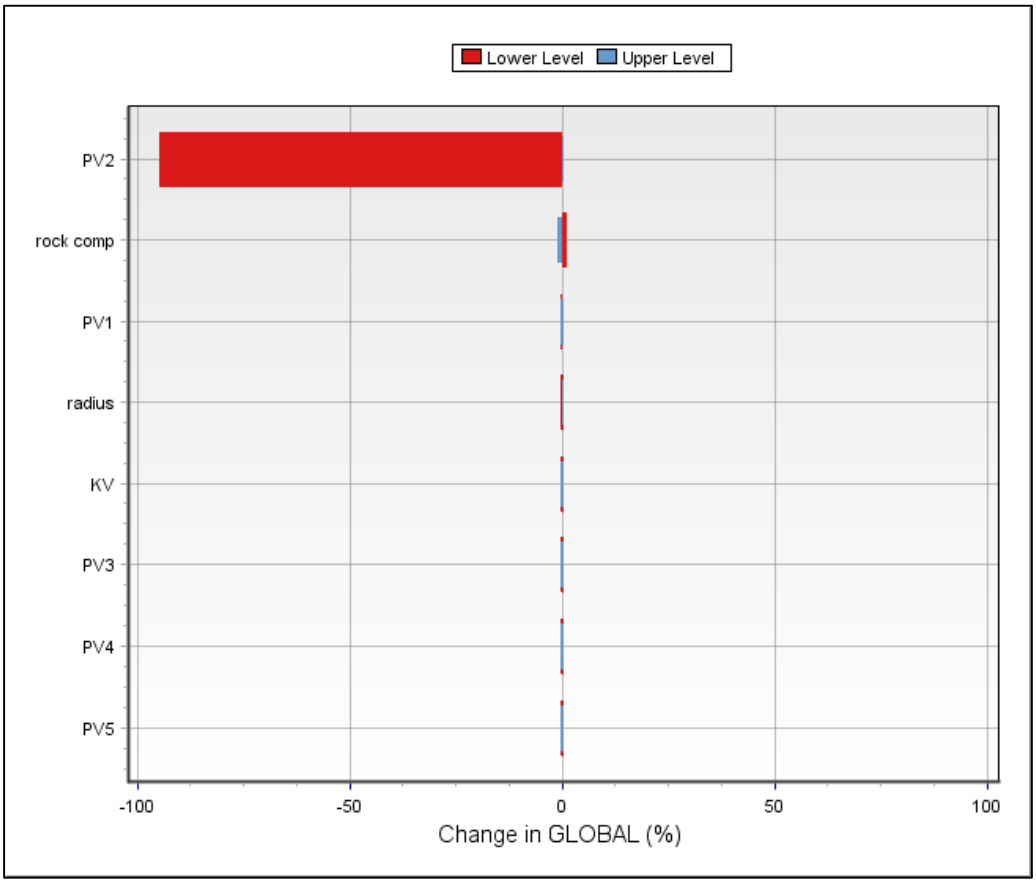

Fig. 39 – Tornado Chart for Case 2

The results for this case are shown in Fig. 40.

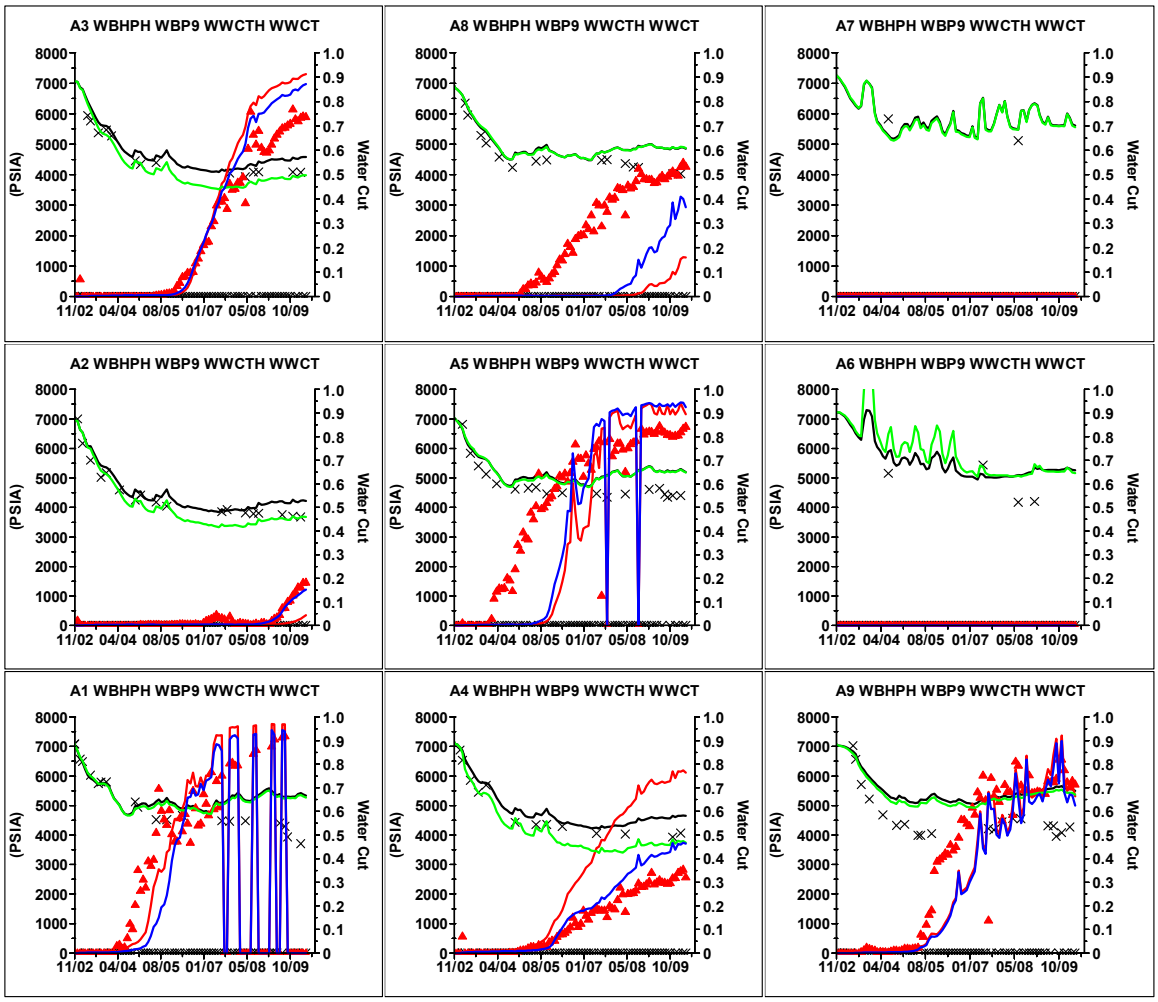

Fig. 40 – Case 2 Results

(Black and Red curves represent the match obtained after energy balance in MEPO. Green and Blue curves represent modified match after the Destiny run.)

The pressure match doesn't degrade in this model to that extent as seen in Case 1 after the Destiny run. The aquifer influx now moves faster through high permeability channels and helps in arresting the pressure decline earlier in the time.

8.3 CASE 3

Geologic Model - Seismic Trend Model

Initial Parameters – PV1, PV2, PV3, PV4, PV5, aquifer radius, Kv/Kh ratio, rock compressibility

Selected Parameters – PV2, rock comp, aq radius

The Tornado chart was found to be similar to what obtained for Case 1 & 2. The results for this case are shown in Fig. 41. I get improvement in the pressure match in Case 3 as well. The water cut match obtained for Case 2 and 3 models do not look very different from each other. The reservoir description before and after the Destiny run are compared in the Fig. 42.

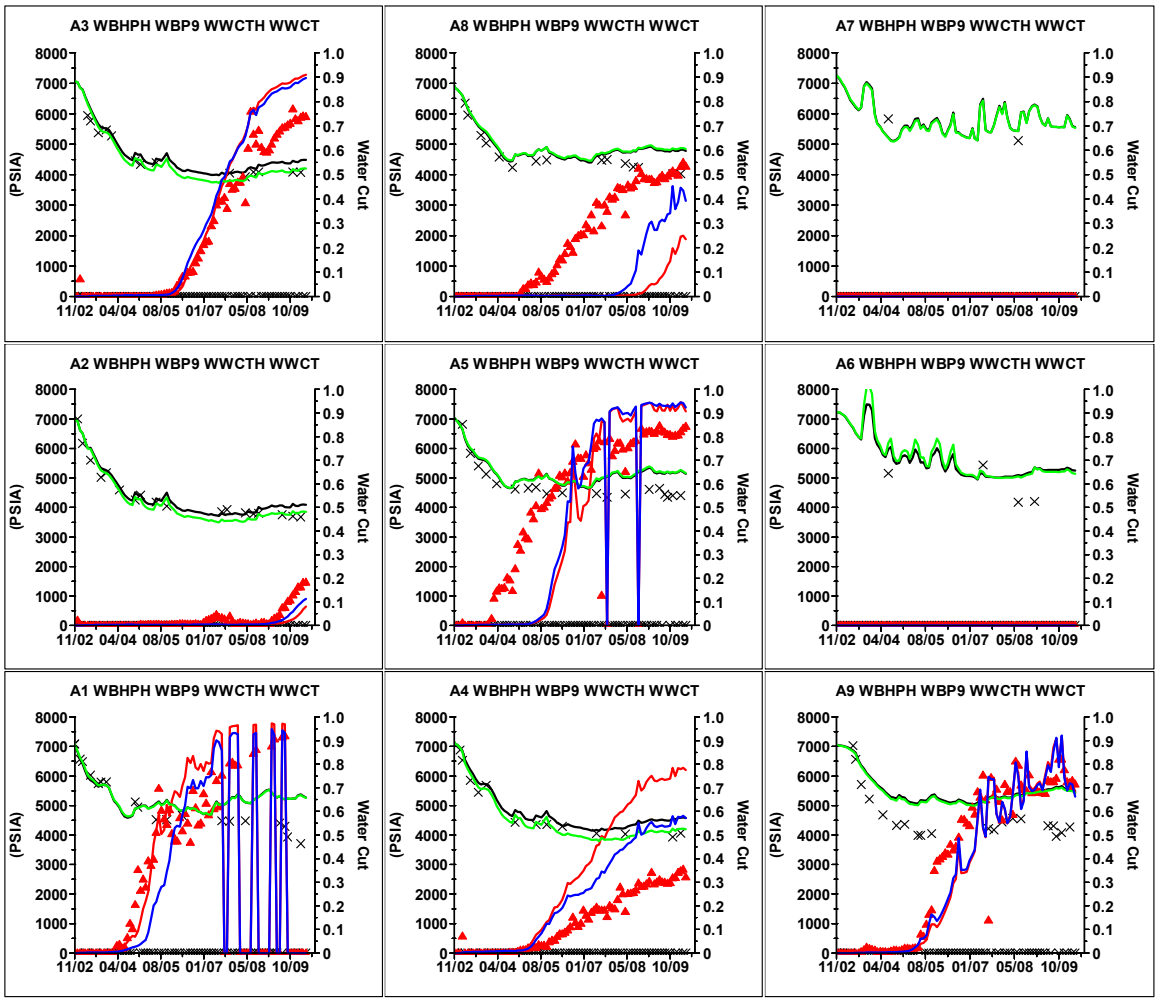

Fig. 41 - Case 3 Results

(Black and Red curves represent the match obtained after energy balance in MEPO. Green and Blue curves represent modified match after the Destiny run.)

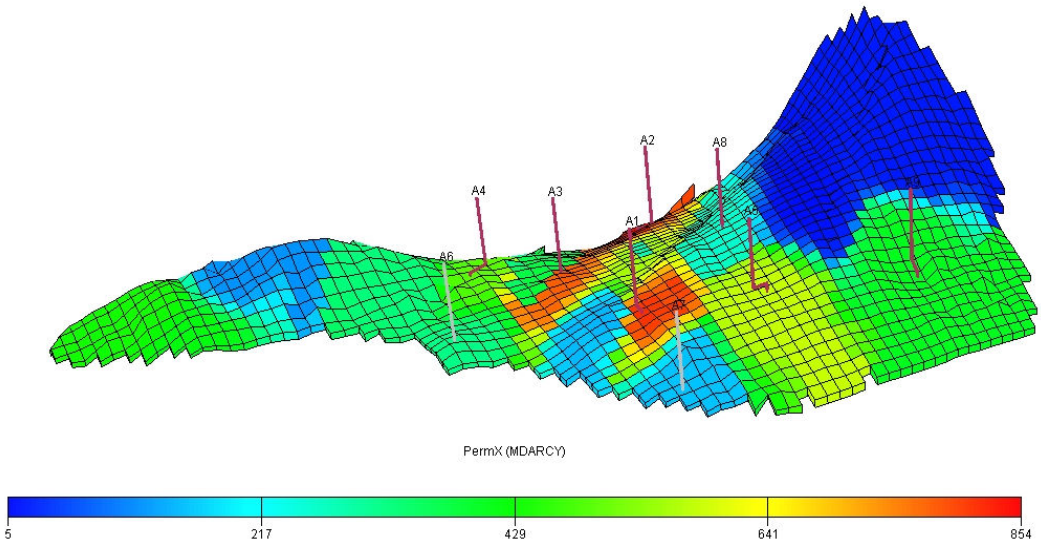

Case 1 – After MEPO

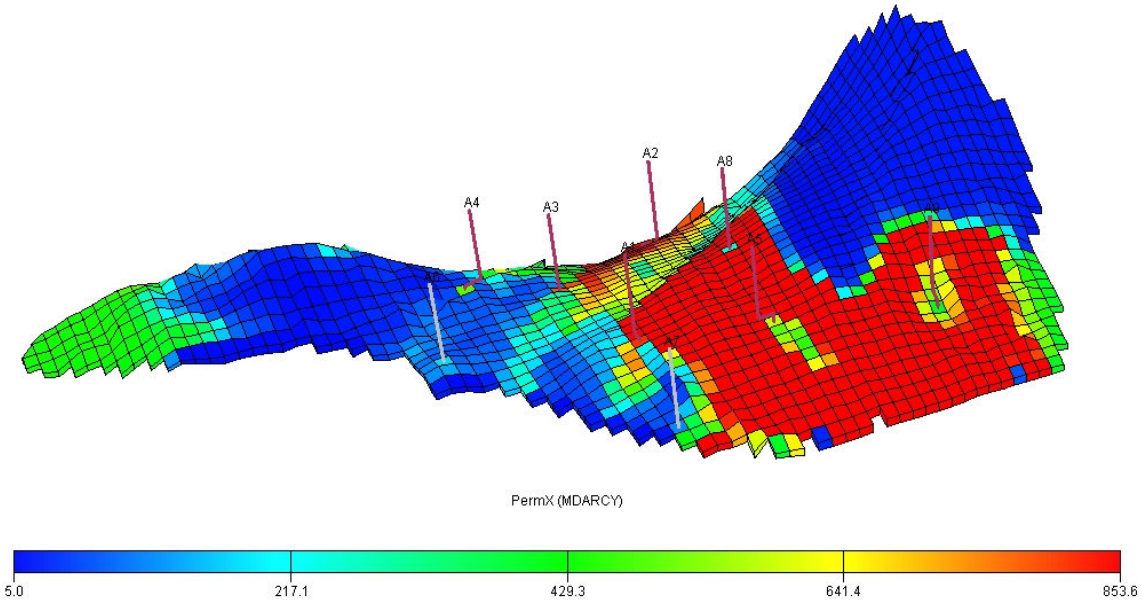

Case 1 – After Destiny

Fig. 42 – Case 1 - 3 Comparison

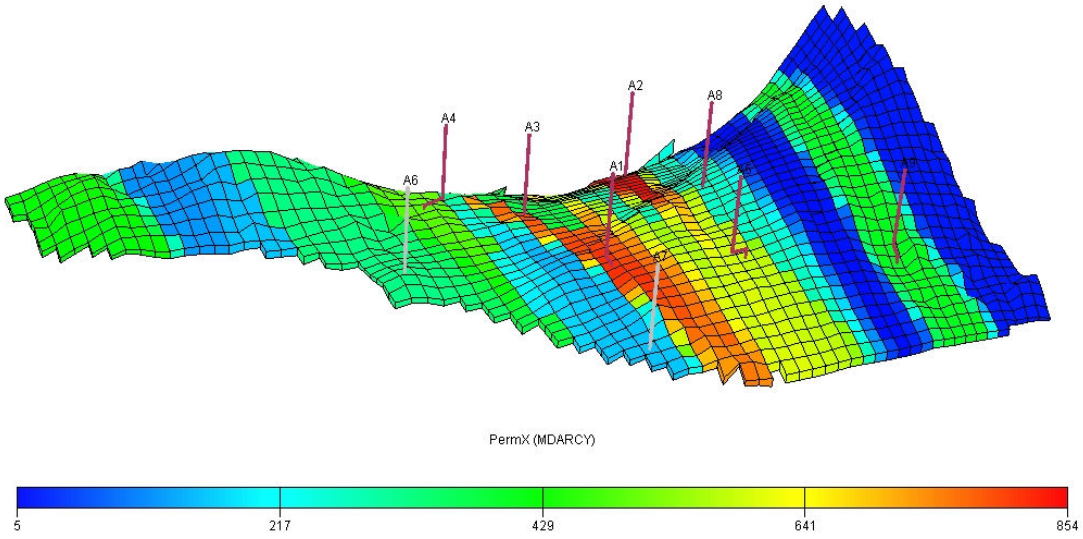

Case 2 – After MEPO

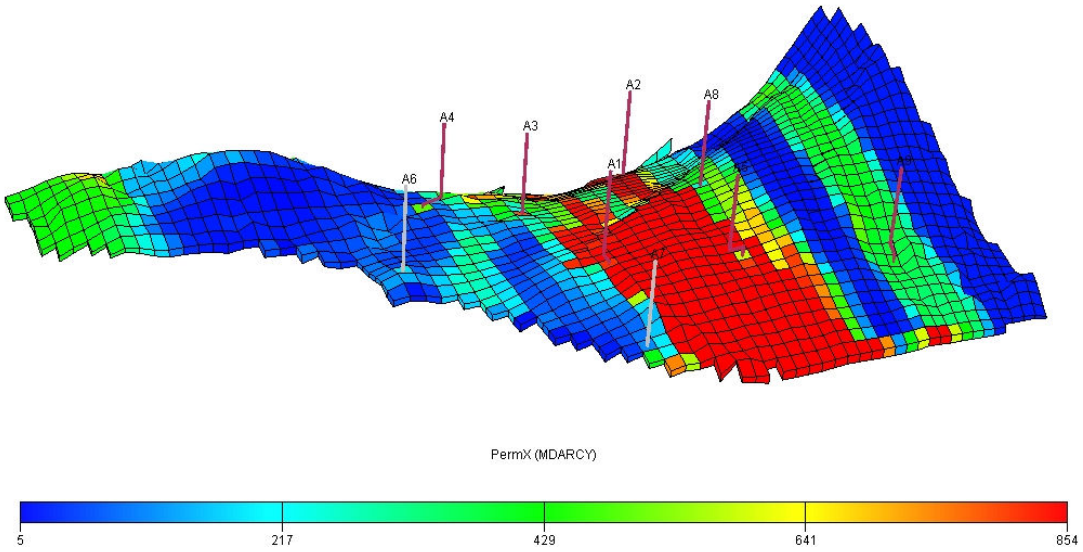

Case 2 – After Destiny

Fig. 42 – Continued

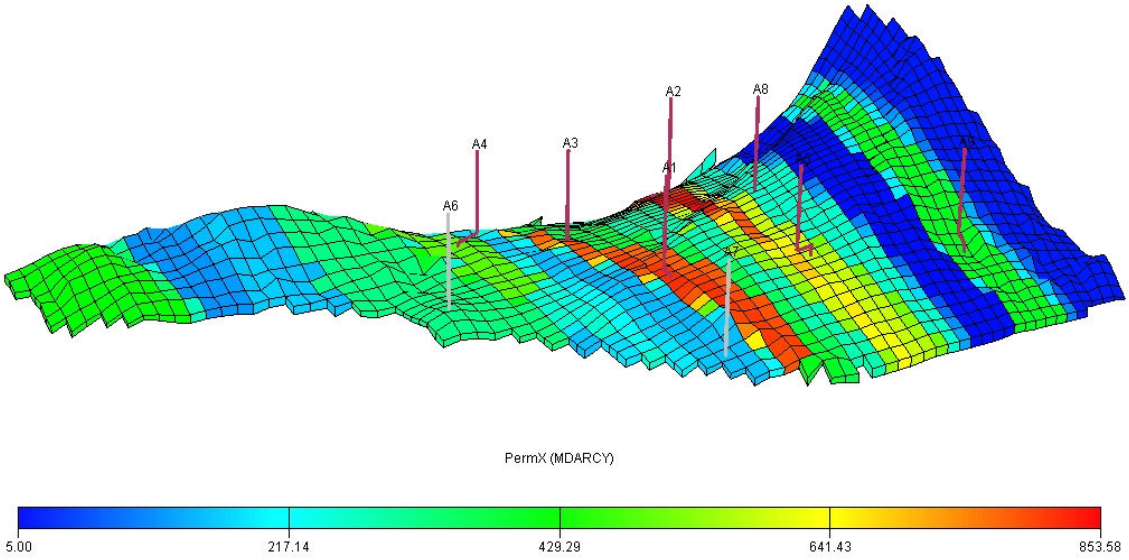

Case 3 – After MEPO

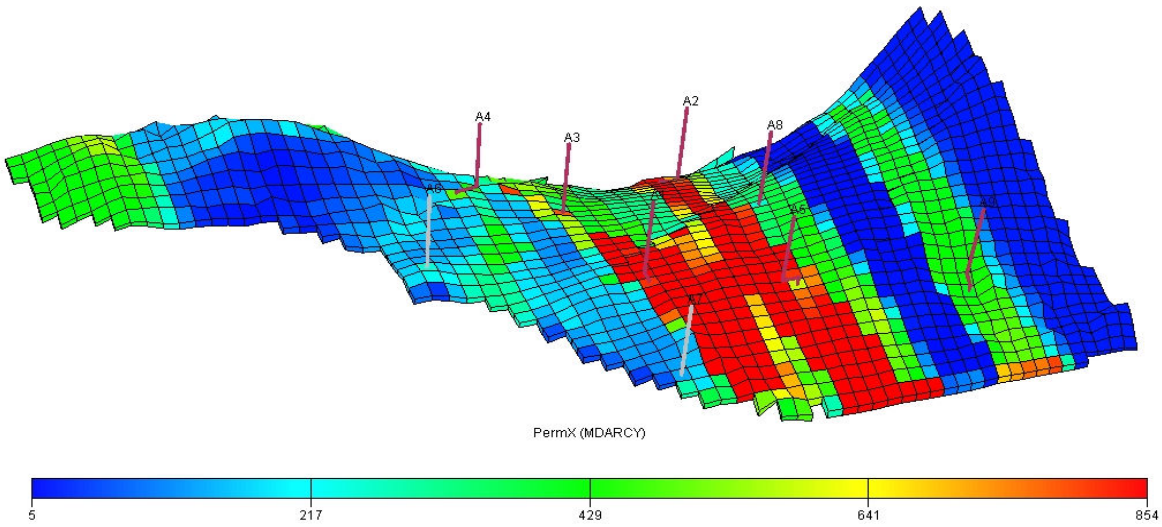

Case 3 – After Destiny

Fig. 42 – Continued

In cases 1 and 2, the contrast between the channel and non-channel sand is completely lost. However in Case 3, we can visualize some of the geologic features of the reservoir. There are two parallel channel sequences (in red) & region of low permeability in between which depicts non channel facies as inferred from the seismic RMS amplitude map (Fig. 27). The seismic conditioning in the static model thus helps in improving the AHM performance. Though I am able to get history match from multiple models, the model which exploits the seismic information is performing marginally better than the other models. However, this is still far from the adequate reservoir description. For better results, it becomes imperative that the methodology be applied in connection with the geology of the field and more elaborately. To include more uncertainty parameters, I defined more regions as shown in Fig. 43. The regions were defined as per the signature seen in seismic RMS amplitude map of the reservoir. The well test in well A5 and A8 suggest channel widths ranging from 800-1500 m. Therefore, region 7 limits the channel boundary in which well A5 and A8 are completed. Region 6 represents the overbank facies region, whereas region 2 represents the main producing region of the reservoir. Now the entire methodology was repeated with more uncertainty parameters.

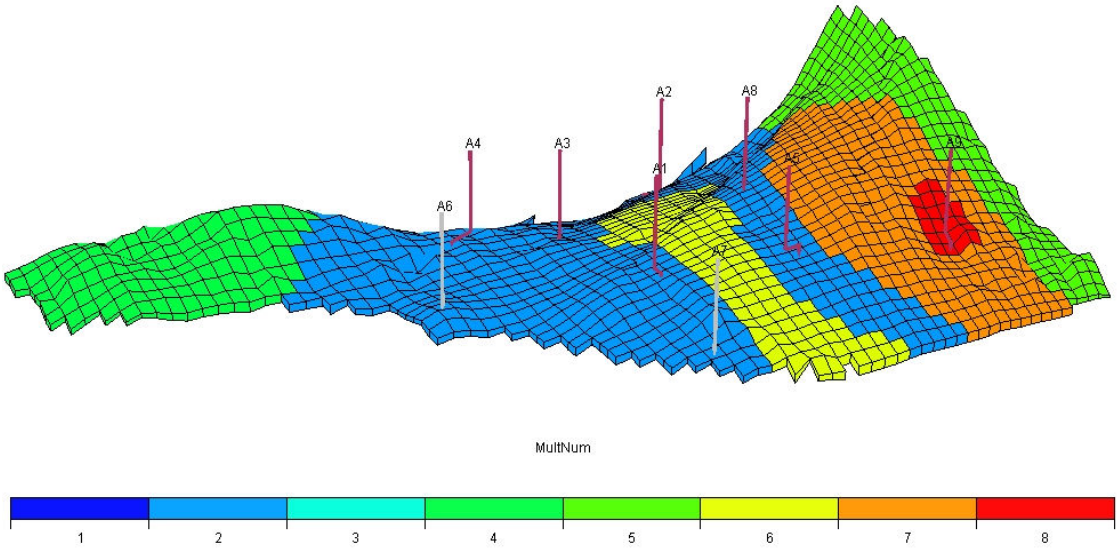

Fig. 43 – New Regions Defined

8.4 CASE 4

Geologic Model - Seismic Trend Model with more regions

Initial Parameters – PV multipliers for all regions, Perm multipliers for all regions, aquifer radius, K_v/K_h ratio, rock comp (19 parameters)

Selected Parameters – PV2, PV6, PV7, K2, K6, K7, rock comp, aq radius (Fig. 44)

The selected parameters were optimized in two cycles as there are more in this case than earlier and the result is shown in Fig. 45.

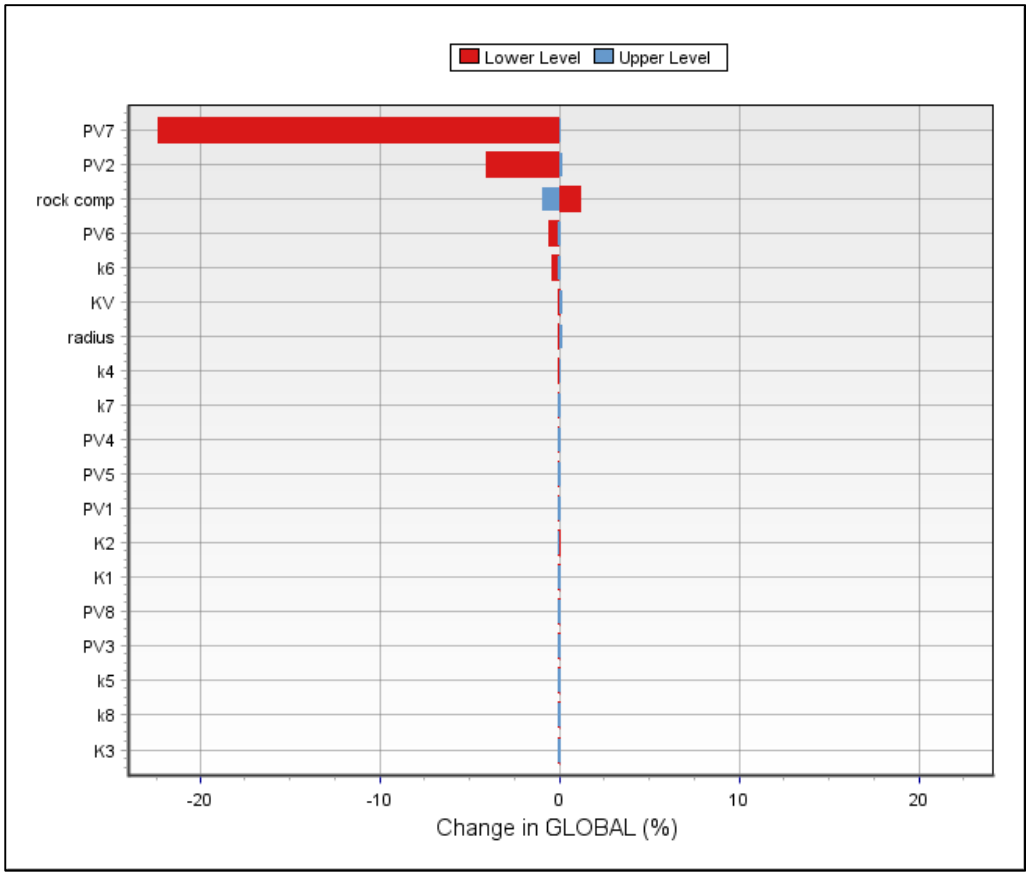

Fig. 44 – Tornado Chart for Case 4

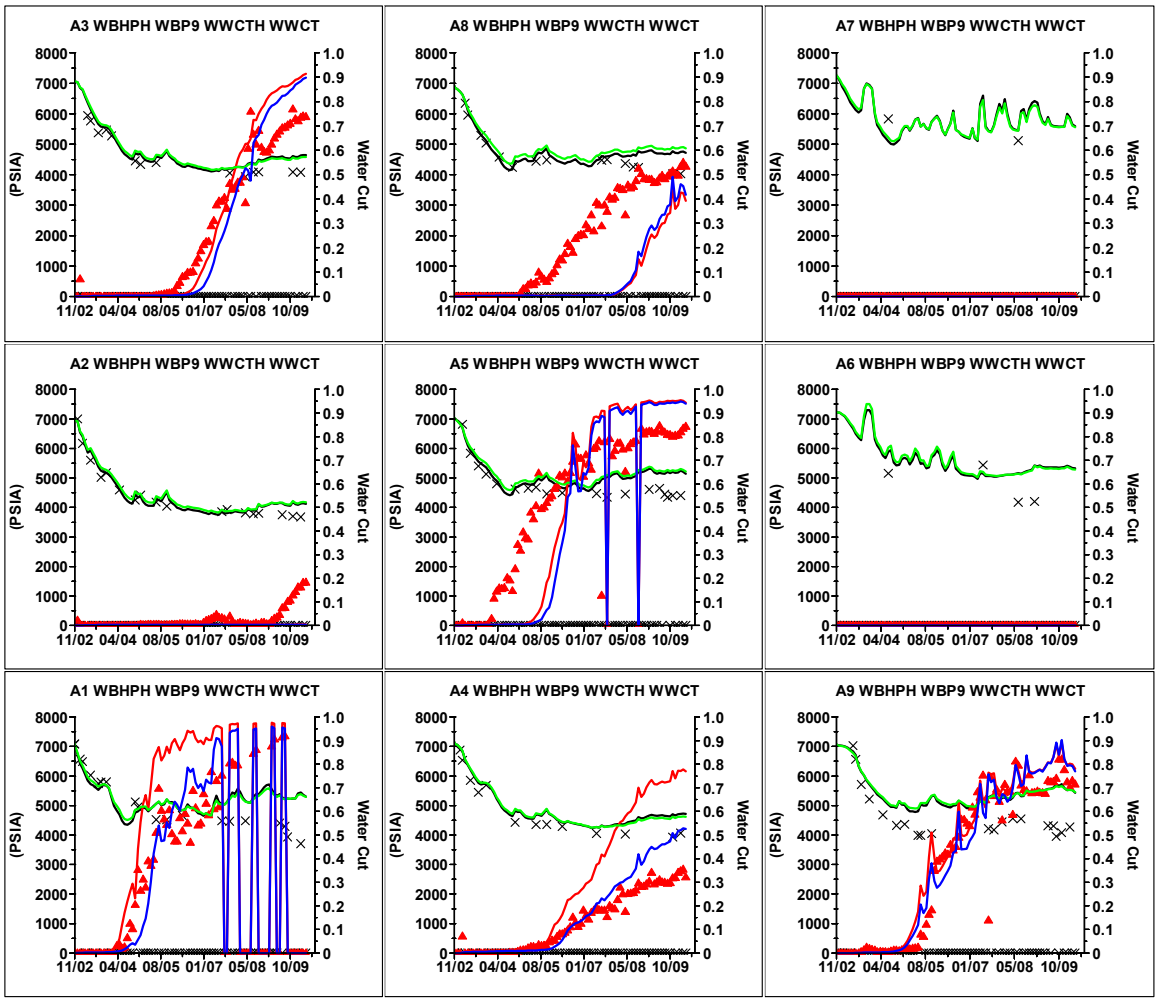

Fig. 45 - Case 4 Results

(Black and Red curves represent the match obtained after energy balance in MEPO. Green and Blue curves represent modified match after the Destiny run.)

The reservoir description for this case is shown in Fig. 46.

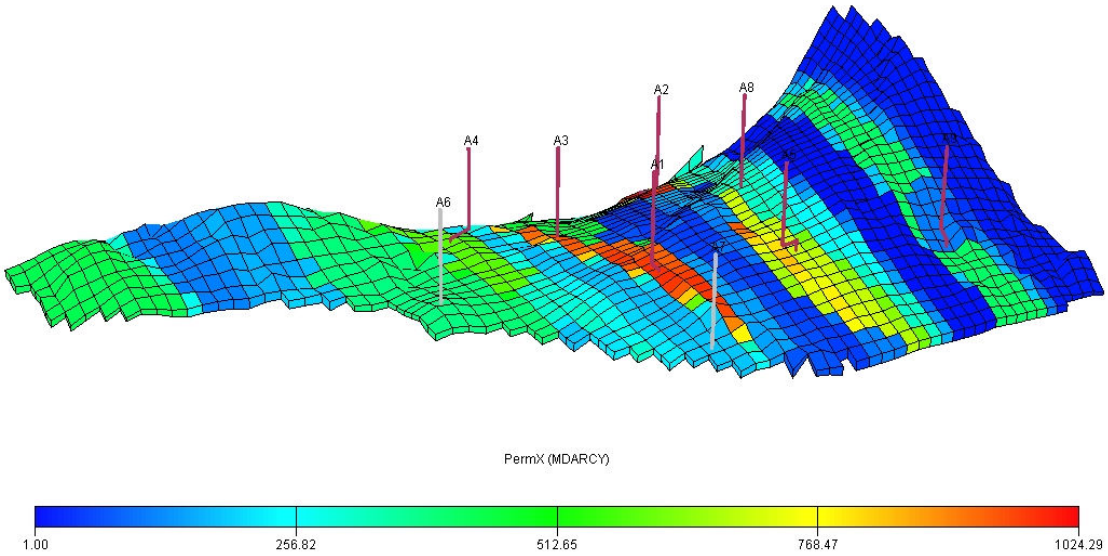

Case 4 – After MEPO

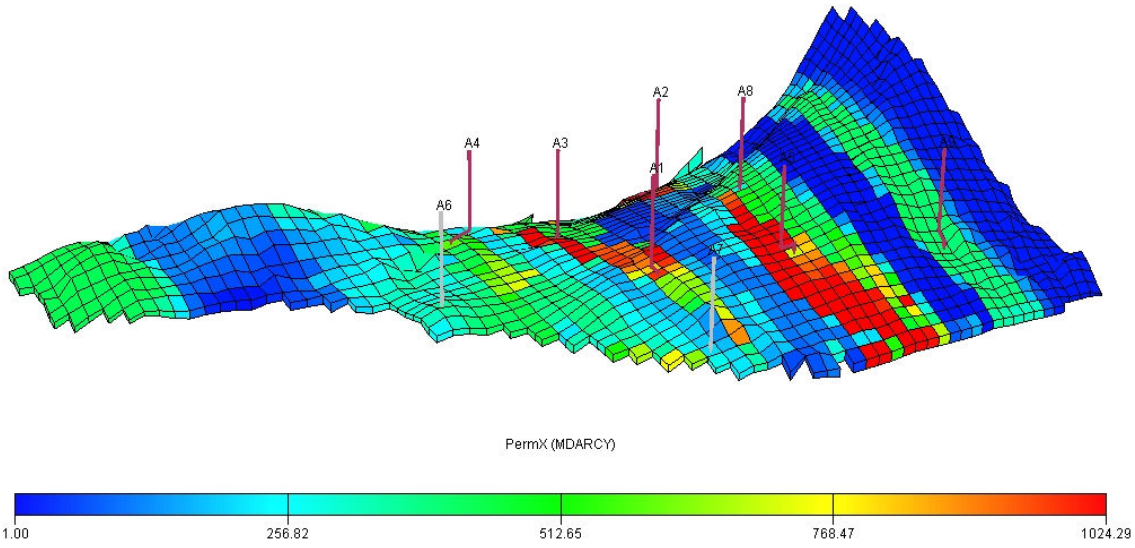

Case 4 – After Destiny

Fig. 46 - Case 4 Reservoir Description

Here the contrast between the two facies is better accentuated. The initial geologic model features remain better preserved in this model. The channel sequences remain discernible after the Destiny run also. Thus as I apply the methodology with more detail, the final model is more relevant to the expected geologic description. However, in Case 4, there is distinct upward pressure trend in all the wells in late time. So with minor aquifer strength adjustment, the result could be improved as seen in Fig. 47.

After I found the best model that worked with the low resolution model, I experimented that on a high resolution model with 22 layers with M2 sand interval divided into 20 layers. This was also required to reconcile the OOIP thus obtained with that observed from the material balance. This is discussed in detail in the discussion and conclusion section. The regions for high resolution model were defined as in Case 4.

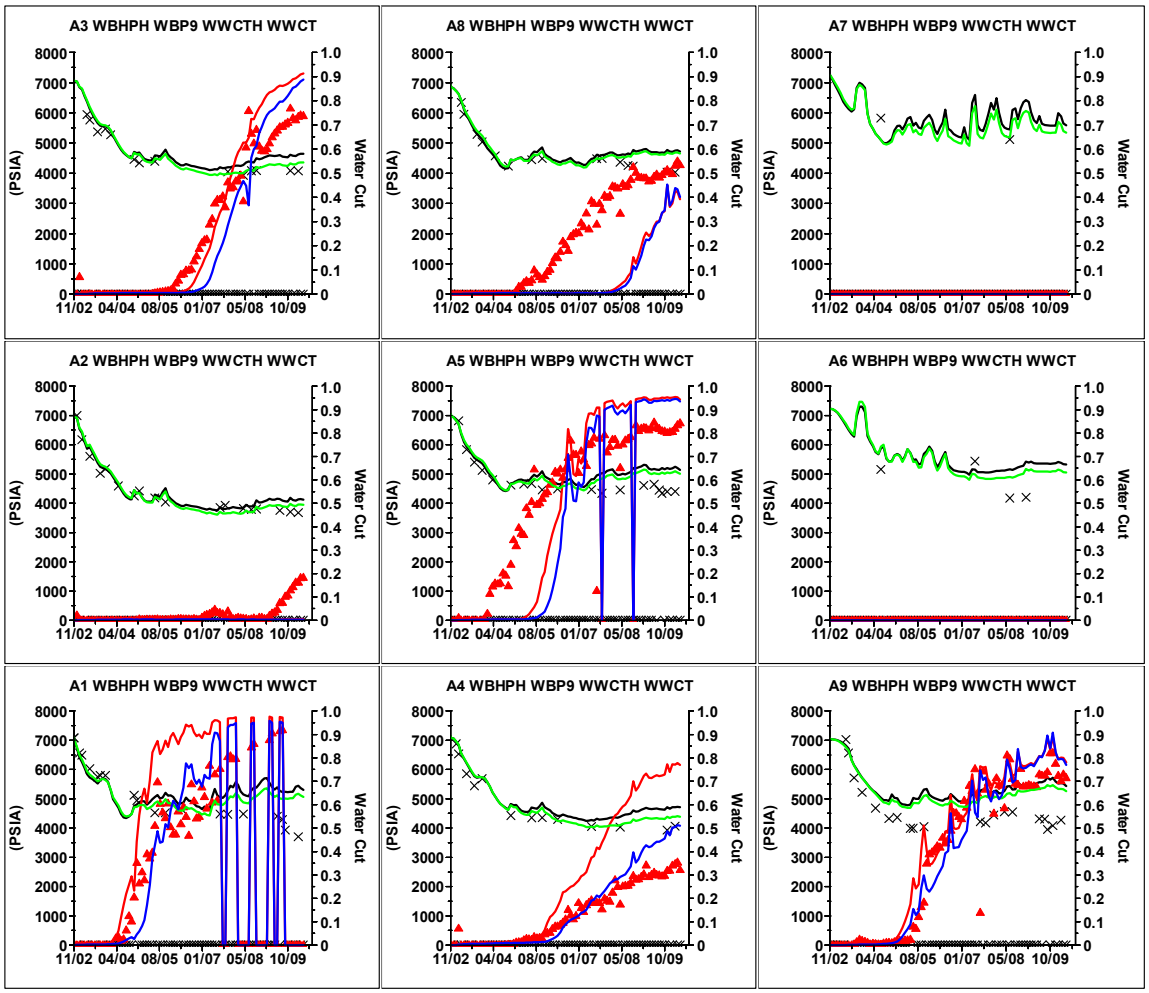

Fig. 47 - Case 4 Adjusted Aquifer Results

(Black and Red curves represent the match obtained after energy balance in MEPO. Green and Blue curves represent modified match after the Destiny run.)

8.5 CASE 5

Geological Model - High Resolution Seismic Trend Model with 8 regions.

Initial Parameters – PV multipliers for all regions, Perm multipliers for all regions, aquifer radius, Kv/Kh ratio, rock comp (19 parameters)

Selected Parameters – PV2, PV6, PV7, K6, rock comp, aq radius (Fig. 48)

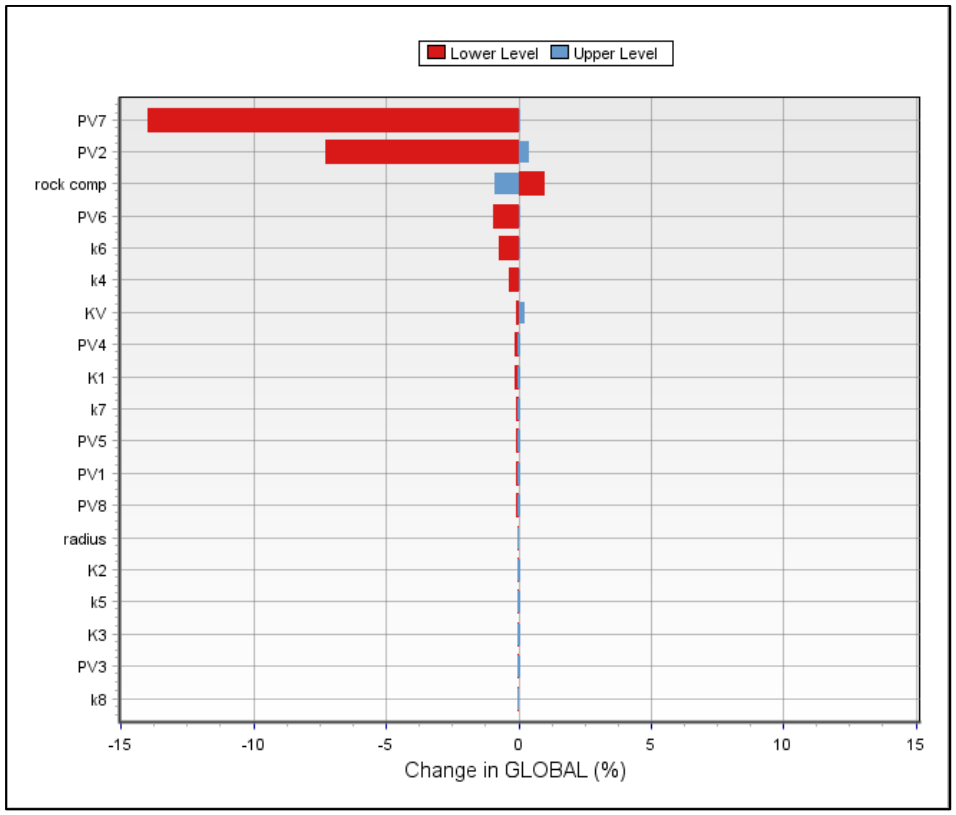

Fig. 48 – Tornado Chart for Case 5

The results for this case are shown in Fig. 49.

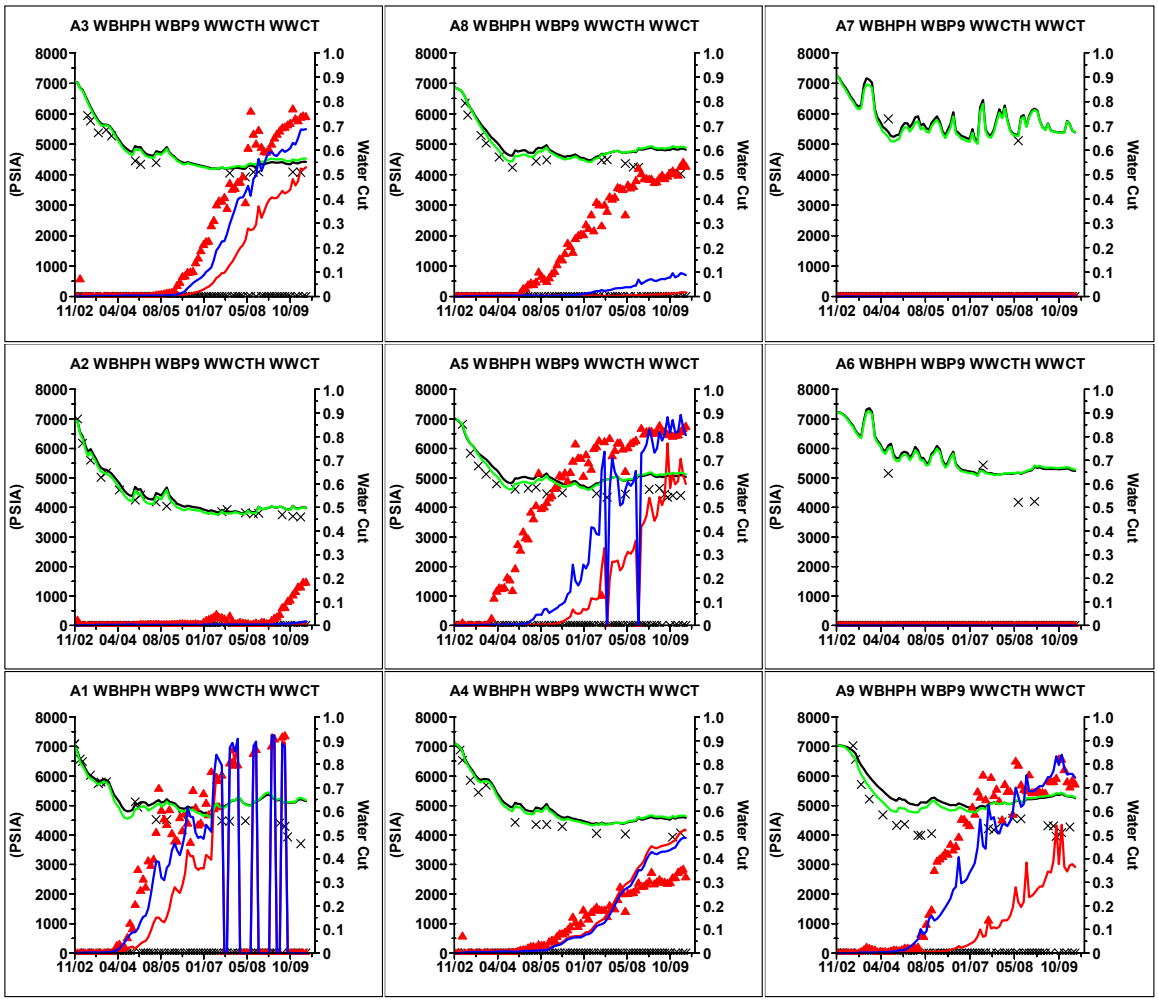

Fig. 49 - Case 5 Results

(Black and Red curves represent the match obtained after energy balance in MEPO. Green and Blue curves represent modified match after the Destiny run.)

Here again the predicted reservoir pressure has upward trend in late time. So after adjusting the aquifer strength, the match could be improved as shown in Fig. 50.

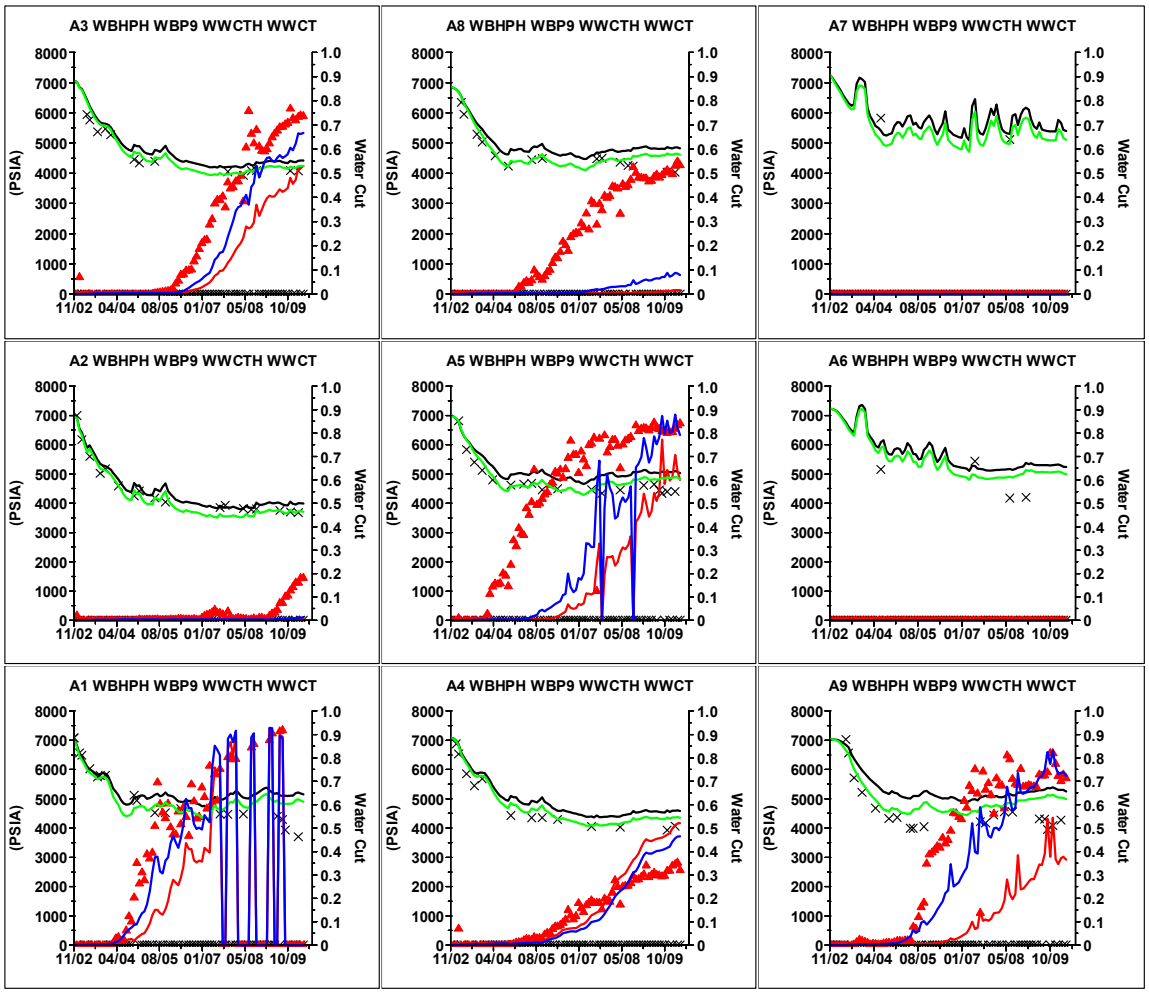

Fig. 50 - Case 5 Adjusted Aquifer Results

(Black and Red curves represent the match obtained after energy balance in MEPO. Green and Blue curves represent modified match after the Destiny run.)

When I compare the results between the high resolution and the low resolution models, the match for wells A1, A3, A4 is improved, whereas the match for other wells are close to each other. The cross-sections displaying water saturation profile when

water breakthrough occurs in well A3 are shown in Fig. 51 - Fig. 53 for cases 3 to 5 respectively

.

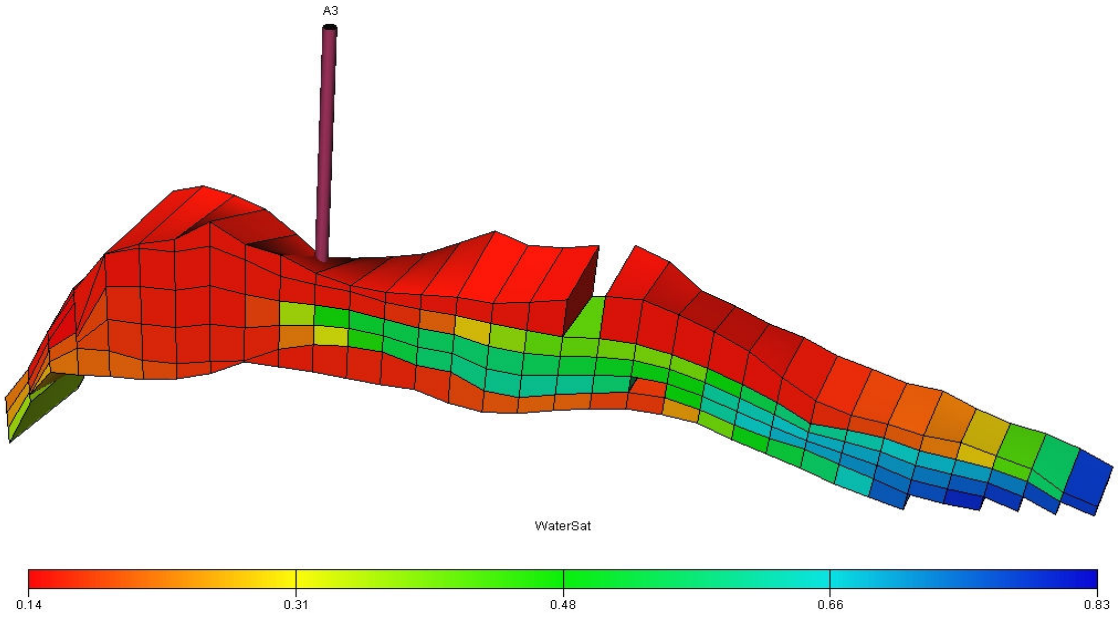

Fig. 51 - Water Breakthrough Profile in Case 3

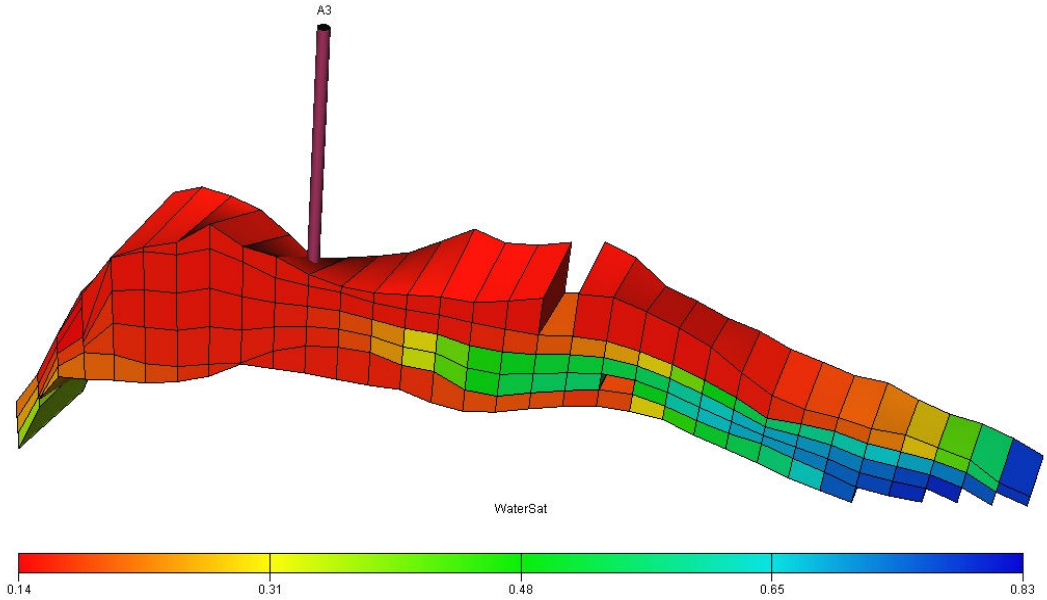

Fig. 52 - Water Breakthrough Profile in Case 4

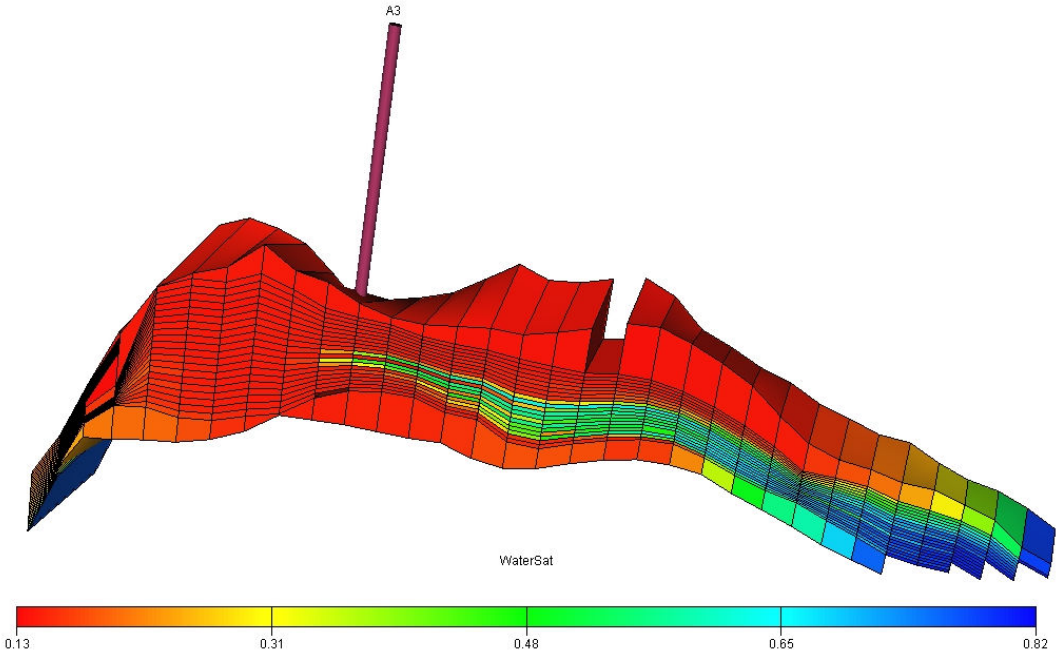

Fig. 53 - Water Breakthrough Profile in Case 5

I can identify the preferential water breakthrough pathways in the reservoir from high resolution model. The model obtained from Case 5 was then examined for other sensitivities. It was tried further for the perm multipliers for all regions and fault transmissibility.

8.6 CASE 6

Geological Model - High Resolution Model with 8 regions obtained from Case 5.

Initial Parameters – Perm multipliers for all regions, Fault transmissibilities

Selected Parameters – k2, k4, k6

The tornado chart (Fig. 54) demonstrates the transmissibilities for the faults represented by F2 and F4 parameters have least effect on the history match. Thus the faults being made sealing or non-sealing have no substantial effect.

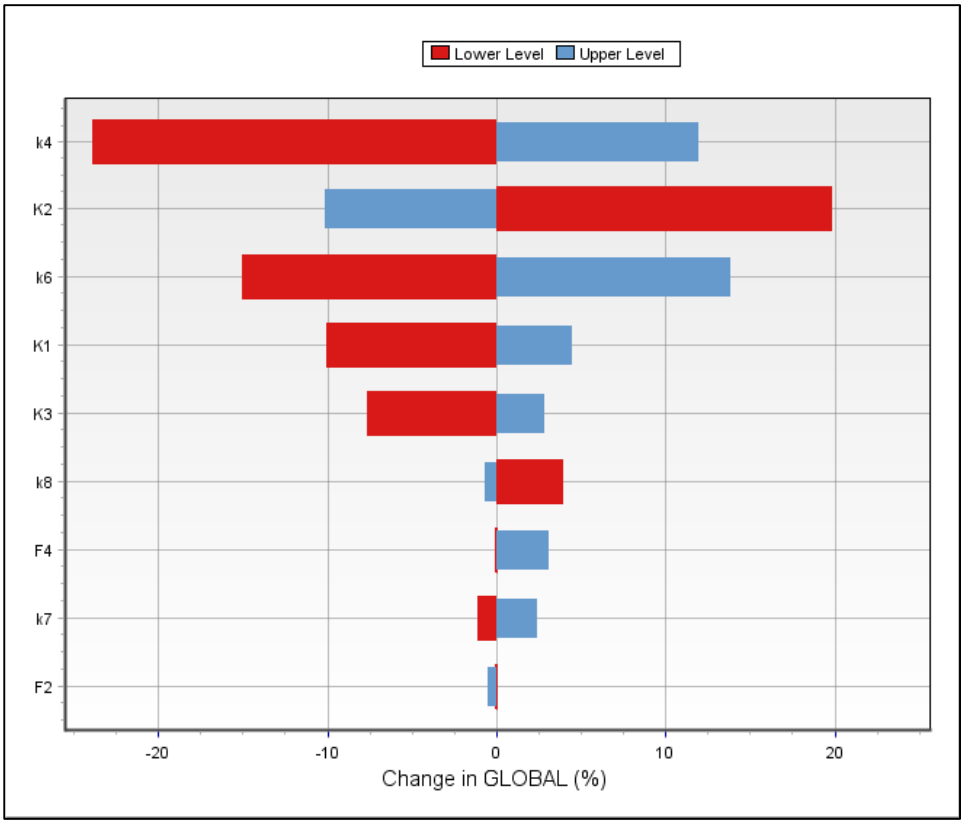

Fig. 54 – Tornado Chart for Case 6

With the selected parameters, the result could not be further improved. Therefore the next sensitivity was run on the relative permeability data.

8.7 CASE 7

Geological Model - Case 5 model with new relative permeability curves

The results for this case when compared with Case 5 are shown in Fig. 55.

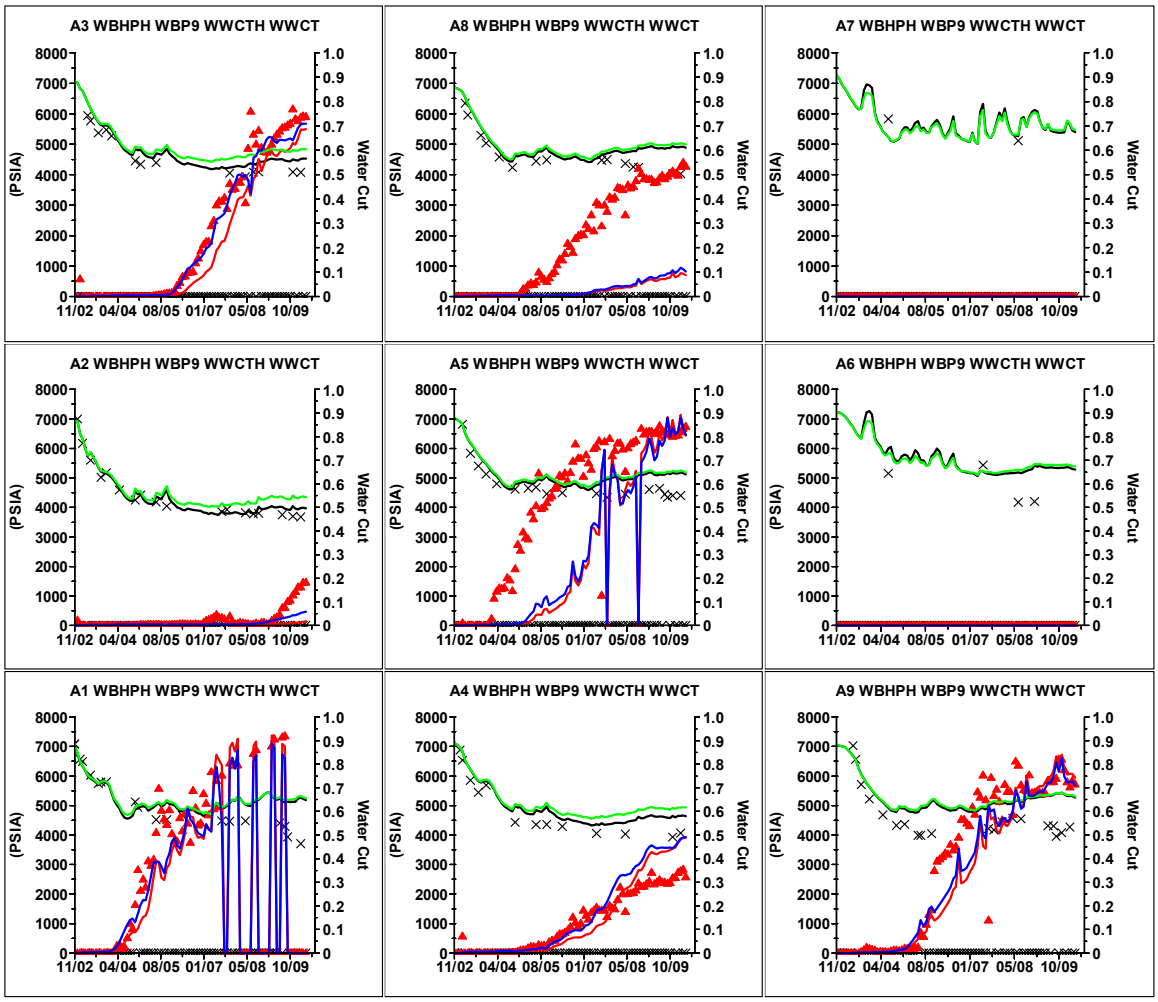

Fig. 55 - Case 7 Results compared with Case 5

(Black and Red curves represent the match obtained for Case 5. Green and Blue curves represent match for Case 7.)

The water cut match for wells A1, A2, A3, and A9 is slightly improved with this sensitivity. However, increased mobility in the reservoir supplements the drop in reservoir pressure more at the wells, thus higher bottom hole pressures are observed with new relative permeability curves.

The model obtained from Case 7 was then taken through the entire methodology to improve further. However this time the objective function was reduced to account for only the wells having major mismatch in history match results, which were A8 and A9. The objective function was based on bottom hole pressures of both the wells and water cut for well A8. I ran the sensitivity for this case and the results are shown in Fig. 56 and Fig. 57.

8.8 CASE 8

Geological Model - Case 7 model

Initial Parameters – PV multipliers for all regions, Perm multipliers for all regions, aquifer radius, Kv/Kh ratio, rock comp (19 parameters)

Selected Parameters – PV2, PV3, PV7, k2, aq radius

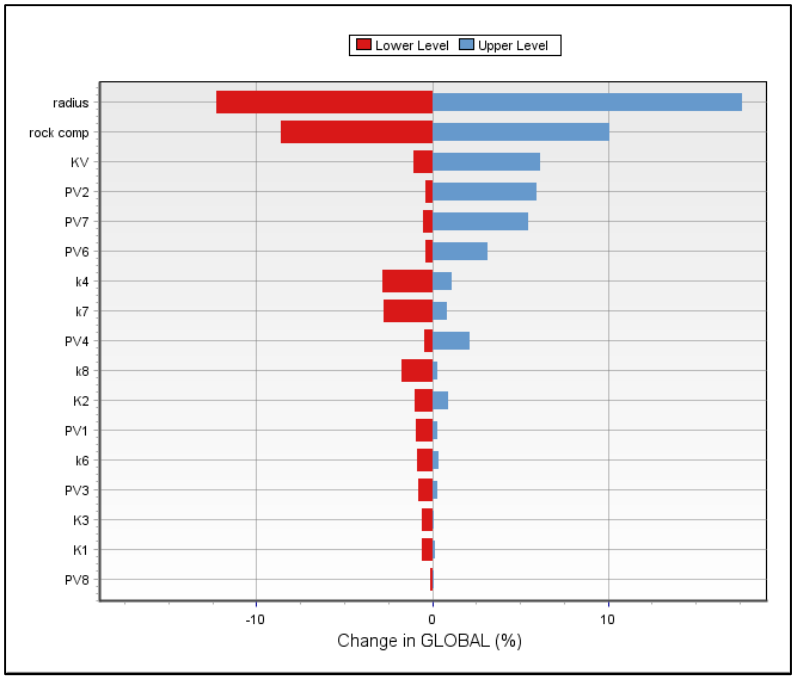

Fig. 56 – Tornado Chart for Case 8

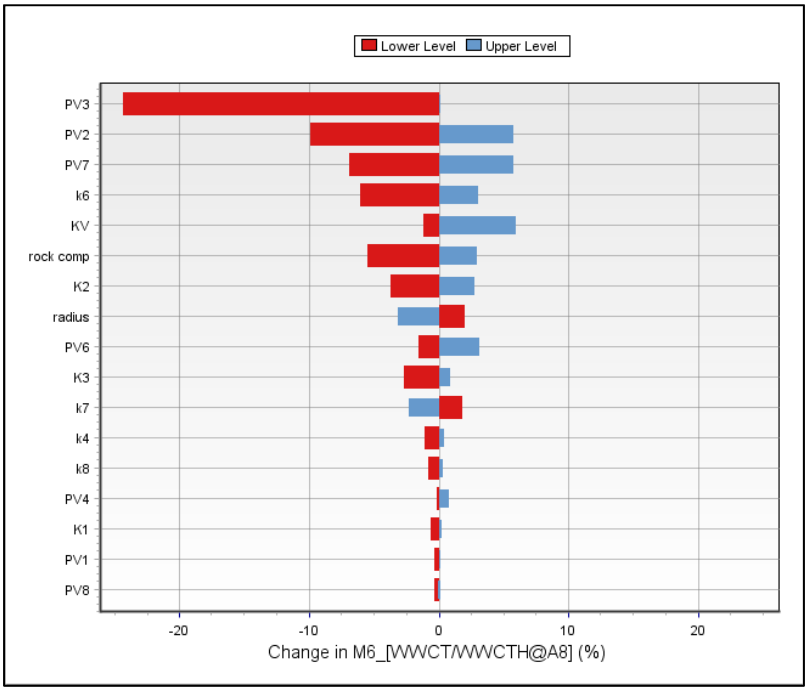

Fig. 57 – Tornado Chart for A8 water cut

The tornado chart for A8 water cut specifies that parameter PV3, not considered in ES algorithm for previous cases, affects it most. The results obtained for this case are shown in Fig. 58.

This does help in improving the water cut match at well A8. I am able to fine tune further our water cut history match, however in doing so the pressure match is being compromised. In all the wells, I see pressure rising in the late time which is due to more aquifer influx. If I again manually adjust the aquifer strength, I can get the results as obtained shown in Fig. 59. I now get close matches in bottom hole pressure trend in each well; however the water cut match is less satisfactory.

The different simulation models developed so far are compared in Fig. 60.

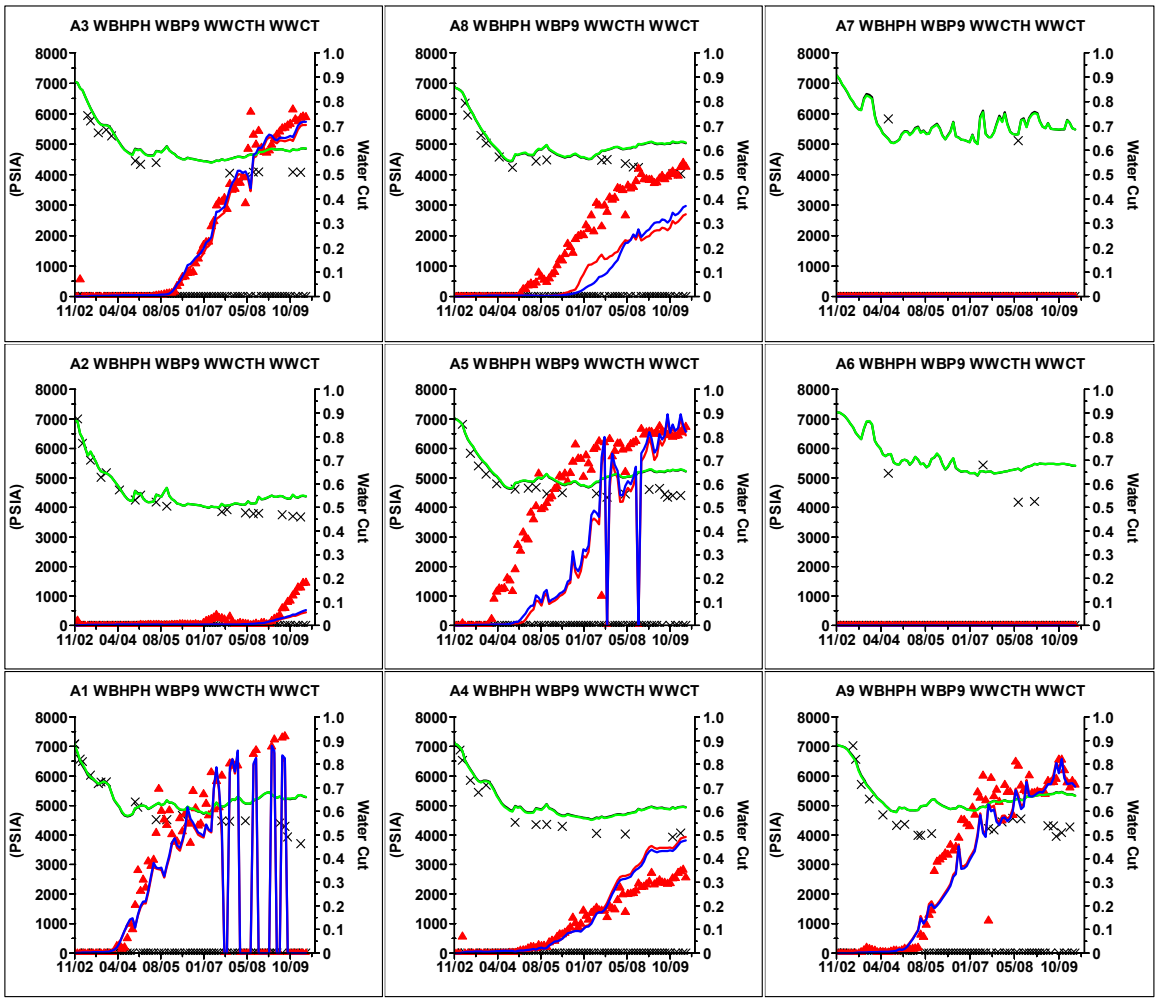

Fig. 58 – Case 8 Results

(Black and Red curves represent the match obtained after energy balance in MEPO. Green and Blue curves represent modified match after the Destiny run.)

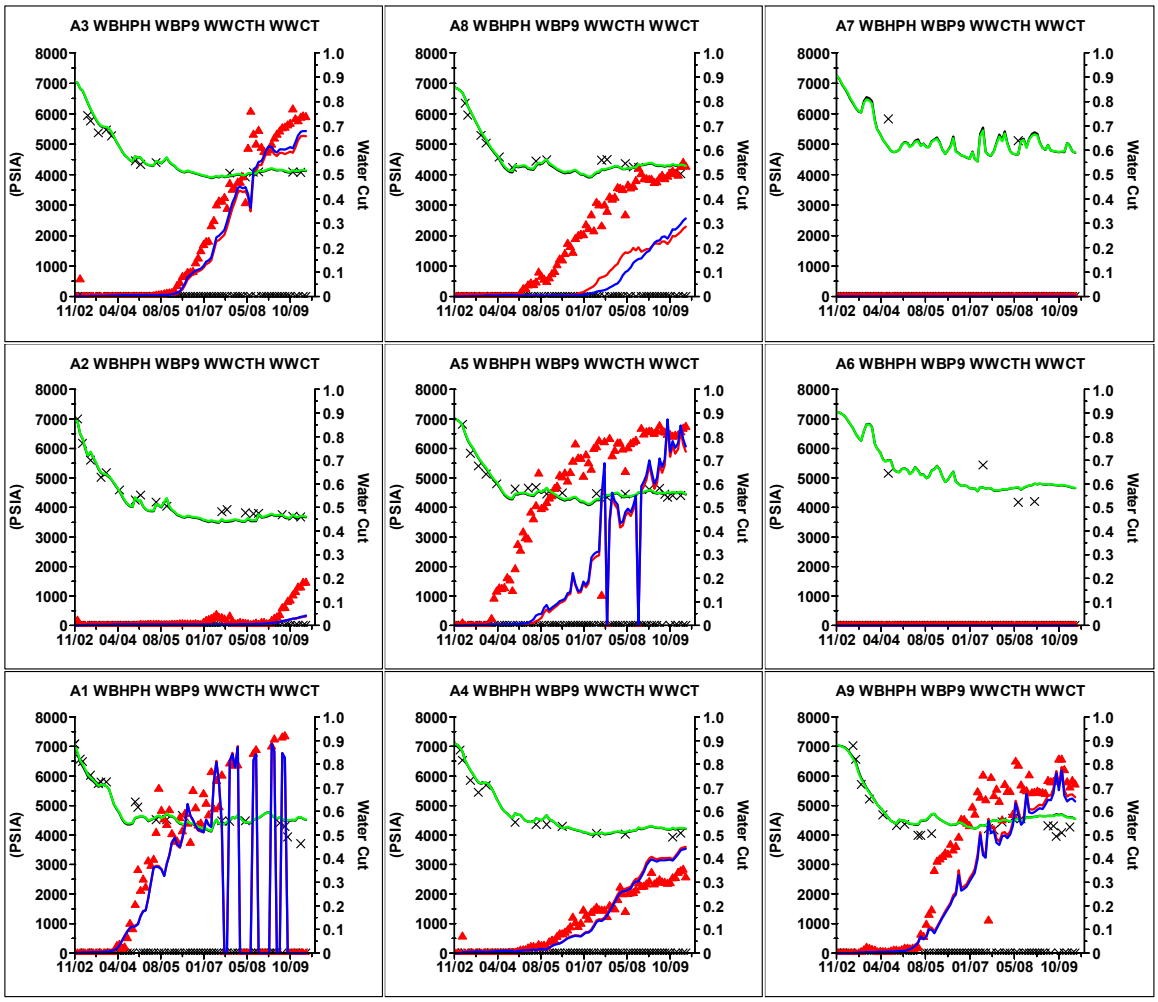

Fig. 59 – Case 8 Results with Adjusted Aquifer Strength

(Black and Red curves represent the match obtained after energy balance in MEPO. Green and Blue curves represent modified match after the Destiny run.)

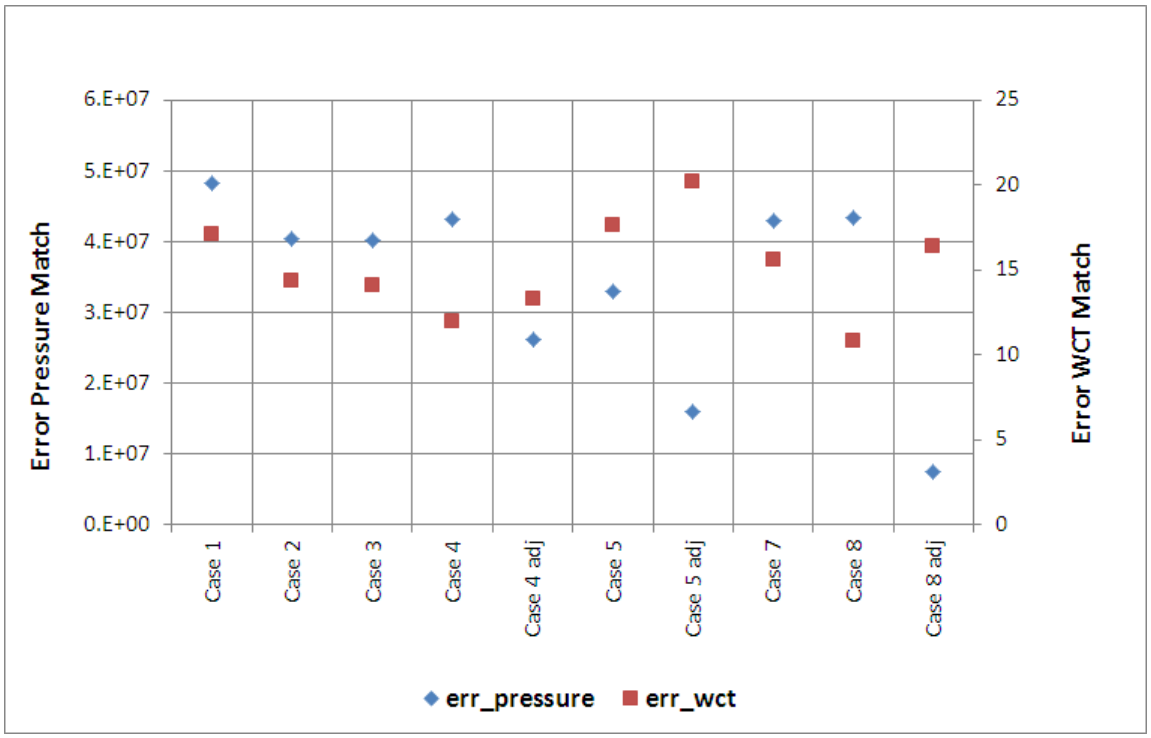

Fig. 60 – Simulation Cases Compared

The model obtained after adjusting the aquifer strength in Case 8 gives us the best match for reservoir pressure. The AHM fails to improve the pressure match and water cut match together in the extended reservoir uncertainty study from Case 4 onwards. However, the pressure match is certainly improved in these models after adjusting the aquifer strength.

9. DISCUSSION AND CONCLUSIONS

I started the reservoir uncertainty study by considering multiple geologic scenarios and dynamic parameters. Based on the uncertainty study, multiple initial models were prepared. As suggested in TDRM, these models may be simplistic in nature and need not incorporate the geologic information in detail. Based on the screening of the initial 32 different static models, I understand the following characteristics about the reservoir.

a) The E-W trend NTG models can now be rejected with evidence.
b) The uniform trend models can be ignored also, but they were included in the history matching to give a wider range of calibrated models.
c) The reservoir has high permeability contrast across channel and non-channel facies. This formed the basis to assess the relative contrast using permeability multipliers for the corresponding regions.

Thereafter, I selected three different models. The simplest model had no channel orientation given. Its Destiny result shows that the pressure falls at the wells in the attempt to improve water production. This implies that the aquifer support is not propagating preferentially towards the wells. The water influx instead of advancing in the channel gets distributed in the reservoir as there is no channel architecture. In the geologic trend model and seismic trend model, I get improved pressure match after the whole AHM methodology. The initial three cases with five regions involve global changes to the initial model. The further improvement possible from this methodology in

reservoir description then necessitates that large scale changes are made that are not uniform globally. Thus, the AHM was then applied with more regions in the model which does improve the results and reservoir description. The initial four sensitivities were run with the low vertical resolution models. The OOIP as obtained from the different cases are shown in Table 13.

Table 13 - OOIP for different Cases

Case	OOIP (MMSTB)
Case 1	231.6
Case 2	223.5
Case 3	223.8
Case 4	214.5
Case 5	234.8

The OOIP in Case 4 gets reduced which is also expected as I introduced channels like region in this case. The pore volume outside the channel is expected to be lower, and this brings down the OOIP in this case. However, this OOIP value doesn't conform well to the OOIP cumulative distribution curve obtained from the material balance analysis. I then attempted the AHM with more vertical resolution in the model that will provide more pathways for water breakthrough. The high resolution vertical model improved the result further with OOIP reconciling better with the material balance prediction. I ran other dynamic sensitivities like relative permeability and fault transmissibility on the high resolution vertical model. I was able to refine the history match for pressure after investigating all the uncertainty parameters identified earlier.

However, working with simple models restricted the improvement in water cut match unless adversely impacting the pressure match quality.

The break-up of pore volumes and permeability multipliers for the main sand M2 is shown in Table 14 for different cases.

Table 14 - Pore Volume and Permeability Multipliers for different Cases

Regions		**Region 2**		**Region 6**		**Region 7**	
Cases	**Parameter**	**Before Pressure Match**	**After Pressure Match**	**Before Pressure Match**	**After Pressure Match**	**Before Pressure Match**	**After Pressure Match**
Case 1	PV	0.5	0.24	NA	NA	NA	NA
Case 2	PV	0.5	0.26	NA	NA	NA	NA
Case 3	PV	0.5	0.25	NA	NA	NA	NA
Case 4	PV	0.8	0.35	0.5	0.14	0.8	0.2
	Perm	1	1.2	1	0.2	1	1
Case 5	PV	0.6	0.41	0.4	0.2	0.5	0.2
	Perm	1	1	0.5	0.3	1	1
Case 8	PV	0.5	0.42	0.3	0.2	0.3	0.2
	Perm	1	1	0.3	0.3	1	1

The pore volume break-up specifies that as more regions are defined in M2 sands, the pore volume fraction gets relatively distributed in the channel and non-channel regions. This shows the OOIP is more contained in the channel region.

Table 15 and Table 16 provide the aquifer strength and rock compressibility values for the different cases.

Table 15 - Aquifer Strength for different Cases

Cases	Aquifer Radius, ft	
	Before Pressure Match	After Pressure Match
Case 1	800	905
Case 2	800	925
Case 3	800	895
Case 4	800	1065
Case 5	800	856
Case 8	800	896

Table 16 - Rock Compressibility for different Cases

Cases	Rock Comp, 1/psia	
	Before Pressure Match	After Pressure Match
Case 1	13.88E-5	3E-5
Case 2	13.88E-5	3E-5
Case 3	13.88E-5	3E-5
Case 4	13.88E-5	3E-5
Case 5	13.88E-5	3E-5
Case 8	13.88E-5	3E-5

The rock compressibility governs the initial decline in reservoir pressure. I observed in each case the trend in the initial reservoir pressure drop is better matched by using rock compressibility of 3E-5 1/psia. In the late time, aquifer influx becomes the major drive mechanism. However, high aquifer strength contributed to greater mismatch

in the late time pressure trend. So, ultimately there is a trade-off between the quality of pressure history match and the water cut history match. The aquifer strength had to be reduced to maintain the energy balance.

In summary, the following conclusions can be derived from this study. Some of these conclusions are field specific while others are about the general methodology of the use of AHM with multiple initial geologic models.

a) The use of multiple simple geologic models is extremely useful in screening possible geologic scenarios and especially for discarding unreasonable alternative models. This significantly reduced the subsurface uncertainty and increased confidence in the remaining models. These conclusions may be drawn without performing a full history matching workflow.
b) The screening models were most useful in evaluating the large scale architecture of the reservoir. For this reservoir specifically, the E-W channel models were discarded, and the non-channel sheet-like reservoir description was not very likely. The N-S channel model and the N-S seismic trend channel model consistently performed better against field history.
c) The screening models were also indicative of reservoir trends within the channels. Models with more heterogeneity within the channels (shorter correlation lengths and/or stochastic permeability) consistently performed better than models which were more homogeneous.
d) The AHM methodology was very effective in exploring a large number of parameters, running the simulation cases, and generating the calibrated reservoir

models. The calibration step consistently worked better if the models had more spatial detail, instead of the simple models used for screening.

e) The AHM methodology implemented a sequence of pressure and water cut history matching. Water cut history match damages the pressure history match for some cases, but not others. An examination of specific models indicated that a better geologic description minimized this interference; a better geologic model tended to bring these changes into alignment.

f) Although low (vertical) resolution simulation models may be used for most of the history matching process, it was necessary to increase the vertical resolution to adequately represent the interplay of gravity and reservoir heterogeneity within each channel, after water breakthrough.

g) The comparison of early and late time pressure trends can be used to obtain information on field scale effective relative permeability. The field scale curves were obtained from the laboratory measurements by increasing the multiphase mobility as would be the case for segregated flow. This is expected to be a general field scale effect since the corresponding core scale curves would indicate an extreme reduction in mobility for two phase flow, which is only expected to occur for well-mixed flow.

h) After a certain class of reservoir models was explored, AHM ceases to improve the match further unless additional geological uncertainties are tested.

In addition, I then investigated how the cases developed so far perform on forward prediction. The following cases were selected for the forward prediction scenario -

a) Case 1 – Uniform Trend Model (low resolution)
b) Case 2 - Geologic Trend Model (low resolution)
c) Case 3 – Seismic Trend Model with 5 regions (low resolution)
d) Case 4- Seismic Trend Model with 8 regions (low resolution) and adjusted aquifer strength
e) Case 5- Seismic Trend Model with 8 regions (high resolution) and adjusted aquifer strength
f) Case 8- Case 5 with adjusted relative permeability and aquifer strength.

The forward predictions were run on BHP control mode with the minimum shut in pressure limit set at 4000 psi for all the producing wells and injection at the wells maintained at the last measured rate. This pressure limit was chosen because it is the onset pressure for the asphaltene deposition from the reservoir crude. The cumulative oil produced after 20 years is compared for the above models in Fig. 61 and tabulated in Table 17.

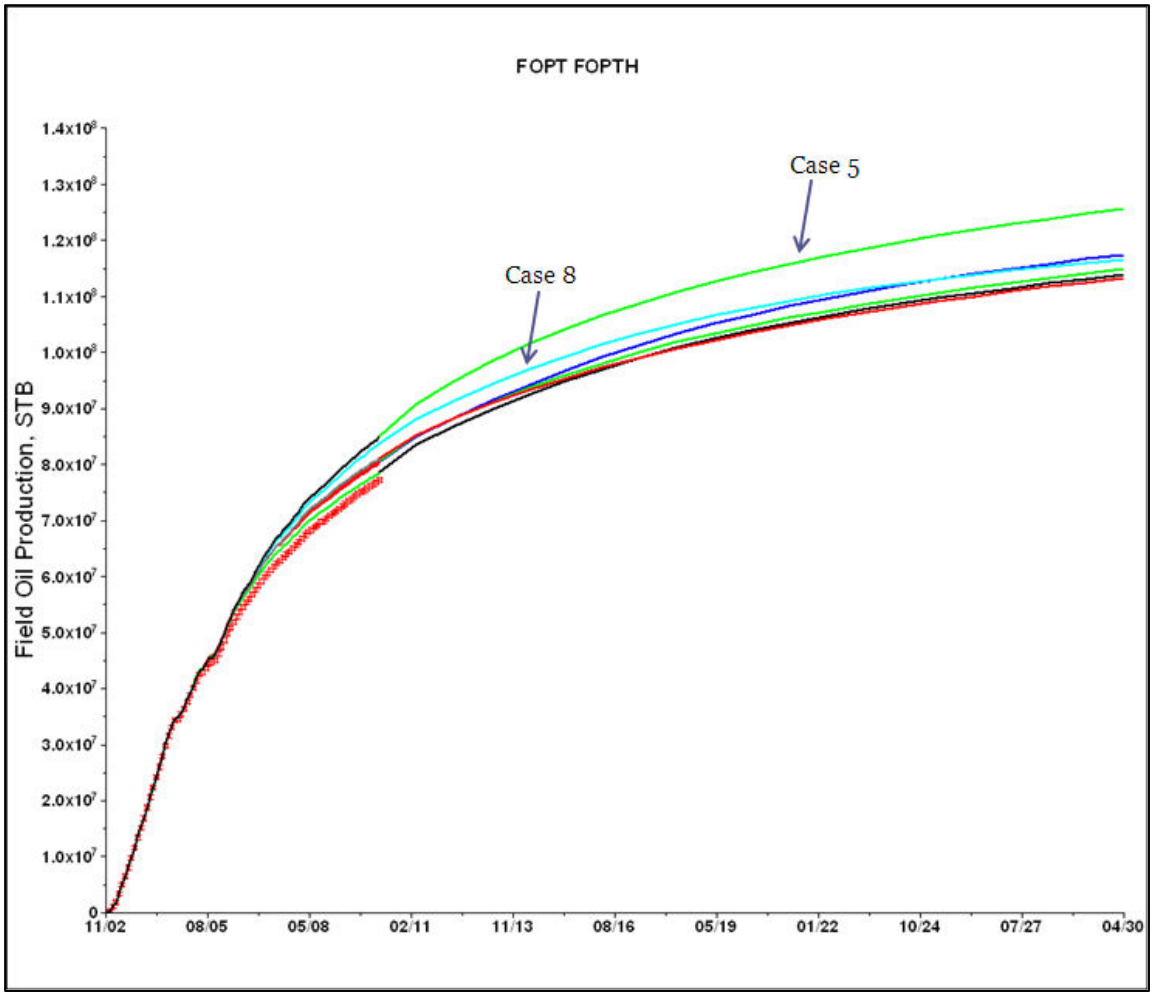

Fig. 61 – Forward Predictions compared for different Cases

Table 17 - Total Oil Production after 20 Years

Model	Case 1	Case 2	Case 3	Case 4	Case 5	Case 8
FOPT (MMSTB)	117.5	114.9	113.9	113.2	125.5	116.5

The simulation models arrived from different starting models have a small variation in total field oil production with exception in Case 5. The predictions after twenty more years are stacked in the range of 113 – 118 MMSTB. The observed field production history lies lower to the field history simulated from all the simulation models. Therefore, it is very unlikely that field production may exceed the predictions. However, these predictions leave uncertainty on the lower bound, which may not be the case if applied in other reservoir study.

REFERENCES

Back, T. 1996. *Evolutionary Algorithms in Theory and Practice,* Chap. 2, 68-73. New York: Oxford Univ. Press.

Back, T., Hammel, U., and Schwefel, H.P. 1997. Evolutionary Computation: Comments on the History and Current State. *Evolutionary Computation, IEEE Transactions* **1** (1): 3-17.

Box, G.E.P. and Draper, N.R. 1987. *Empirical Model-Building and Response Surfaces*. New York: Wiley.

Castellini, A., Yeten, B., Singh, U., Vahedi, A., Sawiris, R. 2006. History Matching and Uncertainty Quantification Assisted by Global Optimization Techniques. *In 10th European Conference on the Mathematics of Oil Recovery*, 4 - 7 September Amsterdam, Netherlands.

Cheng, H., Wen, X.-H., Milliken, W.J. et al. 2004. Field Experiences with Assisted and Automatic History Matching Using Streamline Models. Paper SPE 89857 presented at the SPE Annual Technical Conference and Exhibition, Houston, Texas, 26-29 September.

Cheng, H., Dehghani, K., and Billiter, T.C. 2008. A Structured Approach for Probabilistic-Assisted History Matching Using Evolutionary Algorithms: Tengiz Field Applications. Paper SPE 116212 presented at the SPE Annual Technical Conference and Exhibition, Denver, Colorado, USA, 21-24 September.

Clavier, C., Hoyle, W., and Meunier, D. 1971. Quantitative Interpretation of Thermal Neutron Decay Time Logs: Part I. *SPE J. Pet Tech* **23** (06): 743-755. SPE-2658-A.

Eide, A.L., Holden, L., Reiso, E., and Aanonsen, S.I. 1994. Automatic History Matching by use of Response Surfaces and Experimental Design. *In 4th European Conference on the Mathematics of Oil Recovery*, 7–10 June, Roros, Norway.

Emanuel, A.S. and Milliken, W.J. 1998. History Matching Finite Difference Models with 3d Streamlines. Paper SPE 49000 presented at the SPE Annual Technical Conference and Exhibition, New Orleans, Louisiana, 27-30 September.

Friedmann, F., Chawathe, A., and Larue, D.K. 2001. Assessing Uncertainty in Channelized Reservoirs Using Experimental Designs. Paper SPE 71622 presented at the SPE Annual Technical Conference and Exhibition, New Orleans, Louisiana, 30 September - 3 October 2001.

He, Z., Datta-Gupta, A., and Yoon, S. 2001. Streamline-Based Production Data Integration under Changing Field Conditions. Paper SPE 71333 presented at the SPE Annual Technical Conference and Exhibition, New Orleans, Louisiana, 30 September - 3 October.

Landa, J.L. and Guyaguler, B. 2003. A Methodology for History Matching and the Assessment of Uncertainties Associated with Flow Prediction. Paper SPE 84465 presented at the SPE Annual Technical Conference and Exhibition, Denver, Colorado, 5-8 October.

Ligero, E.L., Madeira, M.G., and Schiozer, D.J. 2005. Comparison of Techniques for Risk Analysis Applied to Petroleum-Field Development. Paper SPE 94806 presented at the SPE Latin American and Caribbean Petroleum Engineering Conference, Rio de Janeiro, Brazil, 20-23 June.

Luo, Y. and Schuster, G.T. 1991. Wave-equation traveltime inversion. *Geophysics* **56** (5): 645-653.

Milliken, W.J., Emanuel, A.S., and Chakravarty, A. 2000. Applications of 3d Streamline Simulation to Assist History Matching. Paper SPE 63155 presented at the SPE Annual Technical Conference and Exhibition, Dallas, Texas, 1-4 October.

Moulds, T.P., Trussell, P., Haseldonckx, S.A. et al. 2005. Magnus Field: Reservoir Management in a Mature Field Combining Waterflood, EOR, and New Area Developments. Paper SPE 96292 presented at the Offshore Europe, Aberdeen, United Kingdom, 6-9 September.

Myers, R.H. and Montgomery, D.C. 1995. *Response Surface Methodology: Process and Product Optimization Using Designed Experiments*. New York: Wiley.

Rechenberg, I. 1973. *Evolution Strategy: Optimization of Technical Systems according to the Principles of Biological Evolution* (in German). Stuttgart, Germany: Frommann-Holzboog.

Schwefel, H.P. 1975. Evolution Strategy and Numerical Optimization (in German). PhD dissertation, Technical University of Berlin, Germany (1974/1975).

Steiber, S.J. 1970. Pulsed Neutron Capture Log Evaluation - Louisiana Gulf Coast. Paper SPE 2961 presented at the Fall Meeting of the Society of Petroleum Engineers of AIME, Houston, Texas.

Vasco, D.W., Yoon, S., and Datta-Gupta, A. 1999. Integrating Dynamic Data into High-Resolution Reservoir Models Using Streamline-Based Analytic Sensitivity Coefficients. *SPE Journal* **4** (4): 389-399. SPE-59253-PA.

White, C.D., Willis, B.J., Narayanan, K. et al. 2001. Identifying and Estimating Significant Geologic Parameters with Experimental Design. *SPE Journal* **6** (3): 311-324. SPE-74140-PA.

White, C.D. and Royer, S.A. 2003. Experimental Design as a Framework for Reservoir Studies. Paper SPE 79676 presented at the SPE Reservoir Simulation Symposium, Houston, Texas, 3-5 February.

Williams, M.A., Keating, J.F., and Barghouty, M.F. 1998. The Stratigraphic Method: A Structured Approach to History-Matching Complex Simulation Models. *SPE Res Eval & Eng* **1** (02): 169-176. SPE-38014-PA.

Williams, G.J.J., Mansfield, M., MacDonald, D.G. et al. 2004. Top-Down Reservoir Modelling. Paper SPE 89974 presented at the SPE Annual Technical Conference and Exhibition, Houston, Texas, 26-29 September.

Worthington, P.F. 2008. The Application of Cutoffs in Integrated Reservoir Studies. *SPE Res Eval & Eng* **11** (06): 968-975. SPE-95428-PA.

Wu, Z. and Datta-Gupta, A. 2002. Rapid History Matching Using a Generalized Travel-Time Inversion Method. *SPE Journal* **7** (2): 113-122. SPE-78359-PA.

VITA

Name: Akshay Aggarwal

Address: Harold Vance Department of Petroleum Engineering
Texas A&M University
3116 TAMU - 507 Richardson Building
College Station, TX 77843-3116

Email Address: akshay.ism@gmail.com/akshay.aggarwal@pe.tamu.edu

Education: B.Tech., Petroleum Engineering, Indian School of Mines, 2006